2023

An investigation of mission designs to the outer solar system supported by centrifugal nuclear thermal propulsion

William Ziehm

AN INVESTIGATION OF MISSION DESIGNS TO THE OUTER SOLAR SYSTEM SUPPORTED BY CENTRIFUGAL NUCLEAR THERMAL PROPULSION

William Ziehm

A THESIS

Submitted in partial fulfillment of the requirements
for the degree of Aerospace Systems Engineering
in
Mechanical and Aerospace Engineering
to
The Graduate School
of
The University of Alabama in Huntsville
December 2023

Approved by:

Dr. Dale Thomas, Research Advisor
Dr. Jason Cassibry, Committee Chair
Dr. Dale Thomas, Committee Member
Dr. Gabe Xu, Committee Member
Dr. George Nelson, Department Chair
Dr. Shankar Mahalingam, College Dean
Dr. Jon Hakkila, Graduate Dean

Abstract

AN INVESTIGATION OF MISSION DESIGNS TO THE OUTER SOLAR SYSTEM SUPPORTED BY CENTRIFUGAL NUCLEAR THERMAL PROPULSION

William Ziehm

A thesis submitted in partial fulfillment of the requirements

for the degree of Aerospace Systems Engineering

Mechanical and Aerospace Engineering
The University of Alabama in Huntsville
December 2023

Centrifugal nuclear thermal propulsion (CNTP) has potential for supporting scientific missions to the outer solar system, shown by investigation of mission and vehicle architectures to the outer planets and Kuiper belt. The patched conic method provided initial guesses for numerical simulation and relationships between parameters of interest for trade studies, recommending engine performance parameters for missions supported by CNTP. Results of the patched conic model were validated by comparison to numerical results, which were within the expected variance for transit time with identical propellant margins based on literature. The trade studies gave a range of performance required to close rendezvous missions to the outer planets for 2 mT payload dry mass. These ranges were 1200-1800 s, 10-70 kN, and 1.5-4 T/W for direct trajectory transit times of 2, 3.5, 7.5, and 10.5 years to Jupiter, Saturn, Uranus, and Neptune. Kuiper belt

missions required 1600-1800 s, >60 kN, and >3.7 for transit times between 10 and 16 years depending on the trajectory type.

Acknowledgements

First, I would like to thank my advisor, Dr. Dale Thomas, for his support and guidance throughout my research.

I would also like to thank my thesis committee members, Dr. Jason Cassibry and Dr. Gabe Xu, for their advice and experience.

I am grateful to my fellow graduate students, and I would especially like to acknowledge Saroj Kumar, Mitchell Schroll, and Nick Morris for their help with my research.

Finally, I would like to thank my family for their considerable care and support.

Table of Contents

List of Figures

List of Tables

List of Symbols

Symbol	Description
I_{sp}	Specific Impulse [s]
T	Thrust [kN]
ΔV	change in velocity [km/s]
V_{∞}^{-}	Incoming hyperbolic velocity with respect to planetary body [km/s]
V_{∞}^{+}	Outgoing hyperbolic velocity with respect to planetary body [km/s]
V_{ϕ}	Velocity of planetary body with respect to Sun [km/s]
V_{DP}	Outgoing velocity with respect to Sun [km/s]
V_{AR}	Incoming velocity with respect to Sun [km/s]
FOM	Figure of merit
TOF	Time of flight, or transit time [yrs]
θ	Reactor operating temperature [K]
V_E	Earth Orbital Velocity [km/s]
P_E	Earth Orbital Period [yrs]
M	Mean anomaly
e	eccentricity
E	Eccentric anomaly [rads]

V	Velocity at a given point [kms]
r	Position at a given point [km]
μ	Gravitational parameter [km^2/s^2]
a	Semi-major axis [km]
h	Angular momentum [km^2/s]
r_p	Periapsis radius [km]
p	Parameter [km]
ν	True anomaly [rads]
i	Inclination [rads]
n	Mean motion [1/s]
δ	Turn-through angle [rads]
D	V_{AR}-ΔV vectors inclusive angle [rads]

Chapter 1. Introduction

1.1 Background on Scientific Missions to the Outer Solar System

Exploring the solar system is a great challenge given its size and the fundamental nature of gravity, and yet this challenge also presents a great reward in the pursuit of knowledge regarding our sun and the planets. The outer solar system in particular has the potential to answer many questions about the processes that shape planetary systems in our past and present [1]. This applies both to the sun and solar system, but also to the planets and smaller planetary objects throughout our solar system. In addition, the search for other life continues parallel to the pursuit of these questions. The National Academy of Science, Engineering, and Medicine is attempting to focus efforts in answering these questions for the next decade by recommending specific and achievable missions to the outer solar system, such as a mission to Uranus by 2040 [2]. Other reasons, besides planetary science, exist as well to explore the outer solar system. These missions often require advanced technology, which is either utilized or must first be developed for each mission. Especially the technologies of propulsion and communication have seen wider development and use as a result of planetary missions [3]. For all the technical benefits missions to the outer solar system provide, curiosity and the desire to explore are in themselves also driving factors in journeying to the farthest places in the solar system.

Several missions have been sent to the outer solar system in the past, accomplishing a variety of scientific tasks while continuously improving technological capability. The Pioneer and Voyager missions were some of the first to visit the outer solar system, conducting the first and in some cases only flybys of each of the outer planets. Pioneers 10 and 11 were the first spacecraft to visit Jupiter and Saturn,

respectively, and continued to make discoveries after their initial flybys [3]. Likewise, Voyager I and II pushed the bounds of knowledge by pursuing flybys of all the gas and ice giants between the two spacecraft before continuing out of the solar system, making discoveries along the way of volcanos on Jupiter's moon Io and exploring the rings of Saturn [4]. Voyager I left the solar system in August 2012, while Voyager II achieved the same milestone in November 2018. As of 2018 they were both still sending information back to the Deep Space Network from interstellar space beyond the solar system [4].

There are other more recent missions to the outer solar system whose objectives were narrower in scope. These missions involved a flyby or planetary capture of a planetary body in order to study the body and its moons in detail. Two planetary captures have been achieved around Jupiter, first by Galileo in 1995 followed by Juno in 2016. Both missions required gravity assists from Venus and Earth in order to reach Jupiter with the allotted program resources and spent many orbits around Jupiter conducting science. More details on the need for gravity assist trajectories are given in section 1.2. During these missions, particular focus was given to measuring the magnetic field and radiation environment near the planet, along with imaging of the atmosphere. Galileo's mission ended in 2003 and was deorbited into Jupiter's atmosphere, while Juno is still conducting research in orbit around Jupiter to this day [5], [6]. Cassini-Huygens conducted research in the Saturn planetary system starting in 2004 after a nearly seven-year journey. In some ways similar to Galileo and Juno, Cassini-Huygens used gravity assists from the inner planets to reach Saturn, where it also conducted a variety of scientific observations which were sent back to Earth [7] . One of the most recent missions to the outer solar system was conducted by the New Horizons spacecraft, which

conducted a gravity assist at Jupiter in order to fly by Pluto and its moons. [8] [9]. The number and variety of missions to the outer solar system have provided a number of scientific discoveries and questions for many of the largest bodies in the outer solar system. At the same time, however, they exemplify the difficulty of reaching the outer solar system by the technological developments which were required for the missions to succeed.

1.2 Applications of Space Nuclear Propulsion

Previous missions to the outer solar system, such as Cassini-Huygens and Juno, used chemical propulsion and a number of gravity assists in order to reach their destination. Due to chemical propulsion being limited to 450 s of specific impulse, gravity assists are sometimes used to enable a small vehicle to perform large ΔV's at the cost of a more complex and sometimes longer trajectory. By contrast, nuclear electric propulsion (NEP) and nuclear thermal propulsion (NTP) enable new trades of an alternative spacecraft architecture for large ΔVs with different requirements for the mission trajectory. These trades can be explored by holding aspects of the vehicle or trajectory fixed [10]. While NEP and NTP introduce new challenges to spacecraft design, new opportunities are gained as well. Examples for each of these are discussed in later sections of this work. Already, a considerable amount of work has been done to define the use case for nuclear propulsion, and NTP in particular has the potential to support different kinds of scientific missions to the outer solar system [11], [12], [13]. In addition to meeting needs for spacecraft propulsion, NTP may also be used in other configurations to provide for versatile options for power as well [14], [15]. For the case of scientific missions to the outer planets, NTP has been shown to have high potential despite its

additional drawbacks. Besides scientific missions, however, NTP is also being considered for crewed missions and is one of the primary candidates for missions focused on sending humans to Mars. As a result, a considerable amount of research involves direct application of NTP to Mars rendezvous missions as well as demonstrations which are capable of being scaled to that task [16], [17].

Solid fuel NTP has a history of testing and development programs, dating back to the 1940's. With the Nuclear Engine for Rocket Vehicle Application (NERVA) program, the U.S. Air Force set out to develop an NTP system for intercontinental ballistic missiles [18]. The program was then taken over by NASA in the late 1950's, which proceeded to accomplish many full-scale tests over the program's lifetime. Later programs would investigate particle bed reactors as well as the development of ceramic-metallic (CERMET) fuels which would each lead to further improvements of the technology [18]. In more recent years NASA has again focused on the potential for NTP to support both manned and unmanned missions, with recommendations for using the technology in the human exploration of Mars, through which insights have been gained in the development, operation, and safety requirements regarding NTP systems [19]. In the near future, more hardware testing is expected with the continuation of the Demonstration Rocket for Agile Cislunar Operation (DRACO) program and the industry progress in manufacturing methods for nuclear reactors [20].

At a much lower technological readiness level, liquid fuel NTP has not yet been physically demonstrated but has also been studied since the 1960s. In contrast to the solid phase fuel elements of solid fuel NTP, liquid fuel NTP contains the liquid phase fuel by porous membranes which allow propellant to move through or near the fuel [21]. Among

several performance advantages, the fuel being liquid phase also removes the risk of fuel elements cracking or breaking due to physical and thermal stresses. In 1963, Princeton published a full system analysis for a liquid NTP propulsion system, which discussed the physical processes and effects which contribute to system operation [22]. Results of the analysis include specific impulse and thrust estimates, as well as chemical analysis and material selection for the physical system. Additionally, an analysis on radiant-heat-transfer liquid-core NTP systems was performed at NASA and likewise presented several aspects of its possible performance and material makeup [23]. Recently more research has been conducted on centrifugal NTP, or CNTP, which contains the liquid fuel in centrifugal fuel elements (CFEs) spinning at high RPM to prevent fuel entrainment in the propellant stream. In 2020 two papers were presented which laid out some of the preliminary analysis and research focal points for further development [24], [25]. Since then, universities have continued research into the viability of CNTP, guided by a list of challenges presented at the International Astronautical Congress (IAC) in 2021 [26]. While many challenges remain, small scale testing of various aspects of the CFEs are undergoing research along with other areas of CNTP steady state operation [27]. Static models of the CFEs are useful in understanding the behavior of fluid-bubble interactions before moving to spinning apparatus which more closely approximate the operation of a CNTP system.

The following work is discussed in sequence by chapters building up to the results and conclusions which relate to the two research questions posed in Chapter 2 after literature review of the state of the art for the application of spacecraft propulsion. Chapter 3 explains the methodology that is utilized to model different trajectories within

chosen mission architectures. Chapter 4 provides an in-depth discussion of a variety of vehicle and mission architectures along with their constraints. Next, the corresponding results are detailed in Chapter 5. Lastly, conclusions are drawn in Chapter 6 based on what the results say about the use-case for CNTP, and future areas of work are also discussed in Chapter 7.

Chapter 2. Literature Review

In this chapter, literature is discussed in further detail, which supports the formulation of two key research questions. First, the current state of technology for missions to the outer solar system is identified in order to establish a case for the development of CNTP and the destinations within its potential to reach. Next, modeling and analysis of CNTP is explored to better understand previous and current estimates of engine performance. Finally, these areas of research are summarized and synthesized into research questions to guide this work.

2.1 Review of Propulsion Technology for Scientific Missions

In general, there are three major types of propulsion systems which have been pursued in use for spacecraft missions. Chemical and electric propulsion in particular have seen wide use in spacecraft, and respectively have supported many missions to the outer planets and the asteroid belt. Nuclear propulsion, on the other hand, has not seen operational use outside of ground test systems, but is currently being pursued as a popular option for future crewed and unmanned missions throughout the solar system. Each of these systems have pros and cons which prioritize its use in some missions over others, and yet there is still a role to be played by future technologies such as CNTP which can support missions that would be challenging for other technologies.

Historically, chemical propulsion has been widely used for missions to the outer solar system. As of 2023, 10 space missions have encountered planetary objects beyond the asteroid belt and all of these missions were supported by chemical propulsion. Some missions consisted of rendezvous with an outer planet, but in order to accomplish the

rendezvous one or more planetary fly-bys were required to achieve the necessary ΔV within the programmatic constraints. Galileo, Cassini, and Juno all fall into this class of mission for their visits to Jupiter, Saturn, and Jupiter respectively [6], [7], [5]. Other missions, such as the Voyager and Pioneer probes, conducted fly-bys or gravity assists of outer planets without a final rendezvous [3], [4]. Table 2.1 gives details for each of the chemical propulsion missions described in this section.

Table 2.1: Summary of Chemical Propulsion Missions to the Outer Solar System.

Mission	Trajectory Type	PGAs	Destination
Pioneer 10 [3]	Direct	None	Jupiter Flyby
Pioneer 11 [3]	Single PGA	Jupiter	Saturn Flyby
Voyager 2 [4]	Multiple PGA	Jupiter, Saturn, Uranus, Neptune	Interstellar Space
Voyager 1 [4]	Multiple PGA	Jupiter, Saturn	Interstellar Space
Galileo [6]	Multiple PGA	Venus, Earth	Jupiter Rendezvous
Ulysses [28]	Single PGA	Jupiter	Heliocentric Polar Orbit
Cassini [7]	Multiple PGA	Venus, Earth, Jupiter	Saturn Rendezvous
Juno [5]	Single PGA	Earth	Jupiter Rendezvous
New Horizons [9]	Single PGA	Jupiter	Kuiper Belt Flybys
Lucy [29]	Multiple PGA	Earth	Trojan Asteroid Flybys

New Horizons, Ulysses, and Lucy all conducted gravity assists of Jupiter or Earth, each for distinct destinations. New Horizons used a gravity assist at Jupiter to reach Pluto where a fly-by was conducted of the dwarf planet and other Kuiper belt objects [9]. Ulysses also conducted a gravity assist at Jupiter, but rather than another close encounter with a planetary object the spacecraft entered a high inclination heliocentric trajectory

[28]. Through several Earth gravity assists, Lucy encountered six Trojan asteroids near Jupiter's orbit [29]. In each of these cases chemical monopropellant or bipropellant propulsion systems were suited for these missions on account of their high thrust and minimal startup/shutdown time, as well as less development work required compared to electric and nuclear propulsion. However, the low specific impulse also meant that gravity assists were often necessary in order to complete missions within programmatic requirements.

No missions to the outer solar system have yet to utilize electric propulsion, however eight missions to the asteroid belt and inner solar system have previously used electric propulsion systems ranging from 15 W to 4.6 kW power [30]. Due to their high specific impulse, large ΔVs can be achieved with many electric propulsion systems, however this comes at the cost of thrust. In many cases, such as with the Dawn or BepiColombo missions, long spiral trajectories were required to reach other planetary bodies, in these cases Vesta and Ceres or Mercury, respectively [31], [32]. Even with the high specific impulse, Hayabusa 2 still required an Earth gravity assist to complete its mission to the asteroid 1999 JU3 [33]. In addition to these examples, it is also helpful to discuss future potential missions which may be supported by electric propulsion. In a response to the call for the 2023 Planetary Science Decadal Survey, a white paper argued in favor of the development of a larger 10-kWe propulsion system to be used for planetary science in the outer solar system [34]. Among others, these missions include a Saturn mission to deliver landers to Enceladus and Titan, a lander mission to Triton/Neptune, and a Pluto rendezvous mission. The proposed transit times for each mission are 9.75 years, 13 years, and 14.7 years, respectively. On account of the long

transit time, the Saturn mission was able to deliver 7200 kg of payload, while the other missions were much smaller at 400 kg and 50 kg, respectively. Overall, these proposed missions show what is projected to be feasible with high power electric propulsion systems.

Similarly, much of the work regarding interplanetary missions supported by nuclear thermal propulsion are in the modeling and analysis stage, due to the low technological readiness of the technology. However, historical testing programs have been key to understanding the requirements of these potential missions. Namely, NERVA, in addition to KIWI and Phoebus, studied multiple operating regimes and failure modes which helped to mature the technology of solid fuel NTP [21]. More recently, solid fuel NTP has gained interest for both crewed and unmanned missions. On the potential of NTP to support manned missions to Mars, historical tests such as NERVA are cited as demonstrating many key system elements which can be scaled up to meet requirements for manned missions [17]. Kumar has likewise published extensive work on the potential for NTP to support scientific missions to the outer planets. Specifically, Jupiter and Saturn are prime candidates for the technology although some missions to the ice giants have also been studied [13], [19]. Liquid fuel NTP, and specifically CNTP, shares many of the strengths of solid fuel NTP. Due to comparable thrust and higher specific impulse as explored in the following section, CNTP has potential to meet missions of a similar kind to solid fuel NTP, in addition to other missions in the far outer solar system.

This section detailed three distinct propulsion technologies, and their use cases related to robotic missions to the outer solar system. First, ten missions to the outer solar

system supported by chemical propulsion were discussed. It was shown that all missions either required one or more gravity assists to complete the mission, or resulted in flyby encounters rather than rendezvous, or both. Next, electric propulsion were shown to have supported missions to the inner solar system and asteroid belt, but not for any missions to the outer solar system. Lastly, the promise of nuclear thermal propulsion was discussed and CNTP specifically was introduced as an advanced technology currently under development. The following section provides more detail on the expected performance for CNTP systems.

2.2 Review of CNTP Performance Analysis

In addition to reviewing the current state of propulsion technologies for missions to the outer solar system, a more in-depth review of CNTP performance is also useful for understanding the realm of feasibility with regards to potential engine performance. Several types of studies are addressed here which identify strengths of CNTP as well as difficulties with future testing and development. Compared to the maximum solid fuel NTP performance of 900-1000 s, each analysis shows much higher expected performance which may contribute to improvements over solid fuel NTP with regards to payload capacity or transit time of missions to the outer solar system.

One of the earliest formal analyses done on CNTP was conducted at Princeton in 1963. The study covered nucleonics, fluid and thermal analysis of fuel/propellant interactions, and potential fuel loss as vapor during steady state operation of CNTP [22]. The chosen engine configuration chosen is a matrix of spinning centrifuges within the reactor moderator, like the CFEs mentioned in the previous chapter. Some of the results include key performance parameters for the engine, such as operating temperature and

pressure, thrust-to-weight ratios, and specific impulse. A summary of these parameters and their values is given in Table 2.2.

Table 2.2: Princeton Study CNTP Performance Values [22].

Parameter	Value
Isp	1200 s
T/W	0.05-0.5
Operating Temperature	3600-3800 K
Operating Pressure	3-100 atm

The study focuses on uranium carbide as fuel, and also selected zirconium carbide as a dilutant to reduce vapor loss of the fissionable material. CFE rotational speeds are concluded to be on the order of 5000 rpm, and further analysis is set aside to investigate heat transfer and bubble formation at high G loadings. Finally, assumptions in the areas of shutdown transients, material vapor pressures, and nucleonics are recognized as needing further research as well.

The next major analysis on CNTP was presented in 2020 at an American Nuclear Society (ANS) conference, and was coordinated by a diverse team representing Dynetics, Southern Research, NASA, Argonne and Idaho National Labs, and The University of Michigan [24]. The study presents a similar engine architecture, with 1 m long CFEs spun by gas turbines. In-depth performance values are given as 1800 s of specific impulse and 5500 K maximum operating temperature, assuming hydrogen propellant. Potential applications of storable propellants such as ammonia, methane, or hydrazine are also mentioned, citing a specific impulse of 900 s. While more in-depth values are not given,

much of the paper is dedicated to modeling and analysis challenges faced in order to reduce the risk of technology demonstration. Three key challenges mentioned within that section are the CFE cylinder wall mass and heat transfer, centrifuge failure accommodation and startup/shutdown transients. Another paper was presented roughly at the same time by a similar coalition of universities working with Argonne National Lab and NASA. The paper focuses on neutronics of the reactor and displayed many charts on sensitivity and relationships of the reactivity coefficient with reactor geometry [25]. However, some macroscopic engine performance is also noted, with operating temperature and specific impulse cited as 4500 K and 1500 s, respectively. Later in 2021 at the IAC, a paper presented by NASA, The University of Alabama at Huntsville, and Pennsylvania State University combined both of these focuses by investigating key challenges to technology development as well as pursuing improvements to reactor and engine analysis [26]. A major contribution put forth by that analysis is discussion of experimental testing intended to better understand bubble formation and movement dynamics within the centrifuge element. Beginning with static apparatus testing using Galinstan and nitrogen, the experimental results tie directly to challenges mentioned by both the Princeton study and the 2020 ANS paper. Additionally, universities are listed by name in association with each of the major development challenges in order to organize and prioritize further research.

As a result of the key studies and analyses previously presented, research has continued to progress in important development areas for CNTP. Particularly in the areas of bubble formation modeling and systems modeling, significant progress has been made in tackling some of the major challenges listed in previous papers. Two major efforts are

being pursued concurrently in the realm of bubble formation. First, a three-dimensional bubble dynamics model is being developed to understand how propellant bubbles within the liquid fuel behave in a centrifuge [35]. The goal of this model is to fully simulate the static and dynamic fluid mechanics inside a rotating CFE and simulate the movement of each bubble via the combination of buoyancy, drag, and other pressure effects inside the liquid. Simultaneously, an experimental apparatus is being developed to understand bubble movement and formation as validation for previous and current simulated data [36]. In addition to each of these efforts, comprehensive systems models have been designed to predict engine performance for CNTP in the context of tying together operation of the reactor with turbomachinery and engine nozzle. Three models have each resulted in different CNTP performance results, based on the assumptions and methodology used for each model. One of the major assumptions used in all of these models is a hexagonal configuration of 19 CFEs within the reactor moderator, as shown in Figure 2.1 [25].

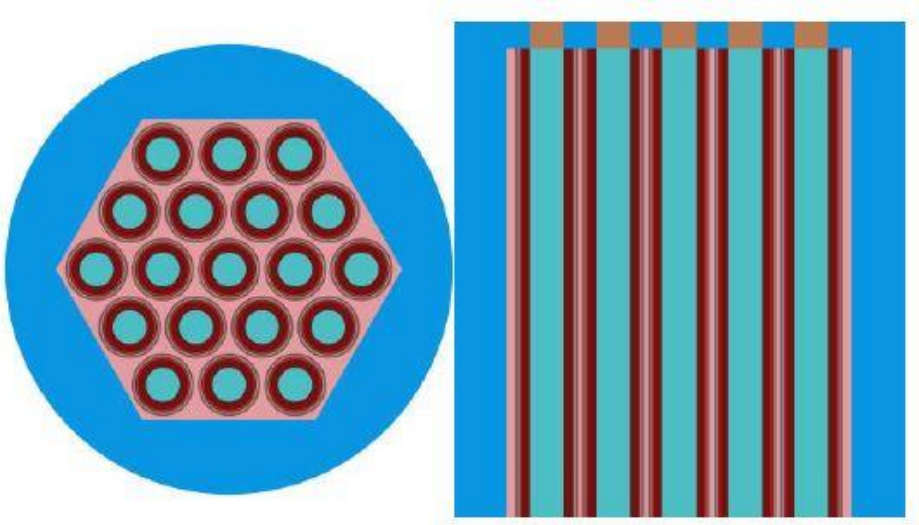

Figure 2.1: Axial (left) and Lateral (right) Cross Sections of 19 CFE Core [25].

The models are highlighted here, designated the baseline, upgraded, and optimized models respectively. In the baseline model, a power balance tracking enthalpy, pressure, and temperature of the propellant supported calculation of engine performance through high-level subsystem models [37]. The upgraded model employed much of the same methodology while refining the nozzle performance calculations with a focus on propellant dissociation and gas kinetics [38]. In the upgraded model, the engine geometric configuration was also changed from the baseline case. Lastly, the optimized model included a genetic algorithm within a Multidisciplinary Design Optimization (MDO) framework to optimize specific impulse [39]. Results for specific impulse and thrust from each analysis are given by Table 2.3 [37], [38], [39].

Table 2.3: Systems Modeling Improvements.

	Baseline Model [37]	Upgraded Model [38]	Optimized Model [39]
Specific Impulse (s)	1150	1600	1605
Thrust (kN)	26	20	49.8

The results of both the baseline and upgraded analysis are used in mission design in this work, due to some of this work being completed alongside the systems models. Additionally, the values presented in this table do not quite reach the expected 1800 s of specific impulse mentioned in previous papers, however this is mostly due to trade-offs of thermal and material constraints within the reactor. One specific source of uncertainty

is the lack of uranium data above 2500 K, which can then result in large variances for material properties at the 5000-5500 K temperatures predicted in the reactor core [39].

Performance studies for CNTP have dated back to the 1960's, and in this section some of the earliest research on CNTP was presented. The early research was then contrasted with more recent studies, which predicted higher performance while still recognizing some of the major challenges faced by development of CNTP. Lastly, specific system and subsystem models were discussed which provided more detailed understanding of internal physics of the engine as well as expected performance parameters which can be used in mission design. However, with the system models there is still a range of performance which is expected from CNTP based on assumptions and simplifications currently being made.

2.3 Research Questions

Modeling of internal dynamics and fluid interactions is necessary for a detailed picture of CNTP operation in addition to neutronics and reactor physics among many other topics of analysis, and yet an operational use-case for CNTP has not yet been fully defined in relation to desired performance parameters for the system. This thesis is intended to provide analysis of several aspects of mission design which can be used to influence the development of CNTP for use-cases that reasonably accommodate both its benefits and difficulties. Two questions can be used to direct the focus of subsequent work:

1) What mission destinations and trajectories are enabled by CNTP given its inherent benefits and constraints?

2) What performance parameters for the CNTP engine are sufficient for the mission architectures of interest, within the bounds of the system's physical capability?

Both research questions are addressed throughout this thesis through the following chapters. Due to the close connectivity between the two questions, the methodology, analysis, and results which pertain to each question are given concurrently, rather than the collection of work relating to one question being discussed followed by the work for the second question.

Chapter 3. Methodology

In Chapter 3, methodologies for the models and studies used in this research are discussed in detail. First, section 3.1 explains the use of patched conics in the models and how these models are structured and utilized. Section 3.2 then discusses the methodology used in two trade studies on CNTP engine performance. Finally, numerical analysis is covered in section 3.3 which includes its contribution to validation.

3.1 Patched Conics

The patched conic method is a basis for the analysis done in this work, as the method offers a simple semi-analytic approach to mission design which would otherwise require complicated numerical solutions. Patched conics is a two-body approximation of orbital mechanics, and in instances where more than one planetary body is present, the two body orbits are "patched" together at the sphere of influence change between the two bodies [40]. While an analytic model is not accurate enough for final mission design, it is often used as a first pass estimate of trajectories. In this way major changes can be made quickly, and some of the underlying dynamics of the trajectory can be understood before moving to numerical simulations of higher precision. A considerable amount of research into interplanetary mission design is done via patched conics, including some analysis for scientific missions to the outer solar system as is a focus of this work [41], [42]. In the case of planetary missions, accurate ephemeris data for planets are still necessary for patched conics despite lower model accuracy overall compared to numerical simulation, as much of the calculations are done based on the position of the planets of interest at specific times.

In mission design for a Mars mission, for example, hyperbolic orbits are used in the Earth and Mars spheres of influence for escape and arrival encounters, and these hyperbolas are patched to an elliptical orbit in the Sun sphere of influence for the majority of the trip. The mechanism by which the orbits are patched together is the patched conic equation which relates the spacecraft velocity with respect to the sun and the spacecraft velocity with respect to the planetary body by accounting for the body's velocity with respect to the sun:

$$V_{\infty}^{-} + V_{\phi} = V_{AR} \tag{3.1}$$

$$V_{\infty}^{+} + V_{\phi} = V_{DP}. \tag{3.2}$$

Eq. 3.1 displays the velocity relation for a spacecraft approaching a planetary body, while Eq. 3.2 is the departing relation. Gauss's solution to Lambert's problem is utilized to solve for the arrival and departure velocities, by using the planet positions and selected time of flight for the mission [43]. The planet velocity is calculated from its position ephemeris, by applying Kepler's equation,

$$M = E - esinE, \tag{3.3}$$

and the energy equation,

$$\frac{V^2}{2} = \frac{\mu}{r} - \frac{\mu}{2a}, \tag{3.4}$$

to the definition of angular momentum

$$h = \sqrt{(\mu a(1 - e^2))}, \tag{3.5}$$

which allow the planetary velocity to be converted to an inertial, cartesian coordinate system for further calculations [40]. Definitions of periapsis,

$$r_p = \mathrm{a}(1 - \mathrm{e}), \tag{3.6}$$

and ΔV,

$$\Delta \mathrm{V} = |V_{new} - V_{old}|, \tag{3.7}$$

are also useful in calculating individual departure and arrival maneuvers [40]. To calculate the inclination change for direct trajectories, the position of the inclination change is found by the orbit equation for a true anomaly 90º before the destination

$$r = \frac{p}{1+ecosv} \tag{3.8}$$

and applying the energy equation once again the velocity at that position is then inserted into the equation

$$\Delta V = 2V_{\Delta V} sin\frac{i}{2}, \tag{3.9}$$

which calculates required ΔV for efficient inclination changes [40]. The time to inclination change can then be calculated via the definition of mean motion,

$$n = \sqrt{\frac{\mu}{a^3}}, \tag{3.10}$$

and Kepler's equation. Gravity assist trajectories require careful checks of the angle swept through by the spacecraft during the encounter, first by matching visvisa

$$visvisa = V_\infty \cdot V_\infty \tag{3.11}$$

for the inbound and outbound trajectories. The available turn-through angle then determines if the required energy for this match is available given the spacecraft velocity

$$cos\delta = \frac{V_\infty^+ \cdot V_\infty^-}{\|V_\infty^+\|\|V_\infty^-\|} \tag{3.12}$$

in a process described by Williams [42]. The turn-through angle is also used to calculate the effective ΔV,

$$\Delta \mathrm{V} = \|V_\infty^+\|\sqrt{(2(1 - cos\delta))}, \tag{3.13}$$

and departure velocity,

$$V_{DP} = \sqrt{(\Delta \mathrm{V}^2 + V_{AR}^2 - 2V_{AR}\Delta \mathrm{V cosD})}, \tag{3.14}$$

for the gravity assist [44]. Appendices B and C give further details for the implementations of these expressions to support the larger models.

As a result of the analytic approach for patched conics, calculations are much faster than numerical propagation of orbits which account for all three bodies. One major assumption which makes this possible is impulsive maneuvers, where maneuvers are treated as having infinite thrust and zero burn time, so that orbit changes are made instantaneously. The criteria of this assumption being reasonable is dependent on the length of the corresponding finite length burn, in addition to the semi-major axis of the orbit [45]. The approach for patched conics is only semi-analytic however, as often numerical iteration is used to define the solar orbit. Lambert's problem describes the process of solving for the orbital elements of an orbit given only the initial and final position of the spacecraft, and the time of flight between the two positions. Solving Lambert's problem gives the solar orbit for interplanetary missions, and multiple solutions have been found for problem [40], [44]. The solution used in this work is Battin's method, which is an improvement over one of the original solutions given by Gauss [43]. In addition to Lambert's problem, boundary conditions for the escape and arrival hyperbolic orbits are needed as constraints when using the patched conic method. These boundary conditions generally come from requirements of the mission and spacecraft, such as periapsis altitudes and delta V capability of the spacecraft. Missions supported by nuclear propulsion require safe orbits which are considered reasonable for the use of nuclear reactors in space where low risk is presented to Earth and infrastructure in low Earth orbit. For NTP systems the minimum altitude for Earth escape is 500 km while the minimum end-of-life altitude is 1000 km [46]. The safe orbit used for these analyses is discussed further in section 3.4.

Another major factor in patched conics is planetary ephemeris as a function of time, and the source for this data can affect the results depending on the accuracy and precision of the data. For this work, planetary ephemeris was acquired from approximate formulas from JPL, which are accurate within 600 arcseconds and 1500 km within the time frame of 1800-2050 AD [47]. Besides model inputs, the selection method for model outputs is also particularly important. For the use of patched conics, when iterating through a large number of initial times, there are several criteria which can be used to select the most optimal trajectory.

A figure of merit (FOM) is used when there are multiple parameters of importance to the optimization of the output, as is often the case when planning interplanetary spacecraft trajectories. In some cases, more complex methods such as genetic algorithms or Monte Carlo simulations are adapted to particular search parameters [48], [49]. However, there is also precedent for defining a FOM as the sum or product of key factors which influence the spacecraft trajectory [50], [51]. In these cases, additional parameters are introduced to nondimensionalize the FOM or contributing terms to enable direct comparisons and relationships. However, much of the literature is focused on low thrust trajectories or low-Earth orbit trajectories; as such a new figure of merit must be defined due to the high thrust of CNTP in addition to its application in this context to interplanetary missions. Additionally, these figures of merit are concerned specifically with the technical optimization of mission parameters, but when it comes to mission design technical factors are not the only drivers of decision for mission planners. Economic factors heavily effect decision making, and so it is useful to capture some of these by keeping in mind the cost of vehicle development as well as the operational cost

of the mission [52], [53]. By constructing the FOM from two parameters which relate to the cost of different aspects of the mission, minimizing the FOM then minimizes the cost of the mission indirectly.

For this research a figure of merit was formulated utilizing mission ΔV and transit time to the destination. Both of these parameters are key to constraining technical aspects of interplanetary missions, and only considering one or the other results in infeasibly long transfer times or ΔV magnitudes which are unable to be achieved with the prescribed launch vehicle or spacecraft constraints. The FOM shown in Eq. 3.15 also accounts for both mission development cost, a factor of vehicle size and therefore vehicle mass which is constrained by mission ΔV requirements, and operational cost (a function of total mission duration) in finding the optimal trajectory for a particular mission [52], [53]:

$$FOM = A\frac{\Delta V}{V_E} + B\frac{TOF}{P_E}. \tag{3.15}$$

The Earth orbital period and Earth orbital velocity terms are characteristic parameters used to nondimensionalize each term. Rather than finding the Earth departure date to minimize ΔV for a given transit time, instead both parameters are accounted for to achieve a trajectory that balances vehicle size and transit time. As a result, for the ΔV vs transit time curves shown in Chapter 5, their minimums do not translate directly to Hohmann transfers. The values of A and B are selected so that nondimensionalizing ΔV and TOF by the Earth orbital velocity and orbital period respectively does not add artificial weight to either term. More specifically, for considering units of km/s for ΔV, the magnitude of Earth orbital velocity is 29.783 km/s [44]. So, A = 29.783 in order to negate the change in magnitude of the ΔV term. Similarly, for considering units of years for TOF, the Earth orbital period is one year and so B = 1. A similar FOM is also utilized

for planetary gravity assist (PGA) trajectories, with the ΔV term modified to decrease the selected transit time. A weight term is included to account for the much larger ΔVs required for Kuiper belt missions compared to missions to the outer planets and can be seen in Eq. 3.16:

$$FOM = 0.5A\frac{\Delta V}{V_E} + B\frac{TOF}{P_E}. \quad (3.16)$$

The approach for selecting A and B values for PGA trajectories is the same as for direct trajectories, however, due to the long transfer times involved, a weighting term does need to be added in order to result in reasonable mission transfer times. This extra weight, applied as a value of 0.5 to the first term, results in 0.5*A = 0.5*29.783 = 14.892, and B = 1. Further details on the implementation of planetary gravity assist (PGA) trajectories in this analysis are given in sections 4.4 and 5.3. Further details are also given in Appendix A.

3.2 Trade Studies

The patched conic method relates parameters of interest for the two trade studies in this work, which involve trading various performance and mission parameters to determine some of the driving factors which influence mission capability for CNTP. In general, these trade studies look at specific impulse and engine thrust-to-weight ratios and how those values affect other parameters such as delta V capability, time of flight, and payload mass capability for destinations in the outer solar system. The first trade study provides an initial estimate of minimum performance required of CNTP for a variety of missions, while the second trade study provides more detailed limits for minimum and maximum engine performance which are able to make use of progress in

CNTP systems modeling that took place over the timespan of this research. These objectives are selected to answer the second research question which is described in section 2.3.

An outline of the trade study methodology is given here which is used in sections 5.1 and 5.4. The methodology is adapted in part from the response surface method (RSM) [54]. In each case, variables of interest are first identified and then relationships between each variable are defined, just as described in RSM. Each of these variables has a range of expected values which are used as a part of the study. However, in this case the objective is not a simple optimization of a single variable or value. As a result, criteria are defined which determine what values are selected for each variable to answer the corresponding question. This step is modified from the SMART methodology outlined by Edwards, who describes steps 1 and 4 of the process as defining trade objectives and collecting metrics [55]. This is similar to defining metrics, or criteria in this case, based on the trade objectives which are not necessarily minimizing or maximizing a single variable. Grumbach similarly used a hybrid trade methodology to define and validate integration principles for complex systems [56]. The individual steps are summarized here, and their application is then discussed in detail for each of the two trade studies:

1) Identify primary and secondary variables of interest

2) Identify relationships between variables of interest

3) Identify criteria by which results will be defined

4) Apply criteria to related variables

For each trade study, each step is conducted in relation to the specific factors in that study, and results of the applied criteria are displayed which in their own way contribute

to the research questions mentioned in section 2.3. The second trade study also includes a sensitivity analysis of one of the relationships, which is also consequential for results of the numerical simulation for direct and PGA trajectories.

The objective of the first study is finding minimum CNTP performance values in order to support missions of varying payload capacities and destinations in the outer solar system. Specifically, the study tracks minimum engine performance required to complete direct trajectory missions to the outer planets and two Kuiper belt objects. The primary variables considered in this study are specific impulse and engine mass. These two variables are chosen to represent engine performance since they are the most directly relevant to vehicle capability in a patched conic model. These two variables, along with thrust, would fully define other engine performance parameters such as thrust-to-weight ratio, exhaust velocity, and mass flow rate, however the patched conic model assumes impulsive maneuvers where thrust is taken to be infinite. As a consequence, only specific impulse and engine mass are considered, and the extension to engine thrust is left for the second trade study. Secondary variables are also included in the first trade study in the form of launch vehicle type and payload mass, with both being used to vary constraints on the CNTP injection stage. These variables are chosen as they fully define constraints on the CNTP injection stage for direct trajectory missions to each of the destinations in the outer solar system.

The relationships used to define the primary and secondary variables consist of the rocket equation and a mass balance of the CNTP vehicle which relates volume constraints from the launch vehicle to volume and mass of the vehicle components such as the spacecraft payload, propellant tank, and CNTP engine. The basis for both of these

relations can be found in Elements of Spacecraft Design [57]. Two criteria for the first trade study are defined, with the first being the average engine mass which closes the mission over the solution space, and the second minimizing the specific impulse at the average engine mass. These criteria are chosen to select a single operating point (one engine mass and one specific impulse) which are attributed to a combination of secondary variables that represent the required capability of CNTP for that mission. The applications of these criteria are shown along with the results in section 5.1. These results are improved upon by the second trade study.

The objective of the second trade study is to investigate how changes to CNTP engine performance change overall mission capability to the outer planets. Given a range of payload masses, this study selects a range of CNTP performance parameters which best deliver those payload masses to each of the gas giants and ice giants with criteria specifying the minimum and maximum performance values. The primary variables of interest for this study are specific impulse, thrust, and engine mass, with all three parameters being directly relevant to vehicle architecture design as well as constraining other engine performance parameters as mentioned within the methodology of the first trade study. Required vehicle ΔV and engine operating temperature are chosen as secondary variables, with operating temperature simplifying a portion of the analysis by relating specific impulse and thrust for a given engine mass. Vehicle ΔV is selected for each destination via the FOM discussed in section 3.1, rather than varying the ΔV or transit time for each destination which significantly complicates the analysis. Besides the relationships used in the first trade study, performance curves for the engine specific impulse and thrust as a function of reactor temperature are used to constrain the variables,

and an analytical approximation for gravity losses developed by Robbins is used to relate thrust to the other variables [38], [45].

Two criteria are used to select ranges for each engine performance variable by the corresponding payload mass delivered to the destination. The criterion for minimum performance is limited by physical payload capability within the range of values considered in the analysis. The variable ranges come from previous analysis of mission design or CNTP systems modeling and are detailed specifically in section 5.4. The criterion for maximum performance is also limited by payload capability, with the specific values used as cutoffs explained in section 5.4. The second trade study is split into two separate analyses, each answering the second research question in a different context. The first analysis treats the three performance parameters as unconstrained, treating the engine as a black box with an unknown number and geometry of CFEs. The second constrains the CNTP engine to a single configuration, with 19 CFEs of a particular size and geometry, which allows specific impulse and thrust to be directly related to each other for a constant engine mass. The purpose of both analyses is to compare the performance requirements for a specific configuration with the general performance requirements, as a template for one method of comparison for specific engine configurations in future research.

Once both configurations are discussed, a sensitivity analysis is performed on the FOM in order to show the effects of different weights on the ΔV and TOF terms. This analysis is based in part on the Brown-Gibson method, which nondimensionalizes a figure of merit for scoring criteria and then applies α and $1-\alpha$ weight terms, with α ranging from 0-1, to show how weighting the selection criteria changes results for the

selected alternative [58]. The sensitivity analysis in this work utilizes the varied α weight to vary dependence on the FOM on ΔV and TOF, however the outputs are not used to select alternatives based on scoring but rather to display how robust results of analyses such as the numerical simulations and trade study are to changing weights of the FOM.

3.3 Trajectory Simulations

Another use case of patched conic results is as initial conditions for numerical propagation of orbital trajectories. For numerical simulations, initial values must be inputted for delta-Vs, time of flights, and other parameters which are then converged with numerical propagators. In addition to the patched conic models providing initial values for numerical simulations, the numerical simulations in turn provide validation for the patched conic models. The simulations converge on results which can be compared to the patched conic models, and percent error can be calculated from the differences in mission ΔV and transfer time. Some differences in results are due to simplifications made in the patched conic models, such as ignoring three body effects or gravity losses, and this does lead to an increase in error between models.

In order to validate the patched conic models, results of the numerical simulations are compared to patched conic results to show the initial guesses were close to the final trajectories. Due to the differences noted above, a variance can be expected between the two sets of results. The magnitude of this variance depends on the mission, but for a direct trajectory to Mars the variance between patched conics and commercial software has been shown between 0.2% and 8.14% [59]. Results in this work are expected to potentially show higher variance than this, due to higher ΔV maneuvers incurring more gravity losses and being further from the impulsive assumption than smaller maneuvers.

To measure variance between the patched conic models and numerical simulation, the vehicle size and shape is matched with less than 1% variance in leftover propellant margin. The transit time of heliocentric trajectories are modified to meet this constraint, and the variance in transit times is measured to establish how well patched conics predicted the trajectory. If the variance in transfer time between the patched conic model and numerical simulation is close to or less than the variance measured by Park and Wright for a variety of different cases, then the patched conic model will be considered valid for use in further analysis.

In this thesis the numerical simulations are conducted using AGI's System Tool Kit (STK) software, which relies on several built-in functions for propagation. Astrogator is the basis for the simulations and is useful for a variety of orbital mechanics analysis [60]. Within Astrogator differential correctors are used to modify each subsequent iteration of values until constraints are matched, and capability also exists to optimize the results from these correctors [61]. For the sake of simplicity, the numerical simulations in this work are non-optimized since much higher priority is given to finding possible or reasonable trajectory solutions rather than the optimal solution.

Chapter 4. Vehicle and Mission Architectures

In Chapter 4, further detail is given on the architectures and constraints used to generate results. Section 4.1 discusses the system analysis which is built upon by the mission design, and how improvements to the system model lead to differences in results. Sections 4.2 and 4.3 focus on the CNTP injection stage design in terms of constraints given by the launch vehicle as well as considerations for the injection stage payload which is delivered to the destination. Choices for the mission architecture also substantially affect results, and these choices are the subject of section 4.4. Lastly, section 4.5 lists some of the constraints on the mission architecture.

4.1 CNTP System Analysis

The analyses in this research performed on the mission and vehicle architectures for CNTP depend primarily on models predicting the performance of CNTP in various conditions. Early mission design analysis which uses a specific impulse of 1150 seconds is based on a systems model of CNTP which includes analysis of turbomachinery, CFEs, and nozzle thermodynamics with the enthalpy of propellant tracked throughout the system [37]. This initial analysis identifies how significantly an increase in specific impulse affects transit time and vehicle size for a similar vehicle architecture. Performance parameters used in this instance are different than those used in numerical simulations, due to this work being carried out in parallel with development of updated CNTP systems models. As a result, more up-to-date numbers were not available at this time. While this portion of the analysis utilizes a different version of the systems model, the specific performance parameters used are not as important as what the difference in

performance between solid fuel NTP and CNTP says about the potential applications of CNTP. Since the systems model gives very conservative estimates of performance in this case, results showing increased capability of CNTP compared to solid fuel NTP would be exaggerated further by using a more updated model.

Later results utilize an upgraded version of this systems model, which includes higher fidelity modeling and especially focuses on the effects of dissociation of the propellant at high temperatures [38]. This upgraded model is used for high-performance simulations by selecting a single operating point for engine performance. Table 4.1 summarizes the different CNTP systems models used in each of the results topics, and the performance parameters of each model.

Table 4.1: Application of Different Systems Model Versions.

Application	Model Version	Performance
Initial Trade Study	N/A	Varies
Comparative Analysis	Baseline Model [37]	Isp: 1150 s Thrust: 26 kN
Outer Planet Simulations	Upgraded Model [38]	Isp: 1600 s Thrust: 20/30 kN
Kuiper Belt Simulations	N/A	Isp: 1600-1700 s Thrust: 60 kN
Final Trade Study	Upgraded Model [38]	Varies

High-performance simulations to the Kuiper belt do not use the same performance parameters described in the upgraded model as the outer planet simulations, due to

necessary changes to specific impulse and thrust in order to close the missions. However, the new specific impulse and thrust are still within the ranges of potential performance as described in the model. In this case, increases to reactor operating temperature and changes to moderator material are sufficient to realize the higher performance [38]. The final trade study is also based on the upgraded model for a portion of the analysis, although rather than using a single performance point the temperature curves for specific impulse and thrust are included in their entirety. Since this trade study is intended to show the effects of changes in engine performance on injection stage capability, sections with constrained engine configurations (meaning the number and size of CFEs are the same as used in the upgraded systems model) as well as unconstrained engine configurations are used to illustrate these effects. The other portion of the final trade study analysis does not use a systems model to predict CNTP engine performance as a result. The topic of different system model versions is also addressed in Chapter 5, when results are given along with the system performance applied to the CNTP engine.

4.2 Vehicle Architecture

Spacecraft are complex systems, with many subsystems and components necessary for mission success. For mission design analysis with CNTP, a simplified model is used for the vehicle. In this case, the injection stage consists of just the engine and propellant tank, with the spacecraft bus and payload attached to the opposite end of the tank. Throughout this work, the term ‘injection stage’ refers to the combination of CNTP engine and propellant tank, while the term ‘vehicle’ refers to the combination of injection stage and spacecraft payload. Figure 4.1 displays a graphic of this vehicle which is borrowed from similar analysis of solid fuel NTP missions [13].

Figure 4.1: Approximate CNTP Vehicle Architecture.

The required engine mass and geometry is pulled from the CNTP system analysis, as is engine performance, and sizing the propellant tank requires iteration to derive the needed mass and volume. To this end several sources are utilized to better understand how spacecraft and propulsion system mass relate to each other [62], [63], [64]. The propellant tank is iteratively solved due to increases in tank mass requiring more propellant to accelerate the extra mass, and in turn more propellant requires a larger tank. Insulation is also accounted for, due to liquid hydrogen being the propellant of choice which must be kept in a liquid state for long periods of time. Passive and active solutions for this problem are feasible, with some research showing little to no active cooling necessary for long periods of time in deep space [65], [66], [67]. Propellants other than hydrogen also have potential in use with CNTP, such as methane or ammonia, especially for those that are not cryogenic which would greatly simplify the stage design. Heavier propellants will also decrease specific impulse, although this is not a major concern for missions where high specific impulse is not required. In this work, hydrogen is the propellant of choice as a result of its use in the systems models discussed in the previous section.

The spacecraft bus size is scaled to the mass for each mission, and in general is defined as an input to the models. Since many of these values dependent on each other to some extent, there is a large collection of parameters which are needed to fully define the CNTP injection stage and payload. The key parameters are listed in Table 4.2.

Table 4.2: Key Vehicle Sizing Parameters.

Parameter	Value Range	Units
Engine Parameters		
Specific Impulse [25], [37]	1150-1800	s
Thrust [38]	10-70	kN
Engine Mass [38]	1650-4000	kg
Length / Diameter [24], [68]	5 / 2	m
Tank Parameters		
Propellant Density [62]	71	kg/m^3
Ullage Volume Fraction [13]	1.03	
Insulation Area Density [62]	2.88	kg/m^2
Propellant/Tank Mass Ratio [62]	0.128	
Payload Parameters		
Dry Mass [5] [69] [70]	800-5000	kg
Length / Diameter [5] [69] [70]	1.5-4.5 / 3-5	m
Payload Mass Fraction [71]	0.4-0.5	
CNTP Vehicle Parameters		
Required ΔV	8-24.5	km/s

The considered value range of each parameter is listed for the variance across simulations and trade studies. Throughout the proceeding analysis, several of these parameters act either as constrained inputs or as free variables depending on the intent of a particular section of analysis. Specific impulse, for instance, is an output in the first trade study constrained by launch vehicle volume, although in other analyses it is used as an input. The value range is the result of analyses giving high and low estimates of CNTP performance, respectively from Gates and Schroll [25], [37]. Meanwhile the value range for thrust, while at first is based on further analysis from Schroll, is extended to incorporate other potential engine configurations in the second trade study [38].

Physical parameters for the engine such as mass and size are also acquired from a variety of sources. Conversely from the thrust, engine mass is at first constrained by launch vehicle fairing volume for a variety of missions in the first trade study, and the range is extended to include analysis from Schroll which predicts lower values [38]. The engine size is selected first in consideration of the 1 m long CFEs and roughly 1 m wide reactor, in addition to estimates of nozzle and turbomachinery sizes which are considered similar to that of the RL-10 engine [24], [68]. The values utilized for hydrogen propellant density, tank insulation area density, and tank mass ratio are all acquired from a source on estimating tank sizes for launch vehicles and spacecraft from the University of Maryland [62]. The ullage volume fraction is chosen so that 3% of the tank volume is dedicated to ullage gases, which allow the pressure of the tank to be precisely controlled. The increase in tank volume for ullage gases is consistent with the methodology used by Kumar for similar analysis of scientific missions to the outer planets using solid fuel NTP [13].

The results of the second trade study give a wide range of payload dry masses, which are largely constrained by the launch vehicle fairing volume. In many of the simulations, however, two specific masses are selected to simplify the analysis and results. In these cases, the values of 800 and 2200 kg are chosen as representatives of NASA New Frontiers and Flagship class missions such as OSIRIS-REx and Galileo, respectively [69], [70]. In the first trade study, 1600 kg is also used as a 'medium' sized payload to contrast with the other selected values as a comparison with another New Frontiers mission, Juno [5]. Similarly, payload length and width are chosen to approximate spacecraft sizes with certain masses based on the same historical data. The payload mass fraction is chosen to give the scientific spacecraft roughly 1 km/s of ΔV, similar to the station keeping capability of Cassini, which is ample propellant for station keeping over the duration of a 4-5 year science phase [71]. In general, however, required ΔV is derived from patched conic models for a given mission architecture. Each listed parameter is an input to determine the mass of propellant and propellant tank which make up the vehicle, and all feed into the vehicle constraints discussed in the following section.

4.3 Vehicle Constraints

Major constraints on the size and mass of the CNTP injection stage come from the fairing size and payload capacity of the launch vehicle used to lift the injection stage into its parking orbit. One major constraint put on the vehicle is that only one launch be required to lift it into orbit, precluding the need for orbital assembly which would dramatically increase the cost and complexity of the mission. Launch vehicle size and launch mass constraints for several launch vehicles considered in this analysis are summarized in Table 4.3.

Table 4.3: Launch Vehicle Constraints.

	Fairing Length (m)	Fairing Width (m)	Maximum Payload to 2000 km (mT)
Vulcan Heavy	21.5	5.2	~26
New Glenn	21.9	7	~45
Starship	18	9	~100

Each of these values were acquired from company websites or user manuals oriented to specifics of the launch vehicle for potential customers [72], [73], [74]. Considerations for these vehicles are given due to large fairing sizes combined with relatively low projected cost.

4.4 Mission Architecture

Two standard architectures are chosen for missions which are modeled for this research. Using the same architecture in both trade studies and numerical simulations allows for more easily comparing data, as well as more cohesive conclusions being drawn from consistent results. Missions to the outer planets are designed using direct trajectories, with no additional encounters between Earth and the destination body. This architecture is also utilized in the initial and expanded trade studies. For simulating missions to the Kuiper belt, a different architecture is also presented. Due to the long transit times and high ΔV necessary, trajectories using PGAs are investigated in order to lower the required ΔV and lower engine performance requirements. However, this comes at the cost of less frequent launch windows as discussed in section 5.3.

In both architectures, the CNTP vehicle begins in a circular parking orbit around Earth at 2000 km altitude. This orbit is chosen for two primary reasons – first, the altitude is high enough to be considered safe from the perspective of the nuclear reactor if the propulsion system fails [46]. However, the safe graveyard orbit listed in the referenced source is only 1100 km. The chosen altitude is much higher than the minimum required for safety purposes due to the performance capability of chosen launch vehicles. Since the CNTP injection stage is volume constrained rather than mass constrained on the launch vehicle, there is extra margin in the chosen launch vehicles' capabilities beyond lifting the injection stage to 1100 km. In order to take full advantage of the launch vehicle capability, the parking orbit is extended to 2000 km to reduce the ΔV required of the injection stage to reach its destination in the outer solar system. The full parameters of this orbit used in numerical simulations are given in Table 4.4.

Table 4.4: Earth Escape Orbital Parameters.

Orbital Parameter	Value
a	8314 km
e	0
i	28.5º
Ω	0º
ω	0º

The first major maneuver is conducted by the CNTP engine, pushing the vehicle out of Earth orbit and onto a heliocentric trajectory toward the destination. At this point, the concept of operations (CONOPS) of each architecture diverges and the vehicle

undergoes different steps depending on the mission. Figure 4.2 displays the CONOPS of direct trajectories, using Jupiter as an example, followed by a summary of the major events.

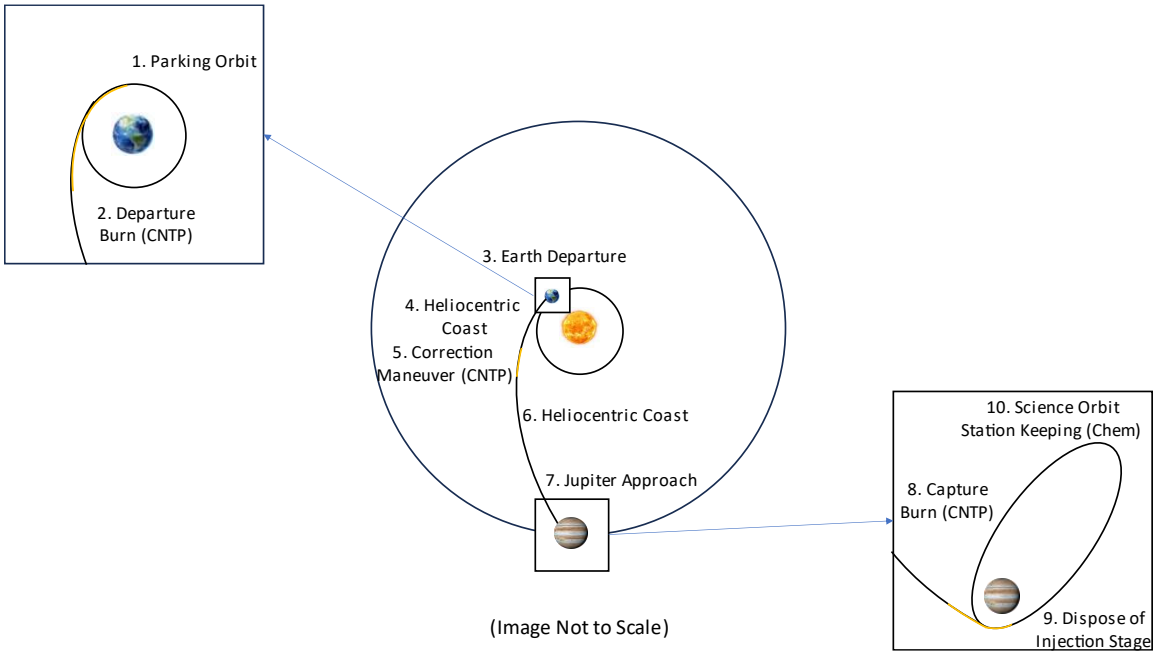

Figure 4.2: Direct Trajectory CONOPS.

For direct trajectories, after a period of coasting, a small correction maneuver is performed to align the vehicle with the correct inclination angle of the destination. In this research, the CNTP engine was used for the correction burn but in future cases a chemical thruster could be considered to decrease the number of restarts required for the nuclear engine. Using a chemical thruster for the correction burn may increase or decrease propellant usage depending on the start-up propellant cost for the CNTP engine, however it would make more sense operationally to use a chemical thruster for small maneuvers due to their much shorter transient start-up/shut down phases. Additionally,

the correction maneuver could be combined with the escape burn near Earth to conserve propellant. However, not only does this incur higher gravity losses being closer to a large gravity well but it also makes convergence more difficult in numerical simulations for larger inclination changes. For this reason, these maneuvers are kept separate for direct transfers. After the correction burn, the vehicle encounters a long coast phase to the sphere of influence of the destination body.

The CONOPS for PGA trajectories is shown by Figure 4.3 with Pluto as an example. For both Kuiper belt objects presented in Chapter 5, a flyby of Jupiter is conducted in order to gain additional ΔV required to reach the far away dwarf planets.

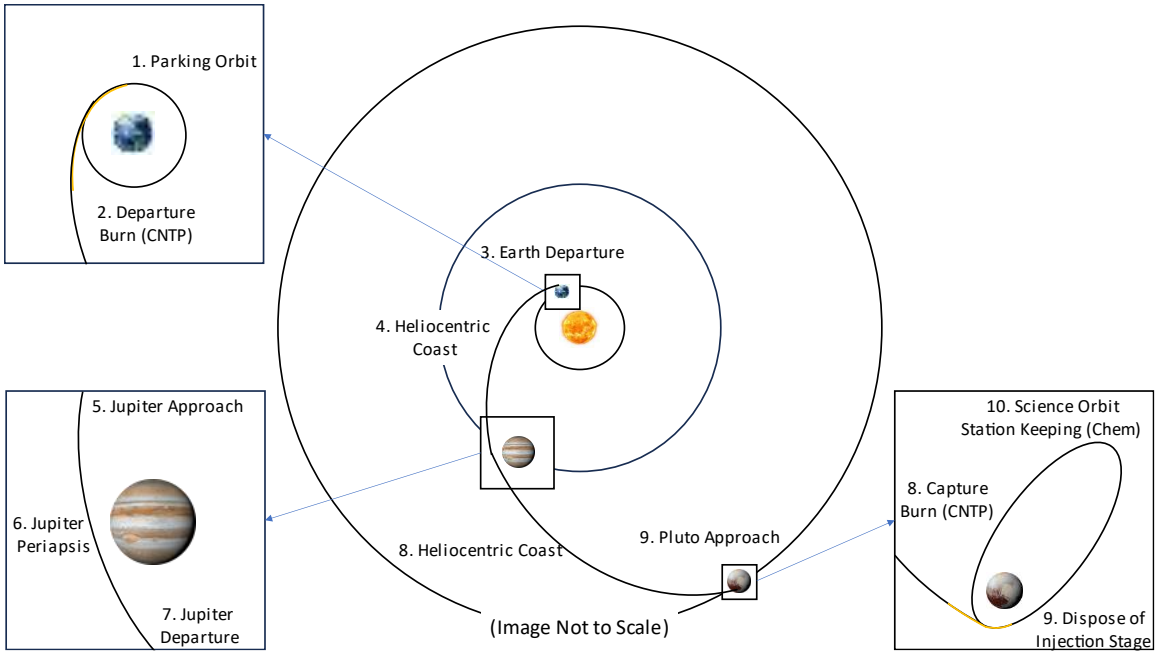

Figure 4.3: PGA Trajectory CONOPS.

In this case, the escape and correction maneuvers are combined since the small inclination of Jupiter, the body providing the gravity assist, does not dramatically

increase the difficulty of closing the mission. As a result, after the departure maneuver from Earth, the vehicle experiences a coast phase until it arrives at the sphere of influence of Jupiter. An effective ΔV is gained by the flyby, and after the encounter the vehicle coasts once again out to the Kuiper belt object. At this point, the capture maneuver is conducted similarly for direct and PGA trajectories.

The final maneuver is conducted by the CNTP engine, which slows down the vehicle into a capture orbit around the destination. While this maneuver could be done by the chemical engine on the scientific spacecraft, it is more mass efficient to accomplish this with the higher performance injection stage. Results backing up this selection are shown in section 4.2. This is a highly elliptical polar orbit, with an eccentricity of 0.95-0.96 targeted for this analysis, and a period between 30 and 60 days depending on the destination. After the capture is complete the propellant tank and CNTP engine separate from the scientific spacecraft and are discarded. Lastly, the science phase may commence using the spacecraft bus and payload, which is outfitted with its own propulsion system. Station keeping during the science phase is not within the prospective use case for CNTP, due to the need for small and precise maneuvers for which chemical propulsion is better suited.

4.5 Mission Constraints

Planet ephemeris, or positions as a function of time, are the greatest constraints on the mission architecture. For direct trajectories, the transfer angle between the body of departure at time of departure and body of approach at time of arrival strongly influences the amount of delta V required to complete the trajectory. In general, the lowest ΔVs are going to be closest to a Hohmann transfer, while trajectories faster or slower than that

will incur penalties to delta V [40]. The alignment of planets is especially important for gravity assist trajectories, where a small perturbation of the planet in either direction results in largely different trajectories for the spacecraft. Another constraint for gravity assists is the available turn-through angle versus the required turn-through angle. If the required energy of the spacecraft is greater than the amount of energy gained from the planet over the course of the encounter, the following solar trajectory is not able to send the spacecraft to its intended destination at the proper time [42].

Requirements of the science phase of the mission also have an impact on the mission trajectory. Historically, polar orbits are beneficial for science missions due to the large variety of latitudes which can be seen by spacecraft over the course of an orbit. To ensure a reasonable length of science phase, additional propellant mass is accounted for in both the numerical simulations and case studies for this research. The spacecraft is outfitted with enough propellant for 4-5 years of science operations once the CNTP injection stage has been discarded. The amount of propellant ranges from 400-900 kg, depending on the dry mass of the spacecraft, and corresponds to a mass fraction of roughly 1.4. For a payload dry mass of 2200 kg, for example, 900 kg of propellant is kept for station keeping.

4.6 Summary

As described in the previous five sections, mission and vehicle architectures are carefully selected for the analysis conducted in this work. In addition, constraints on these architectures are important to recognize for their application. First, systems models of CNTP are discussed and reasoning is given for using different models in different sections of the analysis. Next, a simplified vehicle architecture is shown containing a

CNTP engine, propellant tank, and scientific spacecraft/payload. Constraints on this architecture are also discussed, including constraints on the propellant tank size from the launch vehicle fairing volume and on vehicle mass from launch vehicle payload capability. Mission architectures are then illustrated via two CONOPS diagrams, and details on each maneuver and orbit are given as well. Several constraints on missions are listed, namely for geometry of gravity assists and science phase requirements. These architectures and constraints are applied in chapter 5, where two trade studies are presented on missions to the outer solar system along with patched conic and numerical models of detailed trajectory cases.

Chapter 5. Results

In Chapter 5, multiple analyses of different types are utilized to investigate how CNTP compares to solid fuel NTP, as well as determine the range of CNTP performance parameters best used for each mission architecture. In section 1, an initial trade study is done to estimate the minimum required performance for direct transfers to the four outer planets and two Kuiper belt objects. In section 2, a conservative estimate for CNTP performance is compared to solid fuel NTP to highlight differences in trajectory design and capabilities between the two technologies. These first two analyses provide setup and context for the later results, which are meant to directly answer the research questions set up in Chapter 2. Section 3 uses numerical simulation to validate the patched conic models, as well as provide a general capability baseline for CNTP with a specific set of performance values – this analysis addresses the first research question. Lastly, section 4 displays a more in-depth trade study that investigates a wide range of CNTP performance and its effects on payload capacity to the outer planets, which responds to the second research question.

5.1 Initial Trade Study

Initially, a major question with regards to determining the use case for CNTP is what performance values could be best used as metrics for CNTP. An early analysis uses specific impulse and engine mass as performance metrics to analyze the minimum requirements for a variety of missions. Focusing on direct trajectories to the four outer planets and two Kuiper belt objects, patched conics is first used to determine the required

ΔV to reach each destination as a function of time using direct transfers. Figure 5.1 displays these relationships.

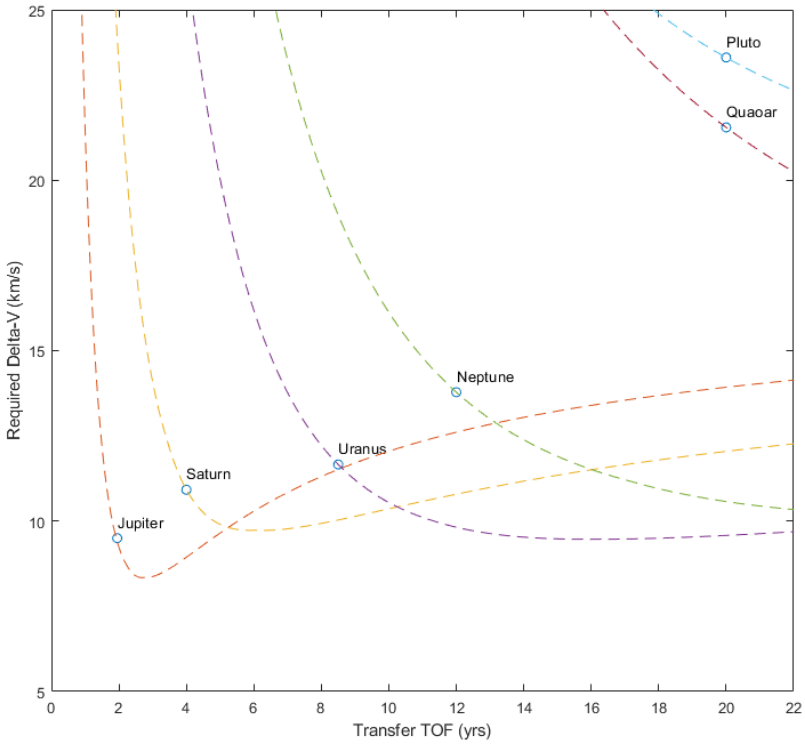

Figure 5.1: ΔV Requirements for Outer Solar System Missions.

At first glance it seems that the minimum of each curve corresponds to a Hohmann transfer to each planetary body, however this is not the case in this instance due to the chosen figure of merit. In addition, for this analysis individual points on the curves were selected rather than iterating through the full dataset. These points are marked in the figure as well. Another major takeaway from Figure 5.1 is the lower ΔV requirement for Quaoar compared to Pluto, given the same transfer time. Despite Quaoar being further from the sun than Pluto by about 4 astronomical units (AU), its inclination

is so much lower, 7 degrees versus 17 degrees, that the larger departure ΔV is offset by the much smaller inclination change maneuver [75].

The next major step in this preliminary trade study was to make assumptions about the mass of the CNTP injection stage as well as the payload. Both mass and volume are needed as constraints to fully integrate the spacecraft model with a reasonable launch vehicle to deliver the system to Earth orbit. For a given payload mass and volume, the rocket equation can be used to calculate the amount of propellant needed. In addition, estimations of tank mass and insulation can be used to fully define the CNTP injection stage within the launch vehicle [62]. The parameter space which allows the missions to close can then be generated, such as Figure 5.2 which shows the mission space for a mission to Jupiter with a Vulcan Heavy launch vehicle.

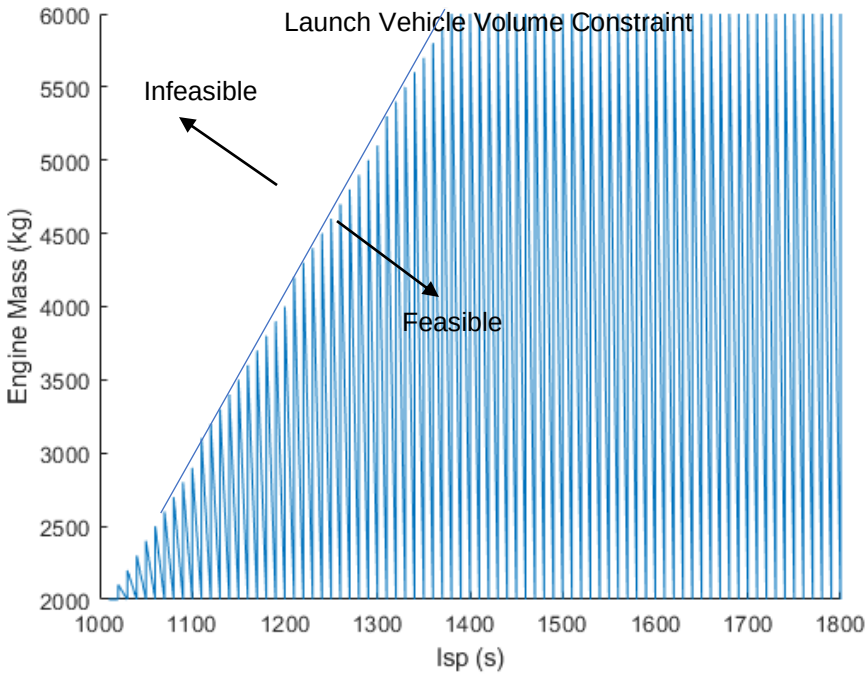

Figure 5.2: Feasible Engine Performance Based on Launch Vehicle for a Jupiter Rendezvous Mission.

The launch vehicle volume constraint is met when the CNTP injection stage and payload fill all available space in the launch vehicle payload fairing, and no more propellant can be fit without unconventional propellant tank shapes. Below the volume constraint line, the combination of engine specific impulse and mass result in a closed mission, while the line itself represents the maximum engine mass for a given specific impulse. To achieve these results, several assumptions had to be made including density of the payload and volume of the CNTP engine. A point can be chosen for average engine mass (in this figure, roughly 4000 kg), which then gives the minimum specific impulse required for that mission. These points can be collected for a wide variety of destinations, payload sizes, and launch vehicles, which results in the data shown in Figure 5.3 and Figure 5.4. The destinations and launch vehicles are labelled for each set of data, and the three bars of similar color for each destination correspond to payload dry masses of 2200 kg, 1600, and 800 kg, respectively.

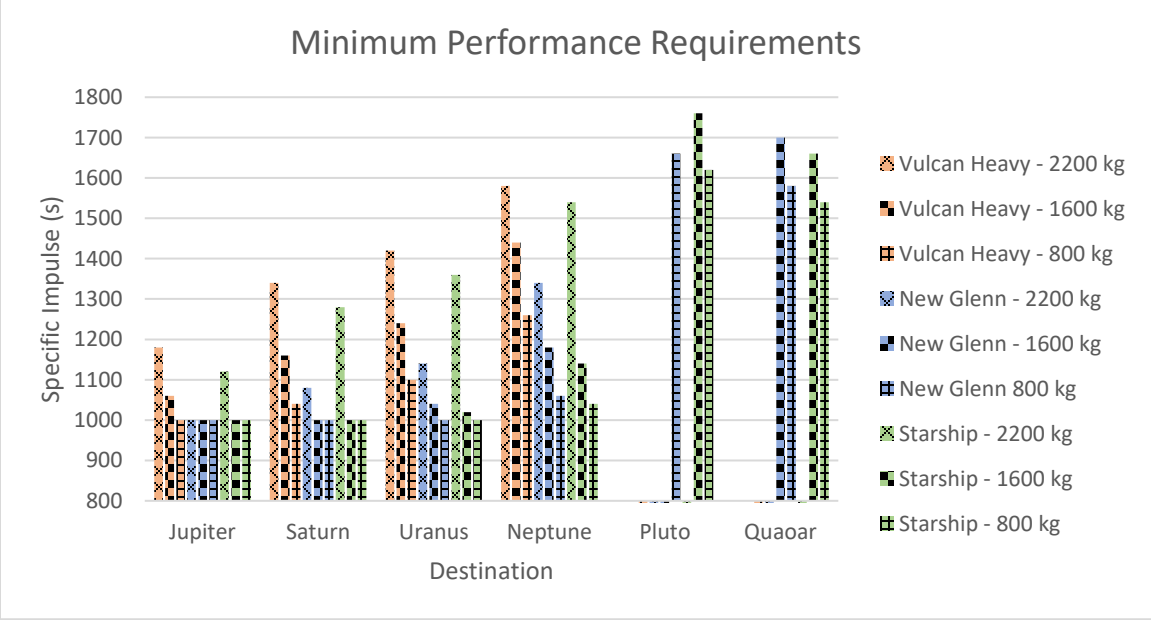

Figure 5.3: Minimum Specific Impulse Requirements for Initial Trade Study.

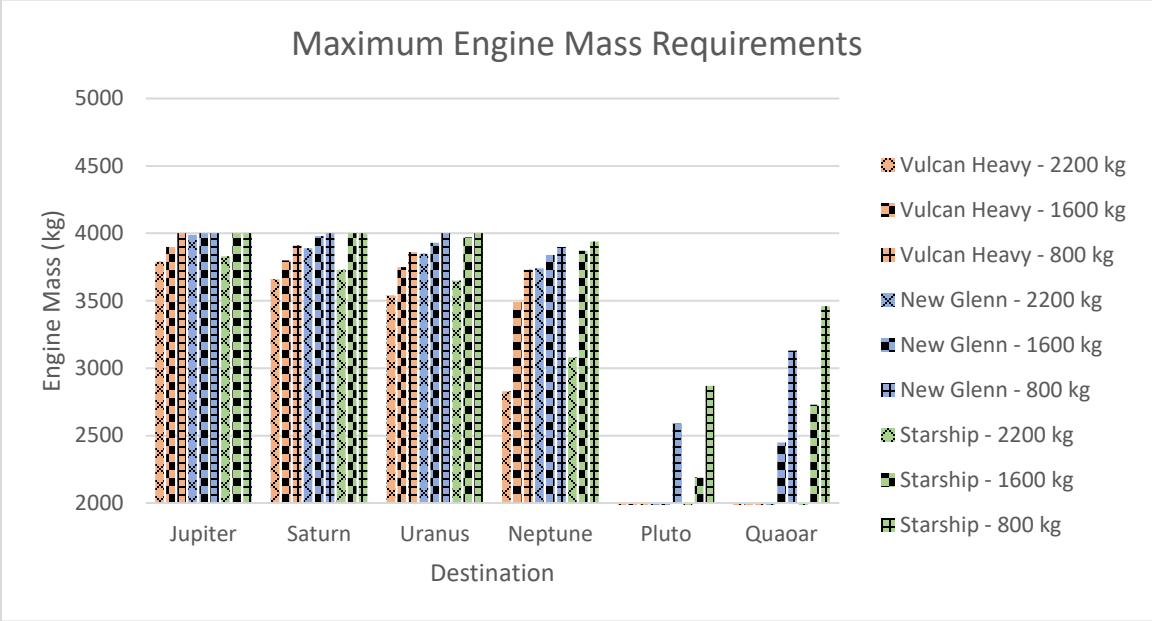

Figure 5.4: Maximum Engine Mass Requirements for Initial Trade Study.

The three bars of each color correspond to payload dry masses of 800, 1600, and 2200 kg, which is shown for destinations including the gas giants, ice giants, and two Kuiper belt objects. Some limitations on the bounds for these figures are 25 km/s of ΔV and 26-degree inclination, which are both roughly limits on vehicle capability assuming only one launch to orbit of the CNTP injection stage and payload combined. The launch vehicle also introduces constraints into the feasible mission trajectory. For the Vulcan Heavy, missions to the Kuiper belt do not close with a transit time of 20 years or less for any of the payload classes. As a result, the Vulcan Heavy has no data for those destinations in Figures 5.3 and 5.4. One additional note is that the relative constancy of the engine mass is an artifact of the method used to identify the minimum specific impulse requirement. Since the specific impulse is taken at the average possible engine

mass, then engine mass is less susceptible to change than the specific impulse requirement.

From these results, ranges of interest can be selected for each factor to facilitate further analysis. Specifically, for specific impulse the range of 1200-1600 s exceeds or meets the minimum criteria for most missions to the outer planets. Likewise, 1600-1800 s looks to be necessary for missions to the Kuiper Belt with the given launch vehicle constraints. In general, engine masses below 3000 kg are below the maximum requirements for engine mass in outer planet missions, while Kuiper Belt missions will require engine masses below 2500 kg for the majority of missions using the described launch vehicles. The engine mass ranges described here are viable as compared to engine mass estimates for solid fuel NTP, which can be as low as 30% less than the 4000 kg from Figure 5.4, or when compared to initial estimates of CNTP reactor mass of 1300 kg, which is expected to be more massive than the turbomachinery or nozzle subsystems [13], [24]. The reactor mass of 1300 kg is confirmed by an unpublished presentation from The Ohio State University, which gives a detailed breakdown of reactor component masses and totals 1336 kg [76]. The mass of the turbomachinery and nozzle are approximated via data for the RS-25, which is roughly similar in size and mass flow rate to the CNTP engine and add 300-400 kg to the engine mass [68]. An analysis by Schroll uses these approximations to give a T/W ratio for CNTP of 1.3, which fits within the bounds of Figure 5.4 for engine thrust less than 51 kN [38].

In summary, the patched conics method is used to identify relationships between transfer time and ΔV to various destinations, which are used to size the CNTP injection stage. Making assumptions for size of CNTP engine and payload, the vehicle is shown to

be volume constrained rather than mass constrained from launch vehicles, which provides boundaries on two performance parameters chosen for the engine. At this point, CNTP looks to be feasible for many scientific missions to the outer planets, and possibly for missions to some Kuiper belt objects. The minimum criteria can then be used with the patched conic model as initial guesses for numerical simulations performed in STK. The transit times to each destination are frozen in this study, and a wider variety of trajectories are pursued by the trade study described in section 5.4.

5.2 Preliminary Comparative Mission Analysis

One of the first numerical simulations conducted within this research compares the performance of solid fuel NTP to estimates of CNTP performance from preliminary systems analysis. The systems analysis carried out by Schroll utilizes an engine configuration employing 19 CFEs which results in performance as given in Table 5.1 [37]. Likewise, the performance values for NTP which are used for this comparison are also included [13].

Table 5.1: Early Approximation of CNTP vs NTP Performance.

Metric	CNTP Value	NTP Value
Number of CFEs	19	N/A
Mass Flow Rate	2.4 kg/s	7.56 kg/s
Thrust	26 kN	66.7 kN
Specific Impulse	1150 s	900 s

The major differences shown in Table 5.1 display some trades between CNTP and solid fuel NTP. While CNTP has significantly higher specific impulse, in this case the thrust is much lower. Additionally, the CNTP specific impulse is much lower than other estimates at 1600-1800 s – the purpose of using this data, which are more conservative than other models that predict much higher performance, is to highlight the differences in trajectory design for two NTP technologies. Since the analysis was performed parallel to the engine modeling, the more conservative data are what was available at the time within the current CNTP research. Despite the opportunity to rerun these results with later systems models, the results shown here are sufficient to convey the similarities and differences in CNTP and solid fuel NTP mission analysis. As a preliminary study, these results are important in that better capability for CNTP compared to solid fuel NTP as a result of the increased performance would mean an even wider gap in capability for CNTP vehicle architectures utilizing the higher predicted performances of later models. Using these performance values, an injection stage can be sized by constraints from the engine and chosen launch vehicle. The CNTP injection stage is fitted to constraints for Vulcan Heavy in this case, which also fits in New Glenn. Subsystem masses are given in Table 5.2 for both CNTP and solid fuel NTP once again.

Table 5.2: Mass Components of Spacecraft and CNTP/NTP Vehicle.

Component	**CNTP Mass (kg)**	**NTP Mass (kg)**
Engine	3,800	2,560
Propellant Tanks	2,000	2,200
Injection Stage Propellant	11,900	12,650
Spacecraft Onboard Propellant	900	2,050

Spacecraft Bus and Payload	2,300	2,300
Total Wet Mass	20,900	21,760

The systems model utilized for this analysis did not include a mass estimate for the engine, so to estimate the CNTP engine mass a conservative number was derived from the results in section 5.1. As shown in Figure 5.4, a mission to Jupiter for CNTP using a ULA Vulcan Heavy requires an engine mass no more than 3800 kg, and so this value was chosen as a 'worst case scenario' for this simulation. Despite this considerable difference in engine masses, the CNTP injection stage requires less propellant overall as a result of the higher specific impulse. Additionally, the CNTP and solid fuel NTP vehicles utilize slightly different CONOPS which account for the significantly lower amount of propellant onboard the scientific spacecraft. As mentioned in section 4.4, the CNTP engine is used for the capture burn at the destination, while the solid fuel NTP CONOPS consists of discarding the injection stage after a deep space correction. Using the CNTP engine for the capture burn is not an arbitrary decision, but an optimization for the performance qualities and vehicle architecture requirements for CNTP. As an example, Figure 5.5 displays a comparison of vehicle mass using a CNTP capture burn versus a chemical capture burn, with the injection stage being discarded after the correction maneuver. This comparison is made for a mission to Jupiter with a Vulcan Heavy launch vehicle.

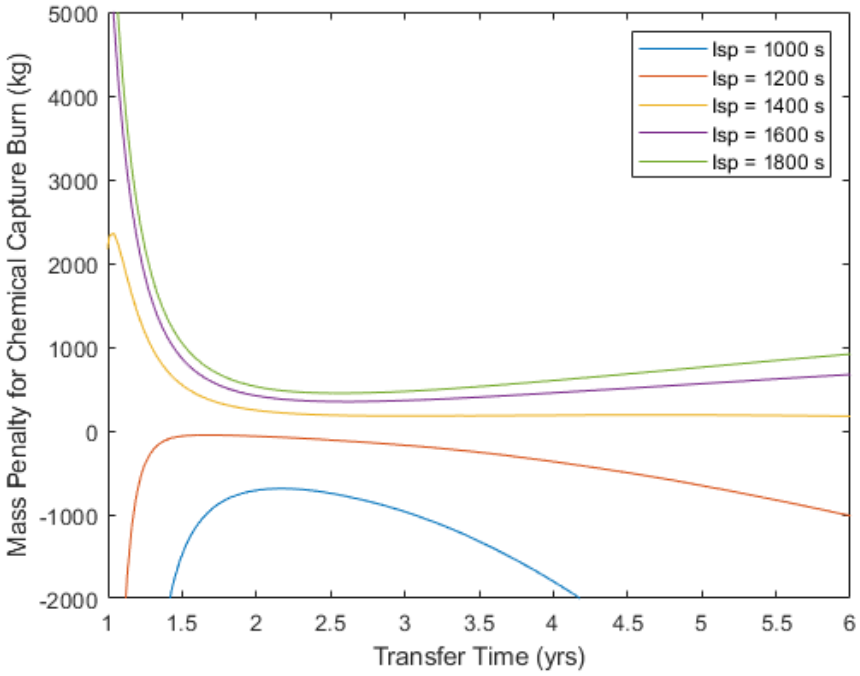

Figure 5.5: Mass Penalty of Chemical Capture Burn.

With higher specific impulse, the increased performance by using the CNTP engine increasingly overcomes the mass penalty of carrying the heavy propellant tank and engine rather than discarding them earlier in the flight. The extent to which this result is true for CNTP depends on the specific impulse, and in this case with a specific impulse of 1150 s, there is a marginal mass difference (less than 100 kg on a 12 mT vehicle) between using the CNTP engine or chemical engine in this case. However, it can also be noted that for CNTP specific impulse of more than 1300 s, the CNTP capture burn is favored, with comparable or greater differences in vehicle mass for other destinations and launch vehicles. The same comparison for solid fuel NTP results in chemical capture being the more mass efficient option against an NTP system with 900 s of specific impulse. However, with the inclusion of gravity losses in the analysis the difference in

mass between the systems is closer to 100-300 kg rather than the 1000 kg suggested by the above plot [77]. Another possible reason for the difference in projected mass penalties is methodology, since in this work the payload mass is held constant and initial vehicle mass modified to meet the different architecture. The analysis for solid fuel NTP instead holds initial vehicle mass constant and varies delivered payload mass.

For the NTP mission the spacecraft itself utilizes its chemical propulsion system for the capture burn in addition to the proceeding station keeping. In both cases, the chemical thruster on the spacecraft has 323 s of specific impulse and 1100 N of thrust. Despite these differences, the trajectory flown by the CNTP injection stage is similar to that of the solid fuel NTP vehicle and is shown in Figure 5.6.

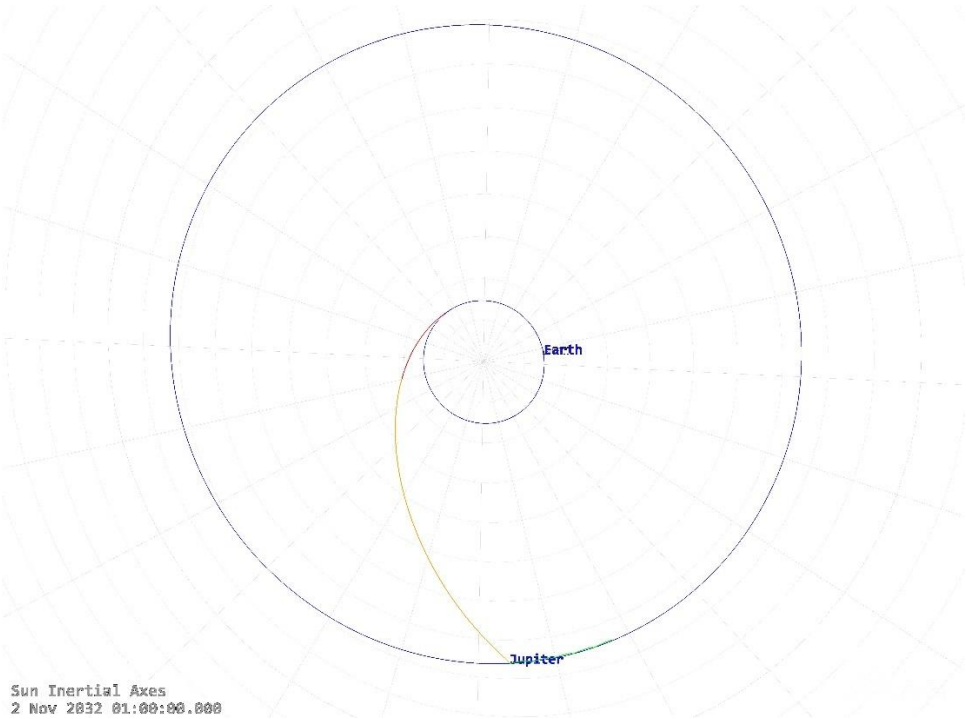

Figure 5.6: Solar View of Spacecraft Trajectory.

The first maneuver for the CNTP injection stage is the departure burn, or Trans-Jovian Injection (TJI). The details of this maneuver, which lasts 73.1 minutes and imparts 7.46 km/s of ΔV, are given in Table 5.3 with a graphic of the burn displayed by Figure 5.7. 10110 kg of propellant are used during the burn, and the thrust vector is aligned with the vehicle velocity vector for the full burn duration.

Table 5.3: TJI Burn Parameters.

Parameter	Initial Value	Final Value
Ephemeris	20 Feb 2031 10:27:37 UTCG	20 Feb 2031 11:40:42 UTCG
Right Ascension	54.96 deg	206.19 deg
Declination	24.03 deg	-13.66 deg
R Magnitude	8374.60 km	26180.84 km
Inclination	28.48 deg	28.49 deg

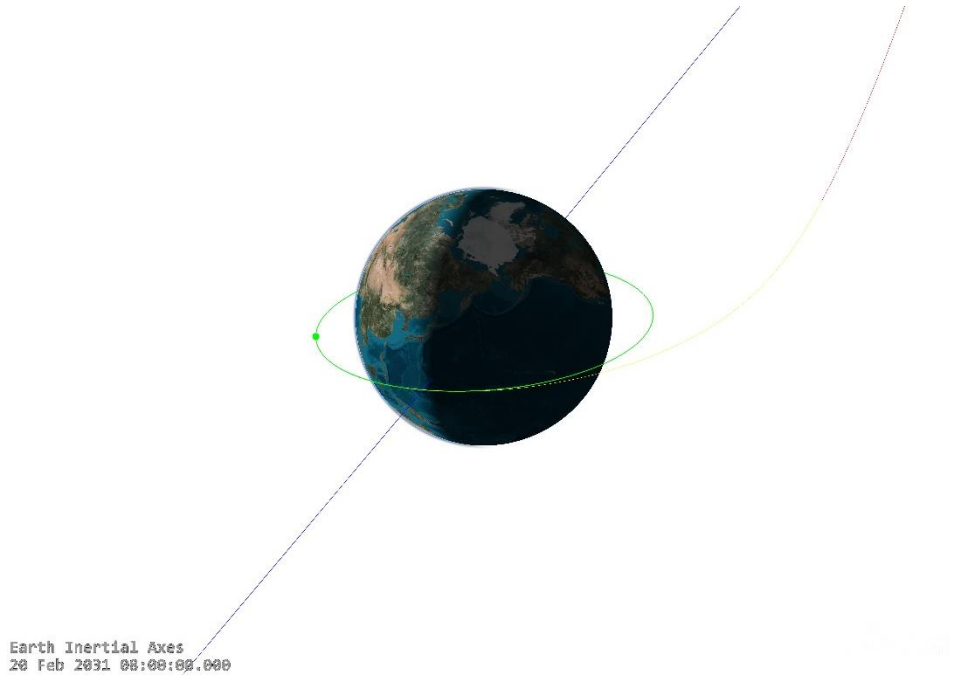

Figure 5.7: Earth View of Spacecraft Trajectory.

After TJI, the CNTP injection stage coasts for 73 days before performing a deep space correction. The small correction consists of a 2.7-minute burn using 374 kg of propellant. 398 m/s ΔV is directed with respect to Earth VNC axes at 17.6º elevation and 10.8º azimuth angles, and after the burn another coast occurs for 547 days before the final maneuver.

Jupiter Orbital Insertion, or JOI, is the capture burn which puts the vehicle in a highly eccentric polar orbit around Jupiter. The maneuver imparts 1.65 km/s of ΔV over 10.25 minutes, and costs 1417 kg of propellant to achieve. During the burn the thrust vector is aligned opposite of the velocity vector, and afterwards the CNTP engine and tank are discarded. The final orbit around Jupiter has a period of 48.8 days and an eccentricity of 0.95, which is utilized for the science phase of the mission. Further details and ephemeris for the maneuver are given in Table 5.4 and Figure 5.8.

Table 5.4: JOI Burn Parameters.

Parameter	Initial Value	Final Value
Ephemeris	2 Nov 2032 00:38:25 UTCG	2 Nov 2032 00:48:40 UTCG
Right Ascension	297.03 deg	297.03 deg
Declination	-21.67 deg	-21.67 deg
R Magnitude	106,933 km	107,012 km
Inclination	79.48 deg	78.21 deg

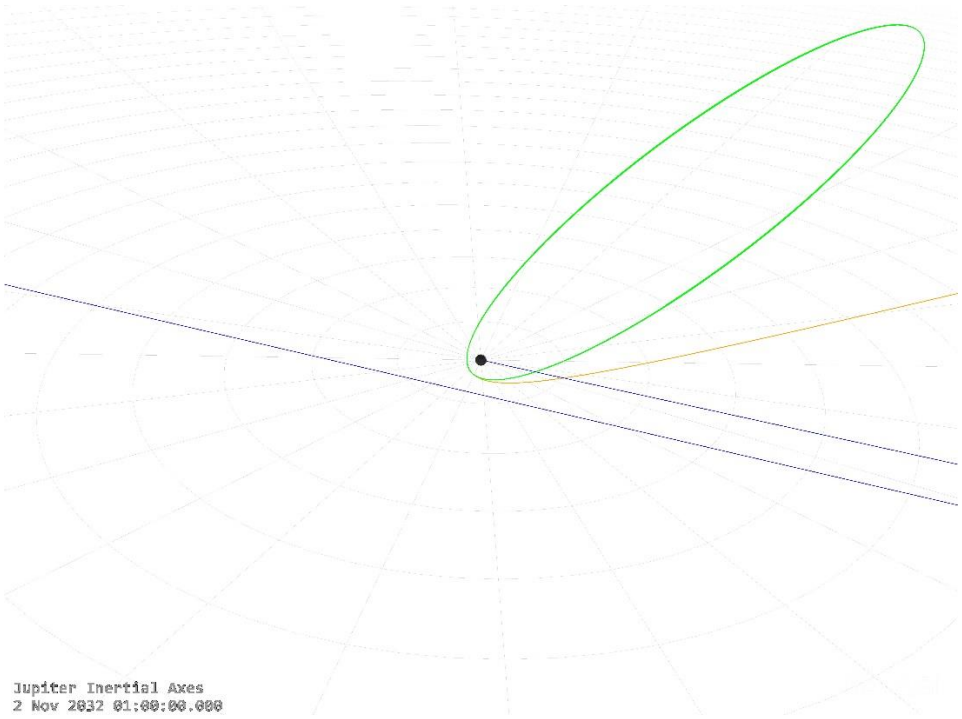

Figure 5.8: Jovian View of JOI Maneuver.

Other than significant differences in propellant and vehicle mass between CNTP and solid fuel NTP, the trajectory is shown to have several differences as well. The result of these differences is a transit time of 1.7 years for a direct trajectory capture mission to Jupiter for CNTP, while the solid fuel NTP trajectory in this comparison takes 2.1 years to reach its destination. With the same payload dry mass in each case, these results show that the increase in specific impulse of CNTP compared to solid fuel NTP, even with its trade-off of lower thrust, can result in significant reductions to transit time even with very conservative estimates for engine mass.

5.3 High Performance Simulations

With preliminary results giving rough estimates of the minimum performance requirements and a detailed comparison to mission design for solid fuel NTP achieved, it

is also helpful to investigate how trajectory and vehicle architecture change with CNTP performance closer to the theoretical maximum. As a result, updated results from the CNTP system model were used to run simulations to all four outer planets. Table 5.5 lists the performance parameters used for this portion of the analysis.

Table 5.5: Updated CNTP Performance Data [38].

Metric	Value
Number of CFEs	19
Engine Mass	1650 kg
Reactor Operating Temperature	4600 K
Reactor Operating Pressure	15 MPa
Thrust (Gas/Ice Giants)	20/30 kN
Specific Impulse	1600 s
Engine T/W Ratio (Gas/Ice Giants)	1.24/1.38

Using these parameters, and a payload dry mass of 2200 kg, the direct trajectory patched conic model is used to generate initial guesses for the required ΔV and propellant mass for each destination body. Two separate launch vehicles are selected to demonstrate the similarity of missions when neither vehicle mass nor volume are close to their constraints, and for this purpose both Vulcan Heavy and New Glenn are used in this model. With numbers gathered for vehicle size, numerical simulations are used to increase fidelity of the patched conic results as well as for validation of the patched conic

model. The results of the patched conic trajectories and shown by Table 5.6 and the numerical simulations are given in Table 5.7.

Table 5.6: Selected Patched Conic Outer Planet Trajectories.

	Jupiter	Saturn	Uranus	Neptune
Initial Mass (kg)	8940	11280	12260	15720
Prop Mass (kg)	3540	5550	6400	9380
ΔV 1 (km/s)	6.248	7.768	8.570	9.451
ΔV 2 (km/s)	0.575	0.997	0.319	1.120
ΔV 3 (km/s)	1.096	1.867	2.696	3.679
TOF (yrs)	2.15	3.38	7.65	10.72

Table 5.7: Simulated Outer Planet Trajectories.

	Jupiter	Saturn	Uranus	Neptune
Initial Mass (kg)	8940	11280	12260	15720
Prop Mass (kg)	3537	5545	6393	9377
ΔV 1 (km/s)	6.568	8.350	9.119	9.929
ΔV 2 (km/s)	0.335	0.617	0.219	0.931
ΔV 3 (km/s)	0.999	1.649	2.225	3.379
TOF (yrs)	2.21	3.56	8.33	11.18

The propellant mass shown in these tables is the predicted propellant required for all three maneuvers, with 900 kg of propellant intended to be left over for station keeping during the mission science phase. As mentioned in section 4.3, the vehicle generated by the patched conic model is matched in the numerical simulations, within 1% of propellant

margins. The variance to measure and compare between patched conic and numerical results is taken from the TOF, and the calculation of variance is given by Eq. 5.1 with results in Table 5.8:

$$\%variance = \frac{|Simulated\ TOF - Approximate\ TOF|}{Simulated\ TOF} * 100\%. \quad (5.1)$$

Table 5.8: Variance between Patched Conic and STK Transit Time for Outer Planets.

Jupiter	Saturn	Uranus	Neptune
2.71%	5.06%	8.16%	4.11%

Variance of the results comes most prominently from neglecting gravity loss and three body effects in the patched conic model, while of these are included in the numerical simulations. The data presented in these tables serve as validation for the patched conic model results which closely resemble results of the higher fidelity numerical simulation. Additionally, the time of flights are comparable to transit times of Voyager 2 out to each of the four planets for example, despite the Voyager 2 mission encountering each planet via flyby while also using each encounter as a gravity assist [4]. The direct trajectories shown here are much less complex, occur more frequently, and result in rendezvous rather than flybys. The validation results are important considering the launch vehicle constraint on the CNTP vehicle. With only one launch of a commercial launch vehicle, a CNTP injection stage can support a capture mission to planets in the outer solar system with much lower transit time than similar rendezvous missions previously flown to destinations such as Jupiter and Saturn. Additionally, with the predicted performance of CNTP at 1600 s of specific impulse and 20/30 kN of thrust,

it is likely that the maximum predicted performance of 1800 s may not be necessary. A lower target specific impulse has the potential to increase temperature and structural margins within the engine and reactor systems. Further elaboration of this conclusion is given with the results in section 5.4.

In addition to missions to the outer planets, missions to the Kuiper belt are also of interest to the scientific community, and some analysis is necessary to explore the feasibility of these missions supported by CNTP. Both direct and PGA transfers are considered for this section, as each have benefits and detriments when using CNTP. The Kuiper belt objects in question are Pluto and Quaoar, and to reiterate the mission architecture to these destinations, capture of the scientific spacecraft around the objects is the goal as opposed to a flyby encounter. The difficulties of these missions primarily come from the extreme distance from the sun as well as high eccentricity from the ecliptic plane, both of which require substantially larger ΔV than capture missions to the outer planets in general. The CNTP engine performance required to close these missions varies based on the type of transfer and destination, and Table 5.9 illustrates the differences between those requirements. An important note can be made here regarding the direct transfer to Pluto, as the trajectory chosen by the FOM for a CNTP rendezvous mission is not feasible with a single launch of a commercial launch vehicle.

Table 5.9: Kuiper Belt Mission Performance Requirements.

	Pluto Direct	Pluto PGA	Quaoar Direct	Quaoar PGA
Isp (s)	1800	1600	1700	1600
Thrust (kN)	-	60	60	60

Engine T/W	-	3.7	3.7	3.7

All of these missions are performed with a thrust of 60 kN and an engine T/W of 3.7. While these values are close to the minimum required for this combination of vehicle and mission architecture, a more in-depth optimization may yield lower values for some cases. Additionally, Starship is the primary launch vehicle used to constrain the CNTP injection stage for this portion of the analysis. While the Vulcan Heavy and New Glenn are included for missions to the outer planets, neither vehicle has the payload mass or volume capacity to support Kuiper Belt missions according to the constraints of this analysis. This result differs from the results of section 5.1, because different criteria are compared to results to determine viability. For the initial trade study, transit time for direct transfers to the Kuiper belt is held constant at 20 years, which can be supported by New Glenn and Starship by that analysis. The transit time was chosen in the previous analysis in a conservative manner so that the required ΔV was within the capability of an injection stage constrained by volume from the launch vehicle. Here, the transit time is selected via a figure of merit. Using the figure of merit significantly reduces the selected transit time, since the injection stage volume is used as a check afterwards rather than the initial basis for transit time selection, but also increases the necessary propellant to close the mission.

As with the outer planet missions, a patched conic model is used to generate initial guesses for the numerical simulation. Both direct and PGA transfers are iterated through over a variety of departure dates and transit times, and the FOM selects a single trajectory based on ΔV and transit time. The set of data which the FOM selects from display the available launch windows for mission in the cases of direct and PGA

trajectories. Figure 5.9 displays the patched conic results for Pluto for PGA architectures, and Figure 5.10 shows the results for Quaoar PGA and direct missions. The direct and PGA transfers are plotted with respect to ΔV and transfer time respectively, as a result of the different driving factors with each trajectory type. Dates of departure are selected to match ephemeris data acquired from JPL's Horizons database which are used in the numerical simulation [75]. As a consequence of no Horizons data for Quaoar past 2030 to use in STK results, Quaoar trajectories are run with dates in the past to meet time constraints for the rendezvous.

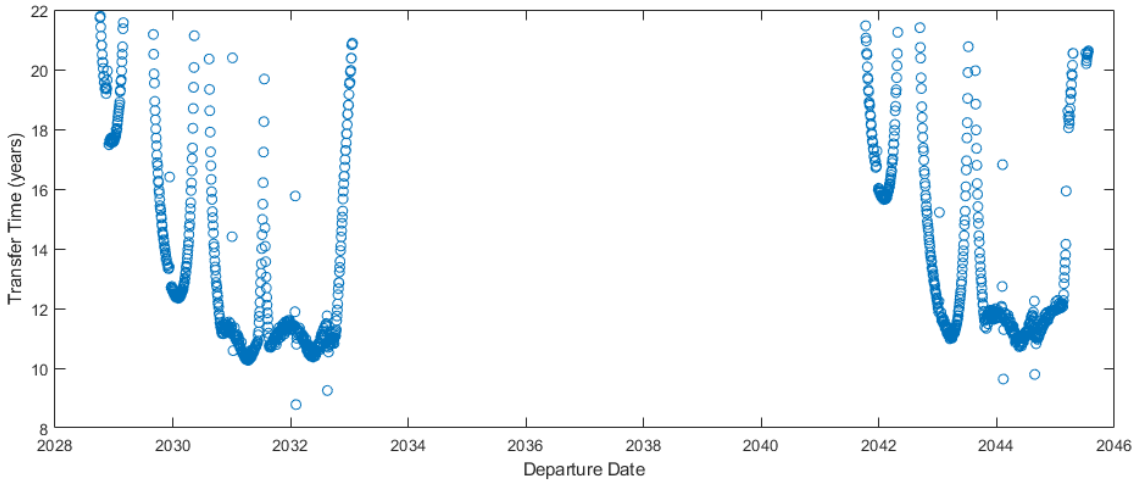

Figure 5.9: Pluto PGA Trajectory Launch Windows.

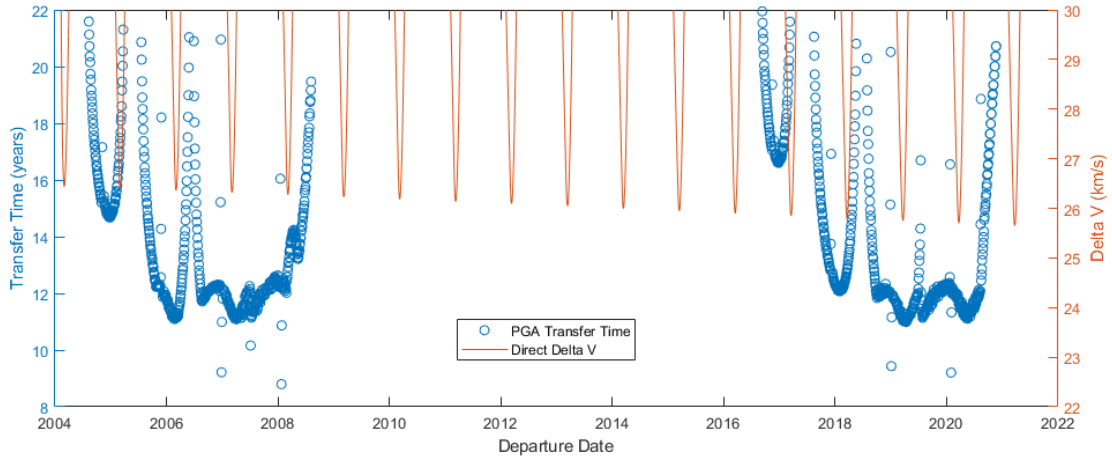

Figure 5.10: Quaoar PGA Trajectory Launch Windows.

Several results are apparent from these plots. First, abnormal slopes in the direct transfer plots appear just to the right of each minimum. Likewise, many transfers in the PGA plot do not fit nicely into the curves made up of most results. These two issues stem from a similar drawback with patched conic models – when two planetary objects have a transfer angle close to 180 degrees, Lambert's problem becomes difficult to solve. Due to division by a very small number, the outputs are unrealistic and cause the noted differences in each of these plots. The direct transfer model attempts to account for this by removing the unrealistic data and using a spline fit to predict what the realistic results should be, however since the results of the PGA model are not a smooth curve, the artifacts remain. Otherwise, the major takeaway from these plots is the relative frequency of launch windows. For direct transfers to the Kuiper belt, launch windows which are feasible for CNTP occur roughly every 12 months, while PGA transfers offer a few windows every twelve years. While the latter are much faster, the cost of these faster transfers is reduced length and frequency of launch windows.

In addition to the ΔV and transfer time results, vehicle masses as a function of transfer time can also be generated for both kinds of trajectories. Using the ΔV associated with each transfer time, Figure 5.11 is generated for Pluto and Quaoar. Engine performance parameters are as shown in Table 5.9 for each case, and the chosen payload dry mass is 800 kg with an expected 400 kg of propellant left for station keeping during the science phase of the mission.

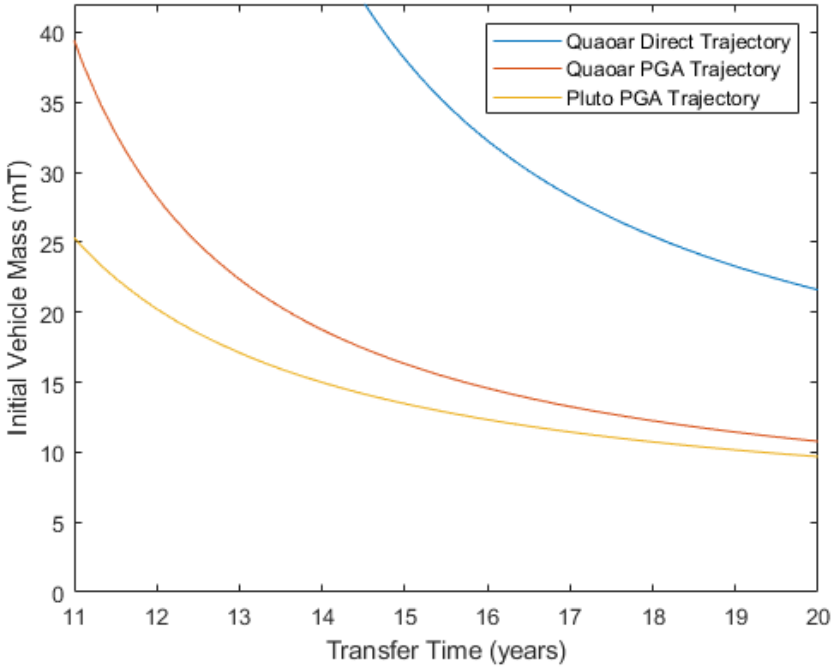

Figure 5.11: CNTP Vehicle Masses for Kuiper Belt Missions.

Figure 5.11 confirms that a CNTP vehicle supporting a capture mission to the Kuiper belt can reach its destination much faster with a PGA trajectory, assuming a similar vehicle size, with other factors remaining the same. However, as noted by Figure 5.10 this once again comes at the cost of launch window availability, while also having

lower requirements for CNTP specific impulse. With the data presented in Figure 5.9 and Figure 5.10 a FOM ranks and then selects a trajectory to be modelled using STK. The comparison of patched conics results vs numerical simulation results is given by Table 5.10 and Table 5.11.

Table 5.10: Selected Patched Conic Kuiper Belt Trajectories.

	Pluto		Quaoar	
	Direct	PGA	Direct	PGA
Initial Mass (kg)	58660	28760	33630	32970
Prop Mass (kg)	48440	22380	26630	26050
ΔV 1 (km/s)	12.515	9.250	10.876	8.576
ΔV 2 (km/s)	11.180	14.401	5.117	15.939
ΔV 3 (km/s)	9.818	n/a	10.184	n/a
TOF 1 (yrs)	13.63	1.04	15.72	1.17
TOF 2 (yrs)	n/a	9.52	n/a	10.32

Table 5.11: Simulated Kuiper Belt Trajectories.

	Pluto		Quaoar	
	Direct	PGA	Direct	PGA
Initial Mass (kg)	n/a	28760	33630	32970
Prop Mass (kg)	n/a	22383	26628	26047
ΔV 1 (km/s)	n/a	10.569	9.930	9.659
ΔV 2 (km/s)	n/a	13.066	5.579	14.830
ΔV 3 (km/s)	n/a	n/a	10.65	n/a

TOF 1 (yrs)	n/a	1.07	15.78	1.21
TOF 2 (yrs)	n/a	10.4	n/a	11.45

A couple of major differences between these tables are important to note. First of all, a direct transfer to Pluto is summarized in Table 5.10 but not Table 5.11, as the trajectory selected by the patched conic model does not close with a single launch of a commercial launch vehicle. Additionally, since direct and PGA trajectories are shown side by side, come columns skip ΔV 3 or TOF 2, depending on the architecture shown. Regardless, just as shown in the outer planets mission design, propellant mass is within 1% of margin assuming 400 kg left over for station keeping once in orbit around the Kuiper belt object. Table 5.12 displays the variances in total transit time for each case.

Table 5.12: Variance between Patched Conic and STK Time of Flight for Kuiper Belt Objects.

Pluto (Direct)	Pluto (PGA)	Quaoar (Direct)	Quaoar (PGA)
n/a	7.93%	0.38%	9.24%

Patched conics has been shown to have up to 8.15% error compared to high fidelity numerical simulations for a direct trajectory to Mars as mentioned in section 3.3 due to the simplifications and assumptions made by the model, so seeing the error near or below 8% does instill confidence in the patched conic model used to generate initial guesses. Additionally, these tables confirm that PGA trajectories enable faster transit times and lower performance requirements than direct trajectories for rendezvous missions to the Kuiper belt using CNTP. Once again, however, this is at the cost of a more complex trajectory and less frequent launch windows.

Compared to the outer planet simulations, the results for PGA trajectories show higher error between the patched conic model and the numerical simulations. A major contributing factor to this difference is the much greater gravity loss associated with longer and larger maneuvers. Since the patched conic models assume instantaneous maneuvers, smaller maneuvers close to large planetary bodies will incur less gravity loss, or gravity drag, as opposed to long maneuvers near objects with very low gravity.

An update to the mass properties calculations for the CNTP engine which occurred after the analysis of these results was completed increased the predicted engine mass as 2800 kg for the specified engine configuration and materials, which differs from the engine mass of 1650 utilized in the presented simulations. The effect of this change varies depending on the mission parameters held constant – with the trade-offs of mission design, the effect can be treated as an increase in transfer time, decrease in delivered payload mass, or increase in vehicle mass. Due to the relatively small vehicles used for outer planet missions, the vehicle mass can be increased by the extra 1150 kg plus mass for additional propellant without significant changes to the trajectory (this may approach the launch vehicle volume constraint for Uranus/Neptune missions supported by Vulcan Heavy). However, if small vehicle size is prioritized then payload mass can be reduced by 1150 kg to a delivered payload dry mass of roughly 900 kg or transfer time may increase, likely by 10-15%. The changes to Kuiper belt missions are more severe, with direct transfers to Quaoar becoming much longer if still feasible at all, and PGA trajectories increasing in transit time by more than 20-25% if additional propellant is not added. Decreases in payload mass or increases in propellant mass to accommodate the

more massive engine are likely not feasible due to the already very large vehicles which deliver a small payload to the destination.

5.4 Updated Trade Study

The objective of this study, as stated in section 3.2, is to define a range of CNTP specific impulse, thrust, and engine mass which are best suited for direct trajectory capture missions to the outer planets. The first method of meeting this objective is treating the engine as a black box, with no direct relationships that constrain the performance parameters to each other. The volume constraint on the CNTP vehicle is chosen to exactly meet the volume provided by the launch vehicle, so the injection stage carries the maximum possible propellant for the given payload mass. In this case, the launch vehicle constraint is chosen so that the Vulcan Heavy or New Glenn could support these CNTP vehicle architectures. The generalized engine configuration is related to the injection stage sizing through a mass balance which requires a certain mass fraction (ratio of dry mass to propellant mass) for a specific ΔV. The required ΔV for each destination is selected by the FOM detailed in section 3.1, is shown in Figure 5.12.

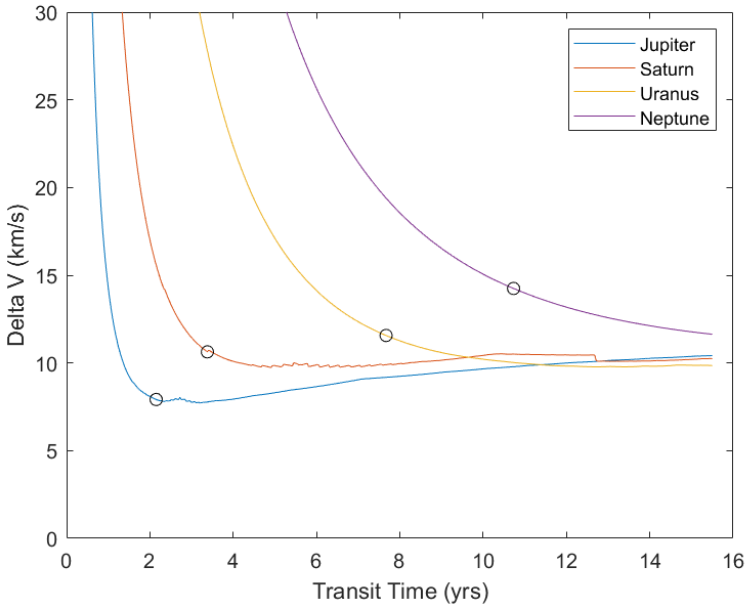

Figure 5.12: Updated ΔV Requirements for Outer Solar System Missions.

The selected points in Figure 5.12 differ from Figure 5.1 due to the use of the FOM described in section 3.1, as well as more precise calculations for planetary positions from their ephemeris. These trajectories are utilized both in this analysis and the proceeding analysis, where the engine configuration is constrained. With the required ΔV selected for each destination, the mass fraction is calculated via the rocket equation, with an analytical approximation used to represent additional ΔV incurred due to gravity drag [57], [45]. These expressions are shown in Eq. 5.2 and 5.3:

$$MF = \frac{m_p}{m_f} = e^{\Delta V^*/gI_{sp}} - 1 \tag{5.2}$$

$$\Delta V^* = \frac{1}{24}\Sigma\left(\frac{\mu}{r^3}t^2\Delta V\right) + \Delta V. \tag{5.3}$$

The mass balance shown by Eq. 5.4 is used to determine the amount of payload deliverable to the destination constrained by the mass fraction and launch vehicle volume. This expression assumes the dry mass of the vehicle consists of only the engine,

propellant tank, and spacecraft payload. Akin details a process which can be used to approximate tank mass as a function of propellant mass [62]:

$$m_p = MF(m_l + m_e + m_t). \tag{5.4}$$

The delivered payload mass can be plotted for each of the primary variables. Figure 5.13-Figure 5.15 display delivered payload mass versus specific impulse, thrust, and engine mass, respectively.

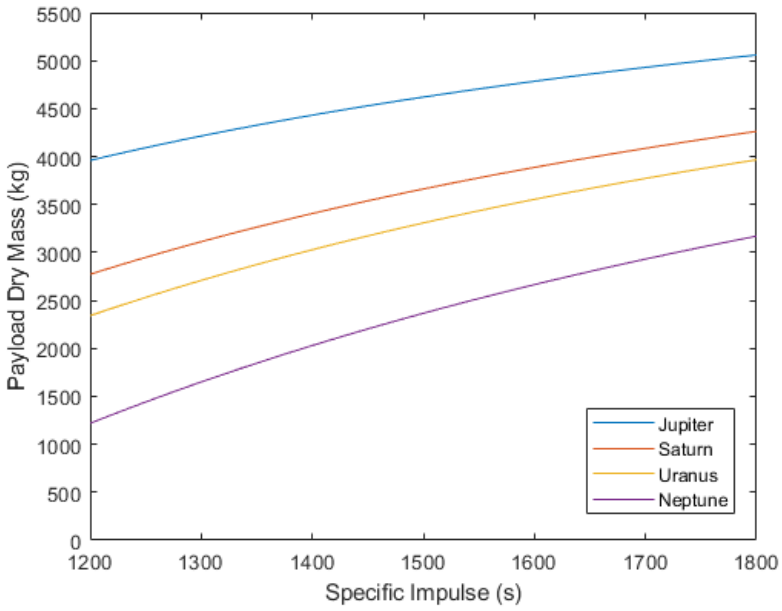

Figure 5.13: Payload Mass versus Specific Impulse.

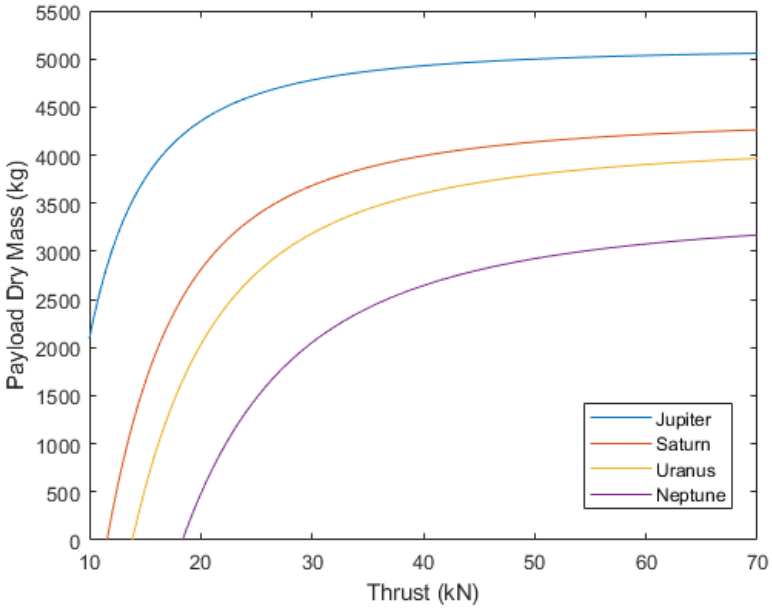

Figure 5.14: Payload Mass versus Engine Thrust.

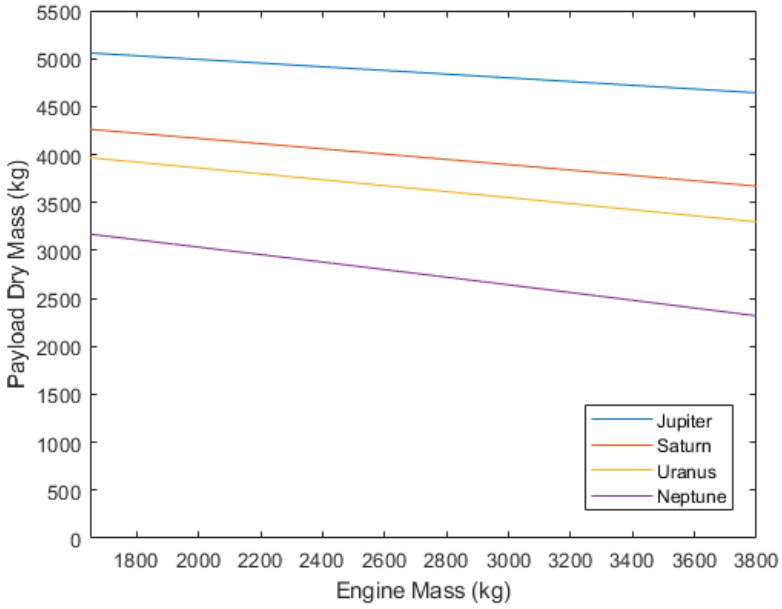

Figure 5.15: Payload Mass versus Engine Mass.

Due to the multidimensional space of parameters being analyzed within this trade study, simplifications were made for the generation of these plots. Each primary variable

is shown plotted against payload mass for the other two parameters being constant at the upper bound. For example, for specific impulse, thrust and engine mass are held constant at 70 kN and 1650 kg, respectively, to generate Figure 5.13. With each relationship well defined, the criteria can now be applied; minimum and maximum performance can be defined by defining a range of payload masses which have previously been used on scientific missions. While more payload mass is always beneficial from a scientific perspective, there is a range of payload masses previously used which can define a narrower range of CNTP performance in order to guide performance targets during development. Therefore, the minimum performance is selected at the lowest payload mass historically delivered to the outer solar system, which is the mass of New Horizons at roughly 480 kg [78]. The maximum performance is selected at the highest payload mass historically delivered to the outer planets that still meets the launch vehicle requirements previously described. The upper bound is then the mass of the Juno spacecraft, at 3600 kg. In any case, if the minimum required performance is below the range of parameters considered, the lower range bound is recorded. Similarly, if the upper payload limit is not feasible within the considered range, the upper bound is recorded. Once the criteria are applied, the results can be tabulated as shown in Table 5.13.

Table 5.13: Engine Performance for Unconstrained Configuration.

	Jupiter		Saturn		Uranus		Neptune	
	Min	Max	Min	Max	Min	Max	Min	Max
Isp (s)	<1200	<1200	<1200	1474	<1200	1620	<1200	>1800
Thrust (kN)	<10	14.2	12.4	28.4	14.9	39.9	20	>70

M_e (kg)	>3800	>3800	>3800	>3800	>3800	2840	>3800	<1650

The engine mass is opposite the other variables, in that a lower number is better in terms of performance. In that sense, minimum and maximum performance correspond to highest and lowest engine mass, respectively. One important result from Table 5.13 is that performance within the bounds that is feasible for CNTP is not required in general for missions to Jupiter in that the performance required for payload between 480 and 3600 kg are lower than the bounds of performance considered in this study. For direct rendezvous missions to Jupiter near the selected transit time solid fuel NTP, a simpler system at a higher technological readiness, may be better suited for these missions with transit times of two years or more. Likewise, even at the highest limit of potential CNTP performance, 3600 kg is outside the range of feasible payload mass for direct rendezvous missions to Neptune with transit times less than 10.5 years. However, in this case there is a range of payload mass for which the mission does close, up to roughly 3200 kg. Missions to Saturn and Uranus do converge using CNTP for the selected transit times. In most cases across all four destinations, engine mass of greater than 3800 kg is able to close the mission at the maximum bound of specific impulse and thrust.

The second method of answering the second research question is constraining the engine to a single configuration, which can be compared to the generalized unconstrained case previously presented. For a constrained engine configuration, the primary variables are the same with operating temperature and required ΔV utilized as secondary variables. Specific impulse and temperature are related via the reactor operating temperature, which means that applying criteria to the reactor operating temperature rather than each performance value individually simplifies the analysis. This relationship is also important

since increasing specific impulse for a given reactor configuration decreases thrust, with the reverse also being true. These relations, given in Eq. 5.5 and 5.6, are taken from curve fits of the optimized systems model of CNTP and are roughly quadratic [39]:

$$I_{sp} = 0.0000083\theta^2 + 0.2040833\theta + 313.0391482 \tag{5.5}$$

$$T = 0.0000464\theta^2 - 0.0698215\theta + 288.6810675. \tag{5.6}$$

The precision of each curve fit is necessary to replicate the shape of the generated curves within the mission design analysis. In addition to the engine performance, the number, layout, and size of CFEs are also constrained, so changing the operating temperature changes the thrust and specific impulse of the engine but the size and weight remain the same. For this configuration the engine mass is held constant at 2800 kg [79]. Calculating deliverable payload mass from a selected ΔV and transit time, and a range of operating temperatures, then leads to a comparison between different temperatures in terms of how much payload they allow to be delivered. Figure 5.16 displays the overall relationship between these values for all four outer planets.

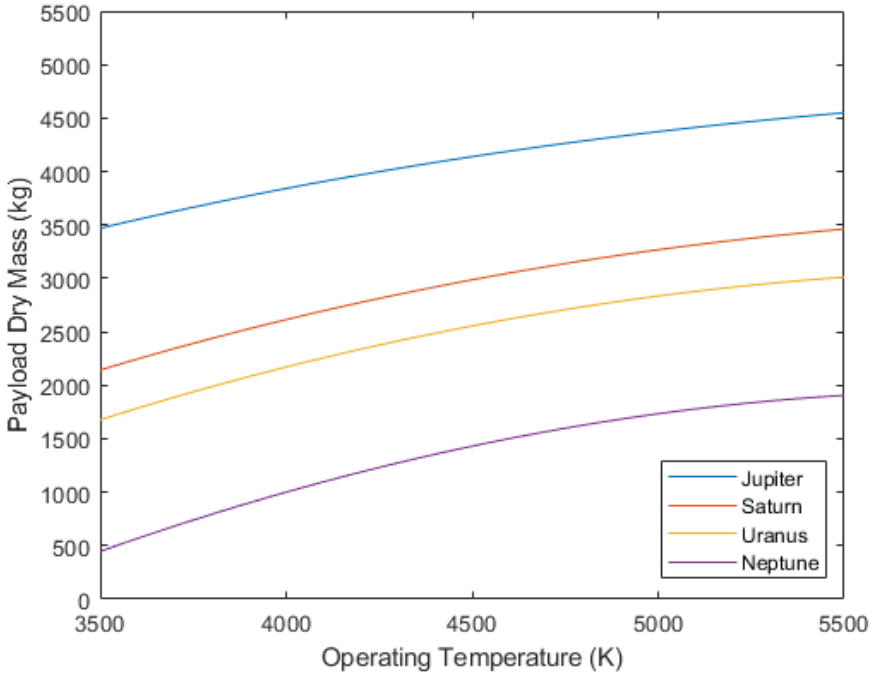

Figure 5.16: Operating Temperature Versus Payload Mass for Constrained Engine Configuration.

The same criteria applied in the previous configuration are also utilized to tabulate results here. In this case, they are applied to select minimum and maximum reactor operating temperatures, which can be used to calculate corresponding specific impulse and thrust. A summary of these results is shown in Table 5.14.

Table 5.14: Engine Performance for Constrained Configuration.

	Jupiter		Saturn		Uranus		Neptune	
	Min	Max	Min	Max	Min	Max	Min	Max
Temperature (K)	<3500	3664	<3500	>5500	<3500	>5500	3528	>5500
Corresponding Isp (s)	1130	1170	1130	1690	1130	1690	1136	1690

Corresponding Thrust (kN)	101.2	95.1	101.2	45	101.2	45	101.1	45

The results in Table 5.14 primarily once again show that direct rendezvous missions to Jupiter do not require performance in the range of CNTP in order to close for payload masses less than 3600 kg, and also concur with the previous analysis in that Neptune requires higher performance than CNTP is capable of for delivering the same amount of payload with the selected transit time. Missions for Saturn and Uranus fall between the payload mass criteria at all reactor temperatures. Diminishing returns on payload capacity for increased performance is also shown by the figure. The methodology shown here is a sample of future analysis, which can be used to compare different engine configurations to show what operating temperatures result in what payload capacity for each configuration. For the constrained case, the payload capacity is slightly lower overall compared to the unconstrained case but is also less sensitive to changes in performance.

Validation of the underlying model is discussed in section 5.3, which compares variance of trajectory transfer time between patched conic and numerical models. Further confidence in the results discussed in sections 5.3 and 5.4 can also be gained by investigating the sensitivity of the FOM for direct trajectories to variation on weights for the ΔV and TOF terms. The robustness of the FOM to variance in the term weights can then be extended to discuss validity of results for both the numerical simulations as well as the second trade study. A summary of the applied sensitivity analysis method is given in section 3.2, which is similar to the Brown-Gibson method but without directly comparing alternatives. Applying a weight term α to the ΔV term and an opposing 1- α

weight to the TOF term allow varying the dependence of the FOM result from only ΔV to both ΔV and TOF to just TOF, and the responses of the selected ΔV and TOF are recorded. Eq. 5.7 displays how these values are inserted into equation 3.3:

$$FOM = \alpha A \frac{\Delta V}{V_E} + (1 - \alpha) B \frac{TOF}{P_E}. \tag{5.7}$$

The results of this analysis are shown in Figure 5.17 and Figure 5.18 for ΔV and TOF, respectively.

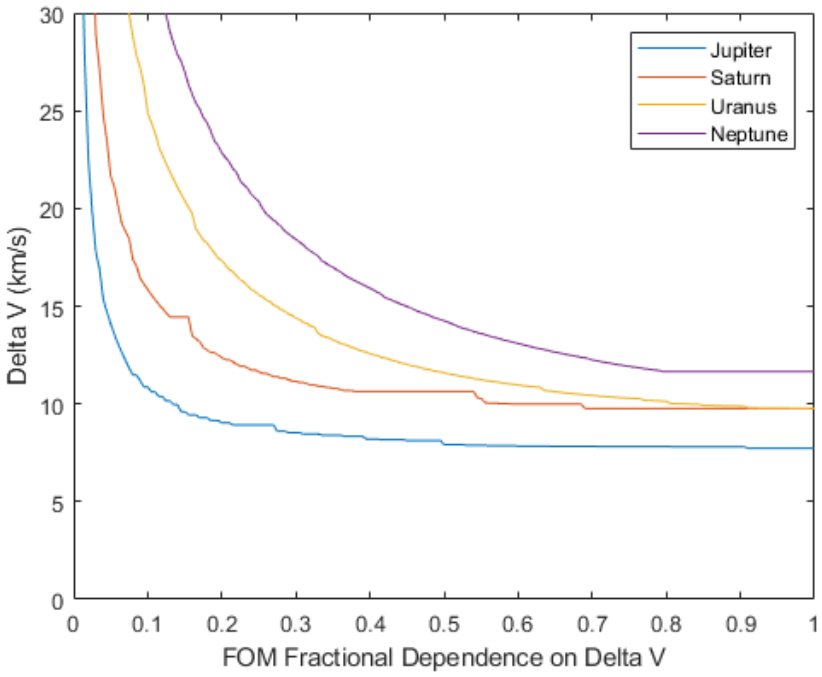

Figure 5.17: FOM Sensitivity of ΔV.

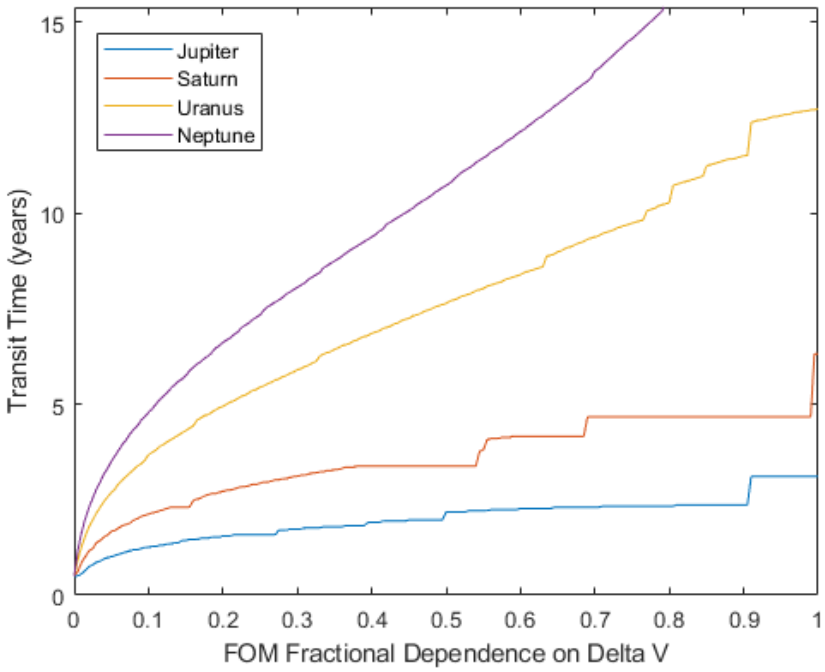

Figure 5.18: FOM Sensitivity of Transit Time.

Since ΔV and transit time are equally weighted for direct missions in previous analyses, the selected transfer time and ΔV for each destination correspond to α = 0.5, which means the weight term is split 50/50 between the two inputs. Overall, the curves for Uranus and Neptune are very smooth but with larger slopes than Jupiter and Saturn, which in turn have more discontinuities. The discontinuities are similar to those in Figure 5.12 which originate from changing departure dates being selected for the lowest ΔV from one transit time to the next. The lower slopes for the Jupiter and Saturn curves show that the FOM result changes very little over much of the weight range, but at times when the result does change the change is large. For these destinations the ΔV and transit time are less sensitive to weights for terms of the FOM, but instead are more sensitive to changes in departure date which are iterated through by the model. This result makes

sense in terms of the physical orbital mechanics, in that destinations which are faster and closer to Earth will have shorter available launch windows than destinations which are further away but move much slower around the sun.

The results displayed in these figures can also be extended to address the validity of using the patched conic model as a basis for the numerical simulations and trade study. The use of patched conics as initial values for numerical simulations is validated in section 5.3 by comparing the results of the patched conic model to the numerical simulations and showing that the variance in transfer time, with other mission details being similar, was close to or less than an expected value from literature. The sensitivity study increases confidence in the patched conic model and FOM by showing that similar results can be expected when the weights to inputs in the FOM are changed. Likewise, the FOM is a significant component of the trade study, since payload masses for each destination are calculated assuming a transfer time which is selected by the FOM. Small changes to the FOM weights result in small or no change to the selected transfer time, and so confidence in these results is increased as well.

Chapter 6. Conclusions

The analyses presented in the preceding sections demonstrate the range of potential for CNTP in supporting missions to the outer solar system. First, a comparison to solid fuel NTP conveys that even a moderate increase in specific impulse can lead to a substantial improvement in capability for scientific missions, including payload mass, transit time, and required propellant mass. Using systems models to predict CNTP performance, it is shown that missions to the outer planets, both gas giants and ice giants, can be performed with engine capabilities of 1600 s specific impulse, 20 kN thrust, and 1.3 T/W. More generally, a range of performance from 1200-1620 s, 10-40 kN, and >1.5 T/W enables access to most direct trajectory missions presented to the outer planets with a payload mass of up to 3600 kg with the exception of Neptune being limited to smaller payloads for transfer times of less than 10.5 years. 1200-1800 s, 10-70 kN, and >4 T/W enables all of the presented mission trajectories to the outer planets. These results are valid for transfer times of 2 years to Jupiter, 3.5 years to Saturn, 7.5 years to Uranus, and 10.5 years to Neptune.

Likewise, capture missions are shown to close to the Kuiper belt with much higher performance requirements of 1600-1800 s of specific impulse and 60 kN of thrust for a T/W ratio of 3.7, although some do require gravity assists in order to reduce transit time and performance requirements. The reduction in transit time for Quaoar is 16 years down to 12 years, and likewise PGA trajectories to Pluto offer transit times of 10-12 years. The preceding analysis results in lower transit times as compared to previous missions flown to the outer solar system - for example, the Juno spacecraft required nearly five years and multiple gravity assists to reach Jupiter compared to the two-year

direct trajectory selected for CNTP [5]. Similarly, many of the scientific missions discussed in chapter 2 consist of longer and/or more complicated trajectories than the proposed CNTP trajectories for rendezvous missions.

6.1 Constraints and Limitations

As mentioned in the opening paragraph, one limitation of the displayed results is the capability of CNTP constrained by a single launch of a commercial launch vehicle to deliver payload to Neptune within a given transfer time. The numerical simulations also show that CNTP within this constraint is not capable of achieving ΔVs much greater than 25 km/s. Just as limitations of the results themselves are shown by the above analysis, limitations of the analysis itself also have an effect on the conclusions for this work. One such example is the simplified vehicle model, which assumes mass for other subsystems not specifically mentioned are accounted for within the payload mass, although a more detailed model would result in more precise vehicle mass estimates. Additionally, engine mass estimates significantly affect the results of each study, and with this analysis being performed in tandem with system modeling for the CNTP engine, many assumptions are still being used to define an engine mass with the current analyses. The final trade study which defines the range of CNTP performance useful for missions to the outer solar system is only performed for the outer planets, and not for direct or PGA trajectories to the Kuiper belt. Time and limitations are constraints throughout this analysis, with some analyses showing further work needed to define mission design aspects within the trade space. These are discussed further in section 6.2, as well as in chapter 7.

6.2 Application of Results

The recommendation of performance ranges lower than the ideal maximum from the opening paragraph of chapter 6 is noteworthy – since specific impulse does not need to be 1800 s in order to accomplish missions to the outer planets, the reactor operating temperature can be lower than the 5500 K listed as a requirement in previous papers [25], [26]. A lower operating temperature could result in larger thermal margins in the reactor, or broaden the range of material choices, which would make the CFEs and therefore engine as a whole easier to fabricate.

Numerous factors are considered in this analysis, primarily focusing on the architecture of the trajectory, the CNTP injection stage vehicle, and their constraints. For the architectures detailed in this thesis, the CNTP injection stage was largely bounded by the volume and capability of the launch vehicle, while the trajectory itself is constrained by the size of injection stage, payload mass, and intended destination. First, a patched conic model is described in detail which uses two-body orbital motion to calculate trajectories with instantaneous maneuvers. The patched conic model used relies on a FOM which weights the transit time versus the required ΔV. A sensitivity analysis on the equation shows that small changes to the weights within the expression lead to small changes or no change to the output. Different factors are considered at this stage to define how the maneuvers are conducted, and here differences in the capture burn from solid fuel NTP are investigated with the use of the spacecraft chemical thruster and the CNTP engine. Specifically, it is shown that for a CNTP engine with a mass of 3800 kg, there is a marginal difference in vehicle mass for a chemical or CNTP capture burn for a Jupiter rendezvous mission with a two-year transit time. The mass difference is in favor of

CNTP for any specific impulse above 1200 s. The CNTP engine is chosen in order to reduce vehicle mass at the cost of stricter requirements for propellant boil-off which may require a passive or active ZBO system.

The propellant chosen in these configurations of CNTP engines is liquid hydrogen, although other propellants could potentially be investigated to gain more thrust at the cost of specific impulse. Later, gravity losses and three-body effects are accounted for via numerical simulation, and further analytic analysis also includes gravity losses to give a conservative estimate of capability. The propulsion and tank systems are the primary spacecraft subsystems covered in this work, with some discussion of thermal control as well. A simplified model is used for the spacecraft which does not fully capture all aspects of mission design, but rather captures the aspects most relevant to the work in this thesis. Subsystems such as power and communication were given placeholder masses for the scientific spacecraft based on estimates from historical missions, but further details were outside the scope of this work and could potentially be investigated with further analysis.

Chapter 7. Future Work

While the work presented in this thesis answers some questions faced by the development of CNTP, there are also other challenges which are outside the scope of this work and which still need to be addressed in the future. First, on the note of constraints and limitations introduced in the previous chapter, other alternatives to vehicle architecture choices made here can be pursued. This work focused primarily on liquid hydrogen as propellant, although other choices may also prove useful with CNTP. Other propellants may decrease the specific impulse of the engine, but at the same time may also increase thrust and storability so are worth further consideration. Assumptions are made regarding the tank insulation and thermal management, but further work pursuing passive ZBO systems would be beneficial for long duration scientific missions. Similarly, other spacecraft subsystems such as power and communication, can provide more in-depth understanding of the driving trade-offs associated with these mission architectures. In regard to the patched conic models and associated FOMs, a cost analysis of previous missions is a future task which will help select better weights for the ΔV and TOF terms. Understanding what portion of mission cost goes to development versus operations will also ensure the best trajectory is selected.

A better operational understanding of CNTP is also vital to making informed decisions on how maneuvers are carried out. In Chapter 4, it is mentioned that the DSM, or correction burn, can potentially be done with chemical thrusters from the payload. The difference this change makes is dependent on the propellant cost of starting up and shutting down the CNTP engine, and due to the higher specific impulse of CNTP this may or may not use less propellant. Regardless of propellant use, chemical thrusters for

short duration maneuvers make more sense operationally due to the complexity of CNTP. In general, these transient operating modes are not considered in this analysis and so also affect the propellant used for departure and capture burns.

References

[1] J. Moore, L. Spilker, J. Bowman, M. Cable, S. Edgington, A. Hendrix, M. Hofstadter, T. Hurford, K. Mandt, A. McEwen, C. Paty, L. Quick, A. Rymer, K. Sayanagi, B. Schmidt and T. Spilker, "Exploration Strategy for the Outer Planets 2023-2032: Goals and Priorities," 2020.

[2] National Academies of Sciences, Engineering, and Medicine, Origins, Worlds, and Life: A Decadal Strategy for Planetary Science and Astrobiology 2023-2032, Washington, DC: The National Academies Press, 2022.

[3] National Aeronautics and Space Administration, "The Pioneer Missions," 26 May 2007. [Online]. Available: https://www.nasa.gov/centers/ames/missions/archive/pioneer.html.

[4] National Aeronautics and Space Administration, "Voyager," 2018. [Online]. Available: https://www.nasa.gov/mission_pages/voyager/overview.

[5] S. J. Bolton, J. Lunine, D. Stevenson, J. E. P. Connerney, S. Levin, T. C. Owen, F. Bagenal, D. Gautier, A. P. Ingersoll, G. S. Orton, T. Guillot, W. Hubbard, J. Bloxham, A. Coradini, S. K. Stephens, P. Mokashi, R. Thorne and R. Thorpe, "The Juno Mission," *Space Science Reviews*, pp. 5-37, 2017.

[6] National Aeronautics and Space Administration, "Missions: Galileo," 27 May 2023. [Online]. Available: https://solarsystem.nasa.gov/missions/galileo/overview/.

[7] C. A. Henry, "An Introduction to the Design of the Cassini Spacecraft," *Space Science Reviews*, pp. 129-153, 2002.

[8] S. A. Stern, H. A. Weaver, J. R. Spencer, H. A. Elliot and t. N. H. T. , "The New Horizons Kuiper Belt Extended Mission," *Space Science Reviews,* 2018.

[9] Y. Guo and R. W. Farquhar, "New Horizons Mission Design," *Space Science Reviews,* pp. 49-74, 2008.

[10] J. R. Laube, S. P. McCall, G. V. Meholic and R. T. Potter, "Orbital Design and Performance Comparison of Chemical and NTP-Powered Stages," in *JANNAF Liquid Propulsion and Spacecraft Propulsion Joint Subcommittee Meeting*, Huntsville, 2022.

[11] C. R. Joyner II, M. Eades, J. Horton, T. Jennings, T. Kokan, D. J. H. Levack, B. J. Muzek and C. B. Reynolds, "LEU NTP Engine System Trades and Mission Options," in *Nuclear and Emerging Technologies for Space*, Richland, Washington, 2019.

[12] S. Kumar, L. D. Thomas and J. T. Cassibry, "Model-Based Approach for Conceptual Mission Design for NTP Enabled Robotic Missions," in *AIAA Propulsion and Energy Forum*, VIRTUAL EVENT, 2021.

[13] S. Kumar, L. D. Thomas and J. T. Cassibry, "Nuclear Thermal Propulsion for Jupiter and Saturn Rendezvous," *Journal of Spacecraft and Rockets,* 2022.

[14] J. Powell, G. Maise, J. Paniagua and S. Borowski, "Compact MITEE-B: Bi-Modal Nuclear Engine for Unique New Planetary Science Missions," in *AIAA/ASME/SAE/ASEE Joint Propulsion Conference & Exhibit*, Indianapolis, Indiana, 2002.

[15] M. Houts, R. Joyner, J. Abrams, J. Witter and P. Venneri, "Versatile Nuclear

Thermal Propulsion," National Aeronautics and Space Administration, 2019.

[16] N. Hatten, K. Hughes, D. C. Folta and A. Valinia, "Fast Earth-Mars Roundtrip Trajectories to Reduce Health and Safety Risks for Crewed Missions," in *AAS/AIAA Astrodynamics Specialist Conference*, 2022.

[17] C. R. Joyner, D. Levack and S. Borowski, "Development of a Small Nuclear Thermal Propulsion Flight Demonstrator Concept that is Scalable to Human Missions," in *AIAA/ASME/SAE/ASEE Joint Propulsion Conference and Exhibit*, Atlanta, Georgia, 2012.

[18] T. Lawrence, "Nuclear Thermal Rocket Propulsion Systems, IAA White Paper," International Academy of Aeronautics, Paris, France, 2005.

[19] S. Kumar, L. D. Thomas, J. T. Cassibry and R. A. Frederick, "Review of Nuclear Thermal Propulsion Technology for Deep Space Missions," in *AIAA Propulsion and Energy Forum*, VIRTUAL EVENT, 2020.

[20] M. D. DeHart, S. Schunert and V. M. Laboure, "INL Nuclear Thermal Propulsion: Project overview, status and future," Idaho National Laboratory, 2023.

[21] R. A. Gabrielli and G. Herdrich, "Review of Nuclear Thermal Propulsion Systems," *Prorgress in Aerospace Sciences*, pp. 92-113, 2015.

[22] S. T. Nelson and J. Grey, "Conceptual Design Study of a Liquid-Core Nuclear Rocket," National Aeronautics and Space Administration, Princeton, New Jersey, 1963.

[23] R. G. Ragsdale, "Performance Potential of a Radiant-Heat-Transfer Liquid-Core Nuclear Rocket Engine," National Aeronautics and Space Administration,

Washington, DC, 1967.

[24] J. Allen, M. Johns, M. Patterson, M. Houts, F. Heidet, N. V. Smith and J. E. Foster, "Overview of High-Performance Centrifugal Nuclear Thermal Rocket Propulsion System," in *Transactions of the American Nuclear Society*, 2020.

[25] J. T. Gates, F. Heidet, M. Jarrett, M. G. Houts, R. S. Raju, E. Fisher, D. Leer and C. M. McSwain, "Preliminary Parametric Studies of a High Performance Centrifugal Nuclear Thermal Rocket System," in *Transactions of the American Nuclear Society*, 2020.

[26] D. Thomas, M. Houts, W. Walters, K. Hollingsworth, R. Frederick and J. Cassibry, "Toward the Engineering Feasibility of the Centrifugal Nuclear Thermal Rocket," in *International Astronautical Congress*, Dubai, United Arab Emirates, 2021.

[27] J. Keese, B. Campbell, M. Schroll, K. Hollingsworth and D. Thomas, "Past Experimental Investigations of Bubbly Flow Applied to Centrifugal Nuclear Thermal Propulsion," in *Science and Technology Forum*, San Diego, CA, 2022.

[28] D. G. Fearn, "The Ulysses Mission: The Ion Propulsion Alternative," IEPC, London, 1991.

[29] J. V. McAdams, J. M. Knittel, K. E. Williams, J. A. Englander, D. H. Ellison, D. R. Stanbridge, B. Sutter and K. Berry, "Redefining Lucy Mission Delta-V During Spacecraft Design Using Trajectory Optimization Within High-Fidelity Monte Carlo Maneuver Analysis," American Astronomical Society, 2020.

[30] D. Lev, R. M. Myers, K. M. Lemmer, J. Kolbeck, H. Koizumi and K. Polzin, "The technological and commerical expansion of electric propulsion," *Acta*

Astronautica, pp. 213-227, 2019.

[31] C. E. Garner, M. D. Rayman, J. R. Brophy and S. C. Mikes, "In-Flight Operation of the Dawn Ion Propulsion System Through Orbit Capture at Vesta," in *48th AIAA/ASME/SAE/ASEE Joint Propulsion Conference & Exhibit*, 2012.

[32] J. Benkhoff, J. v. Casteren, H. Hayakawa, M. Fujimoto, H. Laakso, M. Novara, P. Ferri, H. R. Middleton and R. Ziethe, "BepiColombo - Comprehensive exploration of Mercury: Mission overview and science goals," *Planetary and Space Science,* pp. 2-20, 2010.

[33] K. Nishiyama, S. Hosoda, K. Ueno, R. Tsukizaki and H. Kuninaka, "Development and Testing of the Hayabusa2 Ion Engine System," in *Proceedings of the Joint Conference of the 30th International Symposium on Space Technology and Science 34th International Electric Propulsion Conference (IEPC) and 6th Nanosatellite Symposium*, Hyogo-Kobe, Japan, 2015.

[34] J. R. Casani, M. A. Gibson, D. I. Poston, N. J. Strange, J. O. Elliot, R. L. McNutt, S. L. McCarty, P. R. McClure, S. R. Oleson and C. J. Sotin, "Enabling a New Generation of Outer Solar System Missions: Engineering Design Studies for Nuclear Electric Propulsion," 2020.

[35] P. D. N. Ayuthya and J. Cassibry, "Developing of Three-Dimensional Bubble Dynamics Model for Centrifugal Nuclear Thermal Propulsion," in *Nuclear and Emerging Technologies for Space*, Idaho Falls, Idaho, 2023.

[36] T. Blackman, M. Schroll, R. Frederick and L. D. Thomas, "Continuing Experimental Efforts for Simulating a Centrifugal Nuclear Thermal Rocket

Engine," in *Nuclear and Emerging Technologies for Space*, Idaho Falls, Idaho, 2023.

[37] M. Schroll, J. Keese, R. Frederick and L. D. Thomas, "Baseline Configuration Analysis for Centrifugal Nuclear Thermal Rocket Engine," in *Nuclear and Emerging Technologies for Space*, Cleveland, OH, 2022.

[38] M. Schroll and R. Frederick, *Performance Analysis of Centrifugal Nuclear Thermal Rocket Engine*, Huntsville, Alabama: Academic Workshop (Unpublished), 2022.

[39] M. Schroll, R. Frederick and L. D. Thomas, "Reactor Core Geometry Optimization with Application for Centrifugal Nuclear Thermal Rockets," in *Nucelar and Emerging Technologies for Space*, Idaho Falls, Idaho, 2023.

[40] R. R. Bate, D. D. Mueller, J. E. White and W. W. Saylor, Fundamentals of Astrodynamics, Garden City, New York: Dover Publications, 2020.

[41] J. M. Longuski and S. N. Williams, "Automated Design of Gravity-Assist Trajectories to Mars and the Outer Planets," *Celestial Mechanics and Dynamical Astronomy*, pp. 207-220, 1991.

[42] S. N. Williams and J. M. Longuski, "Automated Design of Multiple Encounter Gravity-Assist Trajectories," in *AIAA/AHA Astrodynamics Conference*, Portland, Oregon, 1990.

[43] R. H. Battin and R. M. Vaughan, "An Elegant Lambert Algorithm," *Journal of Guidance, Control, and Dynamics*, pp. 662-671, 1984.

[44] H. Curtis, Orbital Mechanics for Engineering Students, Elsevier Butterworth-

Heinemann, 2005.

[45] H. M. Robbins, "An Analytical Study of the Impulsive Approximation," in *AIAA Aerospace Sciences Meeting*, New York, 1966.

[46] R. H. Frisbee, S. D. Leifer and S. V. Shah, "Nuclear Safe Orbit Basing Considerations," in *AIAA/NASA/OAI Conference on Advanced SEI Technologies*, Cleveland, OH, 1991.

[47] E. M. Standish, "Approximate Positions of the Planets," 2023. [Online]. Available: https://ssd.jpl.nasa.gov/planets/approx_pos.html.

[48] D. Hennes and D. Izzo, "Interplanetary Trajectory Planning with Monte Carlo Tree Search," in *24th International Joint Conference on Artificial Intelligence*, 2015.

[49] J. W. Hartmann, V. L. Coverstone-Carroll and S. N. Williams, "Optimal Interplanetary Spacecraft Trajectories via a Pareto Genetic Algorithm," *Journal of the Astronautical Sciences,* vol. 46, pp. 267-282, 1998.

[50] G. R. Young, "A New Guidance System Figure-of-Merit," *Journal of Spacecraft and Rockets,* vol. 8, no. 10, pp. 1103-1104, 1971.

[51] J. L. Young, "Coverage Optimization Using a Single Satellite Orbital Figure-of-Merit," Massachusetts Institute of Technology, Cambridge, MA, 2001.

[52] D. Carrelli, D. O'Shaughnessy, T. Strikwerda, J. Kaidy, J. Prince and R. Powell, "Autonomous Aerobraking for Low Cost Interplanetary Missions," *Acta Astronautica,* vol. 93, pp. 467-474, 2014.

[53] D. Fearn and A. Martin, "The Promise of Electric Propulsion for Low Cost Interplanetary Missions," *Acta Astronautica*, vol. 35, pp. 615-624, 1995.

[54] D. L. Thomas, *Experimental Design for Response Surface Methods and Optimization,* University Lecture, 2006.

[55] W. Edwards, "Social Utilities," in *Engineering Economist, Summer Symposium Series*, 1971.

[56] J. L. Grumbach and L. D. Thomas, "Integration Principles for Complex Systems," *Journal of the International Council on Systems Engineering,* vol. 23, no. 6, pp. 684-706, 2020.

[57] C. D. Brown, Elements of Spacecraft Design, American Institute of Aeronautics and Astronautics, 2002.

[58] P. Brown and D. Gibson, "A Quantified Model for Facility Site Selection - Application to a Multiplant Location Problem," *AIIE Transactions,* vol. 4, no. 1, pp. 1-10, 1972.

[59] B. M. A. Park and H. Wright, "Comparison of a Simple Patched Conic Trajectory Code to Commercially Available Software," American Astronomical Society, 2007.

[60] C. Short, P. Ghosh and A. Claybrook, "Revisiting Trajectory Design with STK Astrogator Part 1," in *AAS/AIAA Astrodynamics Specialist Conference*, Portland, Maine, 2019.

[61] P. Gill, E. Wong, W. Murray and M. Saunders, "User's Guide for SNOPT Version 7.7: Software for Large-Scale Nonlinear Programming," 2021.

[62] D. L. Akin, "Mass Estimating Relations," University of Maryland, College Park, MD, 2022.

[63] W. Heineman Jr, "Fundamental Techniques of Weight Estimating and Forecasting for Advnaced Manned Spacecraft and Space Stations," National Aeronautics and Space Administration, Washington, DC, 1971.

[64] S. S. Pietrobon, "Analysis of Propellant Tank Masses," US Human Space Flight Plans Comittee, 2009.

[65] C. Guernsey, R. Baker, D. Plachta and P. Kittel, "Cyrogenic Propulsion with Zero Boil-off Storage Applied to Outer Planetary Exploration," in *AIAA/ASME/SAE/ASEE Joint Propulsion Conference and Exhibit*, 2005.

[66] D. W. Plachta, R. J. Christie, J. M. Jurns and P. Kittel, "Passive ZBO Storage of Liquid Hydrogen and Liquid Oxygen Applied to Space Science Mission Concepts," *Cryogenics*, pp. 89-97, 2006.

[67] N. A. Morris, L. D. Thomas and D. K. Hollingsworth, "Stay Cool - Alternatives for Long-Term Storage of Large Quantities of Liquid Hydrogen on a Mars Transfer Vehicle," *Nuclear Technology*, pp. 860-865, 2021.

[68] Aerojet Rocketdyne, "RL10 Propulsion System," April 2016. [Online]. Available: https://www.rocket.com/sites/default/files/documents/RL10_data_sheet.pdf.

[69] National Aeronautics and Space Administration, "NASA’s OSIRIS-REx Asteroid Sample Return Mission," 24 July 2023. [Online]. Available: https://www.nasa.gov/sites/default/files/atoms/files/osiris_rex_factsheet5-9.pdf.

[70] National Aeronautics and Space Administration, "Galileo Jupiter Arrival, Press Kit," 1995.

[71] European Space Agency, "Cassini Final Mission Report, Appendix A," 2018.

[72] United Launch Alliance, "ULA Vulcan," 25 August 2022. [Online]. Available: https://www.ulalaunch.com/rockets/vulcan-centaur.

[73] Blue Origin, "New Glenn Payload User's Guide, Revision C," 23 August 2022. [Online]. Available: https://yellowdragonblogdotcom.files.wordpress.com/2019/01/new_glenn_payload_users_guide_rev_c.pdf.

[74] Space Exploration Technologies, "Starship," 25 August 2022. [Online]. Available: https://www.spacex.com/vehicles/starship/.

[75] Jet Propulsion Laboratory, "Small-Body Orbits & Ephemerides," June 2023. [Online]. Available: https://ssd.jpl.nasa.gov/sb/orbits.html.

[76] The Ohio State University, "CNTR Core Design," Unpublished, 2023.

[77] S. Kumar, L. D. Thomas and J. T. Cassibry, "Nuclear Thermal Propulsion Trades and Sensitivity Analysis for Robotic Missions (Submitted for Review)," in *AIAA Scitech Forum*, Orlando, Florida, 2024.

[78] A. A. Siddiqi, "Beyond Earth: A Chronicle of Deep Space Exploration, 1958-2016," NASA History Program Office, 2018.

[79] M. Schroll, T. Hampson, R. Frederick and L. D. Thomas, "System Design Optimization for a Centrifugal Nuclear Thermal Rocket," in *International Astronautical Congress*, Baku, Azerbaijan, 2023.

Appendix A. Figure of Merit Details

The figure of merit discussed in section 3.1 combines two key parameters of interest in the design of interplanetary trajectories, namely the required ΔV and transit time of flight. The goal of this FOM is to minimize both parameters, however since decreasing one increases the other a balance must be found. Additionally, since the terms have different units – km/s for the ΔV and years for the transit time are the units best used in this context – additional factors must be included to nondimensionalize the terms so they can be added. The general form of the FOM is given by Eq. 3.15:

$$FOM = \frac{A}{V_E}\Delta V + \frac{B}{P_E}TOF.$$

In this equation, A and B are constants, V_E is the Earth orbital velocity and P_E is the Earth orbital period. While the fractions are used to nondimensionalize the parameters in terms of units, it is important for the relative values of each term to remain the same to prevent artificial weighting in consideration of the FOM value. The nondimensionalizing values were not utilized when writing the patched conic models, which just used the ΔV and TOF terms, and to prevent much of the analysis from having to be redone, A and B are chosen to keep the overall value of the FOM the same in each case. A is selected to the be the same value as V_E to cancel out changes in magnitude for the term as a whole. Since $V_E = 29.783$ km/s, A is chosen so that A = 29.783 as well. The Earth orbital velocity is not unity, and so as a result the exact value of V_E is used to prevent weighing the term for direct transfers. Likewise, for the TOF in years, the Earth orbital period is 1, which means the second term is not changed in magnitude by nondimensionalization and so B is chosen to also be 1. In the case of PGA transfers, a weight of 0.5 is included to output reasonable transit times for the different mission architectures.

Appendix B. Direct Trajectory Patched Conic Model

Main Function

```
% Programmer: Will Ziehm
% Project: Delta V Calculations to an Outer Planet on a Direct Transfer
% Date: January 2023

clc
clear variables
close all

[Sol,Earth,Jupiter,Saturn,Uranus,Neptune,Pluto,Quaoar] = GetEphemeris();

% DESTINATION BODY
% Modify for change in destination %

Dest = Pluto;               %% User Input Based on Desired Destination %%

discon = 5.3;
 % discontinuity factor (1.6,1.9,0.8,1.6,5.3,4.6)

earth.a = 2000 + Earth.r;
earth.e = 0;
 % Initial Earth orbit

dest.a = 50*Dest.r; % use 50*R for STK
dest.e = 0.95;
 % Final destination orbit

%DDate = 0.25:0.0001:0.35; % (Planets)
DDate = 0.28:0.00006:0.34; % (Pluto)
%DDate = 0.08:.00006:.14; % (Quaoar)
 % (centuries past J2000)
TOF = 12.5:0.05:20; % years (1-2.5,2-6,5-10,9-14,12.5-17.5,12.5-17.5)

DV_a = zeros(length(DDate),1);
DV_1a = zeros(length(DDate),1);
DV_2a = zeros(length(DDate),1);
DV_3a = zeros(length(DDate),1);
TOF1_a = zeros(length(DDate),1);
min_DD = zeros(length(DDate),1);
opt_Eartha = cell(length(DDate),1);
opt_Desta = cell(length(DDate),1);
opt_sola = cell(length(DDate),1);
DV = zeros(length(TOF),1);
J = zeros(length(TOF),1);
DV_1 = zeros(length(TOF),1);
DV_2 = zeros(length(TOF),1);
DV_3 = zeros(length(TOF),1);
TOF_1 = zeros(length(TOF),1);
FOM = zeros(length(TOF),1);
```

```
PCDV = zeros(length(TOF),length(DDate));
PCDV1 = zeros(length(TOF),length(DDate));
PCDV2 = zeros(length(TOF),length(DDate));
PCDV3 = zeros(length(TOF),length(DDate));
opt_Earth = cell(length(TOF),1);
opt_Dest = cell(length(TOF),1);
opt_sol = cell(length(TOF),1);

testR = zeros(length(DDate),1);
for i = 1:length(TOF) % iterates through TOF in years
    for j = 1:length(DDate) % iterates through depature dates

        % Planet Positions
        [Earth,Dest] = Planet_Positions(Earth,Dest,DDate(j),TOF(i)/100);

        % Lamberts Black Box

        n = 100;
         % fraction levels
        tol = 1e-8;
         % output tolerance
        kmax = 100;
         % maximum number of iterations
        [sol.a,sol.p,Earth.Vdep,Dest.Varr,~,G,ta] =
Lambert(Earth.R,Dest.R,TOF(i)*(365.25*24*3600),Sol.mu,1,n,tol,kmax);
        %[sol.a,sol.p,Vdep,Varr] =
Lambert2(Earth.R,Dest.R,TOF(i)*(365.25*24*3600),Sol.mu,0,tol,kmax);

        testR(j,:) = ta;%[ta,G,0];
        % discontinuity when transfer angle is ~ 0 rads
        if abs(pi-ta) < 0.1*discon
            sol.a = NaN;
            sol.p = NaN;
            Vdep = [NaN,NaN,NaN];
            Varr = [NaN,NaN,NaN];
        end

        % Earth Departure
        [Earth,DV1] = Departure(Sol,Earth,Dest,sol,earth,DDate(j),TOF(i));

        % Destination Arrival
        [Dest,DV3] = Arrival(Sol,Dest,dest,DDate(j));

        % Inclination Change
        [DV2,TOF1,sol] = inclin_change(Sol,sol,Dest,DDate(j));

        DV_a(j) = DV1 + DV2 + DV3;
        DV_1a(j) = DV1;
        DV_2a(j) = DV2;
        DV_3a(j) = DV3;
        TOF1_a(j) = TOF1;
        opt_Eartha(j) = {Earth};
        opt_Desta(j) = {Dest};
        opt_sola(j) = {sol};
```

```
    end

    [DV(i),J(i)] = min(DV_a);
    min_DD(i) = DDate(J(i));
    DV_1(i) = DV_1a(J(i));
    DV_2(i) = DV_2a(J(i));
    DV_3(i) = DV_3a(J(i));
    TOF_1(i) = TOF1_a(J(i));
    opt_Earth(i) = opt_Eartha(J(i));
    opt_Dest(i) = opt_Desta(J(i));
    opt_sol(i) = opt_sola(J(i));
    FOM(i) = DV(i) + TOF(i);
    PCDV(i,:) = DV_a;
    PCDV1(i,:) = DV_1a;
    PCDV2(i,:) = DV_2a;
    PCDV3(i,:) = DV_3a;
    PCtest(i,:) = testR;
end

[opt.FOM,I] = min(FOM);
opt.TOF = TOF(I);
opt.DV = DV(I);
opt.DD = min_DD(I);
opt.DV1 = DV_1(I);
opt.DV2 = DV_2(I);
opt.DV3 = DV_3(I);
opt.TOF1 = TOF_1(I);
opt.TOF2 = (opt.TOF*365*24*3600) - opt.TOF1;
opt.Earth = opt_Earth(I);
opt.Dest = opt_Dest(I);
opt.sol = opt_sol(I);
```

```
fprintf('Minimum FOM: %0.3f\n',opt.FOM)
fprintf('Optimum TOF: %0.2f years\n',opt.TOF)
fprintf('Optimum DV: %0.3f km/s\n',opt.DV)

%for d = 1:length(DDate)
%end
figure
plot((DDate*100) + 2000,PCDV(I,:))
hold on
xSpline = interp1((DDate*100) + 2000,PCDV(I,:),(DDate*100) + 2000,'spline');
plot((DDate*100) + 2000,xSpline)
hold on
plot((DDate*100) + 2000,PCDV(I,:))
ylabel('Delta-V (km/s)')
xlabel('Departure Date')
ylim([20 35])
xlim([(DDate(1)*100)+2000 (DDate(end)*100)+2000])

figure
plot(TOF,PCDV(:,J(I)))
%hold on
%plot(TOF,DV)
```

```
ylabel('Delta-V (km/s)')
xlabel('Transfer Time (years)')
xlim([1 16])
ylim([0 30])

%figure
%plot(TOF,(PCDV1(:,J(I))./PCDV(:,J(I))))
%hold on
%plot(TOF,(PCDV2(:,J(I))./PCDV(:,J(I))))
%hold on
%plot(TOF,(PCDV3(:,J(I))./PCDV(:,J(I))))

output.DV = PCDV(:,J(I));
output.DV1 = PCDV1(:,J(I));
output.DV2 = PCDV2(:,J(I));
output.DV3 = PCDV3(:,J(I));
output.DV_alt = DV;
save('Saturn.mat',"output")

figure
plot(TOF,DV)
ylabel('Delta-V (km/s)')
xlabel('Transfer Time (years)')
ylim([0 30])

%figure
%plot(DDate,sqrt((testR(:,1).^2)+(testR(:,1).^2)+(testR(:,1).^2)))
%hold on
%plot(DDate,testR(:,1))
%hold on
%plot(TOF,PCtest(:,J(I)))
%hold on
%plot(DDate,testR(:,3))

%figure
%plot(TOF,PCDV(:,677))
%hold on
%plot(TOF,PCDV(:,659))

%figure
%plot(1:length(J),J)
%xlim([0 length(TOF)])
%ylim([0 length(DDate)])
%xlabel('Departure Date Index')
%ylabel('Time of Flight Index')

%figure
%contour(DDate,TOF,PCDV,'ShowText','on','LevelList',[4,6,8,10,12,14,16,18,20,22,24])
%ylabel('Transfer Time (years)')
%xlabel('Departure Date')

%figure
%contour(DDate,TOF,PCtest,'ShowText','on','LevelList',[2.7,2.8,2.9,3,3.1,3.2,3.3,3.4,3.5]
)
```

```
%ylabel('Transfer Time (years)')
%xlabel('Departure Date')
```

```
g = 9.81; % m/s^2
 % gravitational accleration on Earth

% CNTP Performance
Isp = 1800; % s
 % Specific Impulse
m_e = 1650; % kg
 % engine mass

% LV Constraints
R = 4.3; % m (Starship)
 % max tank diameter

m = 800;%[800,1000,1200];
mlp = 0.5*m;
m_o = zeros(length(DV),1);
m_p = zeros(length(DV),1);

figure
for m_ldry = m
    for k = I%1:length(DV)

        m_l = 1.5*m_ldry;%+mlp; % kg

        % Tank estimates
        m_t = 0; % kg
         % tank mass estimate for LH2
        tank_margin = 2;

        while tank_margin > 1
            m_t2 = m_t;
            m_f = m_l + m_e + m_t2; % kg
             % final mission mass
            m_ps = m_f*(exp((DV(k))*1000/(g*Isp))-1); % kg
             % propellant mass
            V_p = m_ps*1.03/71; % m^3
             % full prop volume
            V_pl = V_p - ((4/3)*pi*R^3);
             % cylindrical prop volume
            L = V_pl/(pi*R^2); % m
             % tank cylindrical length
            %if L < 0
            %    R = R - 0.01;
            %    tank_margin = 2;
            %    fprintf('Warning! Tank not full!\n')
            %end
            m_t = (m_ps*0.128) + (2.88*((2*R*pi*L)+(4*pi*R^2)));
             % new tank mass
            tank_margin = abs(m_t - m_t2);
        end
```

```
        m_p(k) = m_ps;
        m_o(k) = m_ps + m_f; % kg
         % initial mission mass
    end

    plot(TOF,m_o./1000)
    hold on
end
ylim([0 42])
xlim([8 20])
legend('Payload Dry Mass: 800 kg','1000 kg','1200 kg')
xlabel('Transfer Time (years)')
ylabel('Initial Vehicle Mass (mT)')
%{
PGAT = load('Quaoar_PGA_TransitTime');
PGAM = load('Quaoar_PGA_Mass');
plot(PGAT.mass_transit,PGAM.m_o./1000)
hold on
PGAT = load('Pluto_PGA_TransitTime');
PGAM = load('Pluto_PGA_Mass');
plot(PGAT.mass_transit,PGAM.m_o./1000)
xlim([11 20])
ylim([0 42])
xlabel('Transfer Time (years)')
ylabel('Initial Vehicle Mass (mT)')
legend('Quaoar Direct Trajectory','Quaoar PGA Trajectory','Pluto PGA Trajectory')
%}
%figure
%plot(m,m_o)

%fprintf('Required Propellant Mass: %0.2f kg\n',m_p)
%fprintf('Spacecraft Total Mass: %0.2f kg\n',m_o)
```

Definition of Planetary Ephemeris

```
function [Sol,Earth,Jupiter,Saturn,Uranus,Neptune,Pluto,Quaoar] = GetEphemeris()

% SOL

Sol.mu = 1.327e11; % km^3/s^2
 % Gravitational parameter of Sol
Sol.AU = 1.496e8; % km
 % Definition of 1 astronomical unit

% EARTH

Earth.mu = 3.9860e5; % km^3/s^2                  %%
 % Gravitational parameter of Earth
Earth.r = 6378.14; % km                          %%
```

```
 % Radius of Earth
Earth.a =@(T) (1.00000261+(T*0.00000562))*Sol.AU; % km
 % Semi-major axis of Earth orbit
Earth.e =@(T) 0.01671123-(T*0.00004392);
 % Eccentricity of Earths orbit
Earth.i =@(T) (-0.00001531-(T*0.01294668))*pi/180; % rads
 % inclination of Earths orbit
Earth.L =@(T) (100.46457166+(T*35999.37244981))*pi/180; % rads
 % mean longitude
Earth.theta =@(T) (102.93768193+(T*0.32327364))*pi/180; % rads
 % longitude of perihelion
Earth.RAAN =@(T) (0.0+(T*0.0))*pi/180; % rads
 % Longitude of ascending node

% JUPITER
Jupiter.mu = 1.26687e8; % km^3/s^2               %%
Jupiter.r = 69911; % km                          %%
Jupiter.a =@(T) (5.20288700-(T*0.00011607))*Sol.AU; % km
Jupiter.e =@(T) 0.04838624-(T*0.00013253);
Jupiter.i =@(T) (1.30439695-(T*0.00183714))*pi/180; % rads
Jupiter.L =@(T) (34.39644051+(T*3034.74612775))*pi/180; % rads
Jupiter.theta =@(T) (14.72847983+(T*0.21252668))*pi/180; % rads
Jupiter.RAAN =@(T) (100.47390909+(T*0.20469106))*pi/180; % rads

% SATURN

Saturn.mu = 3.7931e7; % km^3/s^2
Saturn.r = 58232; % km
Saturn.a =@(T) (9.53667594-(T*0.00125060))*Sol.AU; % km
Saturn.e =@(T) 0.05386179-(T*0.00050991);
Saturn.i =@(T) (2.48599187+(T*0.00193609))*pi/180; % rads
Saturn.L =@(T) (49.95424423+(T*1222.49362201))*pi/180; % rads
Saturn.theta =@(T) (92.59887831-(T*0.41897216))*pi/180; % rads
Saturn.RAAN =@(T) (113.66242448-(T*0.28867794))*pi/180; % rads

% URANUS

Uranus.mu = 5.7940e6; % km^3/s^2
Uranus.r = 25362; % km
Uranus.a =@(T) (19.18916464-(T*0.00196176))*Sol.AU; % km
Uranus.e =@(T) 0.04725744-(T*0.00004397);
Uranus.i =@(T) (0.77263783-(T*0.00242939))*pi/180; % rads
Uranus.L =@(T) (313.23810451+(T*428.48202785))*pi/180; % rads
Uranus.theta =@(T) (170.95427630+(T*0.40805281))*pi/180; % rads
Uranus.RAAN =@(T) (74.01692503+(T*0.04240589))*pi/180; % rads

% NEPTUNE

Neptune.mu = 6.8351e6; % km^3/s^2
Neptune.r = 24624; % km
Neptune.a =@(T) (30.06992276+(T*0.00026291))*Sol.AU; % km
Neptune.e =@(T) 0.00859048+(T*0.00005105);
Neptune.i =@(T) (1.77004347+(T*0.00035372))*pi/180; % rads
```

```
Neptune.L =@(T) (-55.12002969+(T*218.45945325))*pi/180; % rads
Neptune.theta =@(T) (44.96476227-(T*0.32241464))*pi/180; % rads
Neptune.RAAN =@(T) (131.78422574-(T*0.00508664))*pi/180; % rads

% PLUTO

Pluto.mu = 8.724e2; % km^3/s^2
Pluto.r = 1195; % km
Pluto.a =@(T) (39.48211675-(T*0.00031596))*Sol.AU; % km
Pluto.e =@(T) 0.24882730+(T*0.00005170);
Pluto.i =@(T) (17.14001206+(T*0.00004818))*pi/180; % rads
Pluto.L =@(T) (238.92903833+(T*145.20780515))*pi/180; % rads
Pluto.theta =@(T) (224.06891629-(T*0.04062942))*pi/180; % rads
Pluto.RAAN =@(T) (110.30393684-(T*0.01183482))*pi/180; % rads

% QUAOAR (Horizons Small Body Database Lookup)

Quaoar.mu = 93.4332; % km^3/s^2
Quaoar.r = 555; % km
Quaoar.a =@(T) (43.38833028+(T*0))*Sol.AU; % km
Quaoar.e =@(T) 0.04028864+(T*0);
Quaoar.i =@(T) (7.99130083+(T*0))*pi/180; % rads
Quaoar.L =@(T) (281.22046283+(T*125.6157883))*pi/180; % rads
Quaoar.theta =@(T) (346.79068308+(T*0))*pi/180; % rads
Quaoar.RAAN =@(T) (189.10126806+(T*0))*pi/180; % rads

end
```

Calculation of Planet Positions

```
function [Earth,Dest] = Planet_Positions(Earth,Dest,DD,TOF)

T = DD;
% Earth.n*(departure - Earth.tp) = E1 - (Earth.e)*sin(E1); % solve for E, Newton
Earth.E1 = newton(1,Earth.e(T),Earth.L(T)-Earth.theta(T),1000,1e-8);%Earth.n*(DD -
Earth.tp)*365.25*24*3600
Earth.test = Earth.L(T)-Earth.theta(T);
while Earth.E1 > 2*pi
    Earth.E1 = Earth.E1 - (2*pi);
end
r1 = Earth.a(T)*(1 - (Earth.e(T)*cos(Earth.E1)));
%O1 = Earth.theta + (2*atan((((1+Earth.e)/(1-Earth.e))^(1/2))*tan(E1/2)));
O1 = Earth.theta(T)-Earth.RAAN(T)+(2*atan((((1+Earth.e(T))/(1-
Earth.e(T)))^(1/2))*tan(Earth.E1/2)));
%U1 = Earth.RAAN;
U1 = Earth.RAAN(T);
%i1 = Earth.i;
i1 = Earth.i(T);

Earth.DCM = [(cos(U1)*cos(O1))-(sin(U1)*sin(O1)*cos(i1)),-(cos(U1)*sin(O1))-
```

```
(sin(U1)*cos(O1)*cos(i1)),(sin(U1)*sin(i1));...
    (sin(U1)*cos(O1))+(cos(U1)*sin(O1)*cos(i1)),-
(sin(U1)*sin(O1))+(cos(U1)*cos(O1)*cos(i1)),-(cos(U1)*sin(i1));...
    (sin(O1)*sin(i1)),(cos(O1)*sin(i1)),cos(i1)];
 % Including only r components for simplicity
Earth.R = Earth.DCM*[r1;0;0];

T = DD+(TOF);
% Dest.n*(departure + TOF - Dest.tp) = E2 - (Dest.e)*sin(E2); % solve for E, Newton
Dest.E2 = newton(1,Dest.e(T),Dest.L(T)-Dest.theta(T),1000,1e-8); %Dest.n*(DD + TOF -
Dest.tp)*365.25*24*3600
while Dest.E2 > 2*pi
    Dest.E2 = Dest.E2 - (2*pi);
end
r2 = Dest.a(T)*(1 - (Dest.e(T)*cos(Dest.E2)));
%O2 = Dest.theta + (2*atan((((1+Dest.e)/(1-Dest.e))^(1/2))*tan(E2/2)));
O2 = Dest.theta(T)-Dest.RAAN(T)+(2*atan((((1+Dest.e(T))/(1-
Dest.e(T)))^(1/2))*tan(Dest.E2/2)));
%U2 = Dest.RAAN;
U2 = Dest.RAAN(T);
%i2 = Dest.i;
i2 = Dest.i(T);

Dest.DCM = [(cos(U2)*cos(O2))-(sin(U2)*sin(O2)*cos(i2)),-(cos(U2)*sin(O2))-
(sin(U2)*cos(O2)*cos(i2)),(sin(U2)*sin(i2));...
    (sin(U2)*cos(O2))+(cos(U2)*sin(O2)*cos(i2)),-
(sin(U2)*sin(O2))+(cos(U2)*cos(O2)*cos(i2)),-(cos(U2)*sin(i2));...
    (sin(O2)*sin(i2)),(cos(O2)*sin(i2)),cos(i2)];
 % Including only r components for simplicity
Dest.R = Dest.DCM*[r2;0;0];

end
```

Newton Method Solution for Kepler's Equation

```
function num = newton(x_o,c1,c2,max,tol)
% Purpose:  Using Newtons method to numerically approximate any given value
% Inputs:   c1-c3 - variable or constant values needed in chosen equation
%           tol - tolerance for numerical approximation
%           max - maximum number of iterations in loop
% Outputs:  numerically approximated value
    x = zeros(1,max);

    f =@(E,e,M) M - E + e*sin(E);
    fp =@(E,e) e*cos(E) - 1;

    for i = 1:max
        if i == 1
            y = f(x_o,c1,c2);
            yp = fp(x_o,c1);
```

```
            x(1,i) = x_o - (y/yp);
            % calculations for initial run
        else
            y = f(x(1,i-1),c1,c2);
            yp = fp(x(1,i-1),c1);
            x(1,i) = x(1,i-1) - (y/yp);
            % calculations for non-initial run

            if abs(x(1,i)-x(1,i-1)) < tol
                break;
            end
            % ends loop when tolerance is met
        end
    end
    num = x(1,i);
    % final value
end
```

Lambert Solver

```
function [A,P,V1,V2,conv,G,ta] = Lambert(R1,R2,TOF,mu,JJ,n,tol,kmax)
%{
    Programmer: Grant Hecht
    Date:       3/11/2019
    File:       Lambert.m
    Purpose:    This function solves Lambert's Problem using Battin's
                method.

    Inputs:
    R1:     Vector to Pt#1
    R2:     Vector to Pt#2
    TOF:    Time of Flight
    mu:     Gravitational parameter for central body
    JJ:     Integer that determines initial guess for x
                (set JJ = 1 for an ellipse)
                (set JJ = 0 for a parabola or hyperbola)
    n:      Number of continued fracton levels
                (set n = 0 for default of 10)
                (recomend setting n >= 100 for most accurate results)
    tol:    Tolerance to exit iterations
    kmax:   Maximum Iterations


    Outputs:
    V1:     Velocity Vector at Pt#1
    V2:     Velocity Vector at Pt#2
    conv:   Boolean to indicate convergence.

%}
% Defalt Value for n
```

```
n_default = 10;

% If does not converge, set as false
conv = true;

% Sets n to defalt value if n = 0 is passed
if n == 0
    n = n_default;
end

% Find Transfer Angle
ta = acos(dot(R1,R2)/(norm(R1)*norm(R2)));
if R1(1)*R2(2)-R1(2)*R2(1) < 0
    ta = 2*pi - ta;
end

% Find Chord
c = sqrt(norm(R1)^2 + norm(R2)^2 - 2*norm(R1)*norm(R2)*cos(ta));

% Find Semi-Perimeter
s = (norm(R1) + norm(R2) + c)/2;

% Find Lambda
lambda = sqrt(norm(R1)*norm(R2))*cos(ta/2)/s;

% Find w
w = atan((norm(R2)/norm(R1))^0.25)-(pi/4);

% Find l
if (0 < ta) && (ta < pi)
    l = (sin(ta/4)^2+tan(2*w)^2)/(sin(ta/4)^2+tan(2*w)^2+cos(ta/2));
elseif (pi <= ta) && (ta < 2*pi)
    l = (cos(ta/4)^2+tan(2*w)^2-cos(ta/2))/(cos(ta/4)^2+tan(2*w)^2);
else
    fprintf('Cannot Compute for Transfer Angle of 0 or 360 degrees.');
    return
end

% Find m
m = (8*mu.*TOF.^2)/(s^3*(1+lambda)^6);

% For Eliptical Transfer Orbit Use x = l for Initial Guess
% For Hyperbolic or Parabolic Transfer Orbit Use x = 0.
if JJ == 0
    x = 0;
else
    x = l;
end

%Define Velocity Vectors
V1 = zeros(3,1);
V2 = zeros(3,1);
```

```
%Define delta x and counter
DX = 100;
k  = 0;

%Iterate to solve
while abs(DX) > tol

    % Breaks Itteration and sets conv = false if k = kmax
    if k >= kmax
        conv = false;
        break
    end

    % Calculates Continued Fraction PHI for 'n' Levels
    eta = x/(sqrt(1+x)+1)^2;
    f   = 1;
    % Itterate to Calculate levels 4 -> n
    for j = n:-1:4
        ceta = j^2/((2*j)^2-1);
        f = 1 + ceta*eta/f;
    end
    % Finishes Calculation of PHI with levels 1 -> 3
    PHI = 8*(sqrt(1+x)+1)/(3+1/(5+eta+(9/7)*eta/f));

    h1 = (l+x)^2*(1+3*x+PHI)/((1+2*x+l)*(4*x+PHI*(3+x)));
    h2 = m*(x-l+PHI)/((1+2*x+l)*(4*x+PHI*(3+x)));
    B  = 27*h2/(4*(1+h1)^3);
    u  = B/(2*(sqrt(1+B)+1));

    % Calculates Continued Fraction K(u) for 'n' Levels
    f = 1;
    r = n/2-1;
    % Iterate to Calculate Levels 3 -> n
    for j = r:-1:1
        g2n  = 2*(3*j+1)*(6*j-1)/(9*(4*j-1)*(4*j+1));
        g2n1 = 2*(3*j+2)*(6*j+1)/(9*(4*j+1)*(4*j+3));
        f = 1 + g2n*u/(1 + g2n1*u/f);
    end
    % Finishes Calculation of K(u) with levels 1 -> 2
    K = (1/3)/(1+(4/27)*u/f);

    % Calculates New Values for y and x
    yNew = ((1+h1)/3)*(2+sqrt(1+B)/(1+2*u*K^2));
    xNew = sqrt(((1-l)./2).^2+m/yNew.^2)-(1+l)/2;

    % Compares xNew with x
    DX = abs(xNew - x);

    % Sets x and y to xNew and yNew
    x = xNew;
    y = yNew;

    k = k + 1;
```

```
end

%Computes Orbit Parameters and Initial and Final Velocity
A  = m.*s.*(1+lambda).^2/(8.*x.*y.^2);
P0 = c^2*(1+x)^2/(16*A*x);
P  = 4*norm(R1)*norm(R2)*P0*sin(ta/2)^2/c^2;
F  = 1-(norm(R2)/P)*(1-cos(ta));
G  = norm(R1)*norm(R2)*sin(ta)/sqrt(mu*P);
FDOT = sqrt(mu/P)*tan(ta/2)*((1-cos(ta))/P-1/norm(R2)-1/norm(R1));
GDOT = 1-(norm(R1)/P)*(1-cos(ta));
for K=1:3
    V1(K)=(1/G)*(R2(K)-(F*R1(K)));
    V2(K)=FDOT*R1(K)+GDOT*V1(K);
end
end
```

Departure Burn Analysis

```
function [Earth,DV1] = Departure(Sol,Earth,Dest,sol,earth,T,TOF)

Earth.v = sqrt(Sol.mu*((2/norm(Earth.R))-(1/Earth.a(T))));
Earth.h = sqrt(Sol.mu*Earth.a(T)*(1-Earth.e(T)^2));
Earth.y = acos(Earth.h/(Earth.v*norm(Earth.R)));
if Earth.E1 > pi
    Earth.y = -Earth.y;
end
Earth.V = Earth.DCM*[Earth.v*sin(Earth.y);Earth.v*cos(Earth.y);0];
Earth.Vinf = Earth.Vdep - Earth.V;

hyper_a = -Earth.mu/(norm(Earth.Vinf)^2);
r_p = earth.a*(1-earth.e);

hyper_v = sqrt(Earth.mu*((2/r_p)-(1/hyper_a)));
ellip_v = sqrt(Earth.mu*((2/r_p)-(1/earth.a)));

DV1 = hyper_v - ellip_v;
Earth.DV1 = Earth.DCM*[0;DV1;0];

end
```

Arrival Burn Analysis

```
function [Dest,DV2] = Arrival(Sol,Dest,dest,T)

Dest.v = sqrt(Sol.mu*((2/norm(Dest.R))-(1/Dest.a(T))));
Dest.h = sqrt(Sol.mu*Dest.a(T)*(1-Dest.e(T)^2));
Dest.y = acos(Dest.h/(Dest.v*norm(Dest.R)));
if Dest.E2 > pi
```

```
    Dest.y = -Dest.y;
end
Vinf = Dest.Varr - (Dest.DCM*[Dest.v*sin(Dest.y);Dest.v*cos(Dest.y);0]);

hyper_a = -Dest.mu/(norm(Vinf)^2);
r_p = dest.a*(1-dest.e);

hyper_v = sqrt(Dest.mu*((2/r_p)-(1/hyper_a)));
ellip_v = sqrt(Dest.mu*((2/r_p)-(1/dest.a)));

DV2 = hyper_v - ellip_v;

end
```

Inclination Change Analysis

```
function [DV,TOF,sol] = inclin_change(Sol,sol,Dest,T)

sol.e = sqrt(1-(sol.p/sol.a));
 % solar orbit eccentricity
sol.n = sqrt(abs(Sol.mu/sol.a^3));
     % solar mean motion

sol.nu_dest = acos(((sol.p/mag(Dest.R))-1)/sol.e);
 % true anomaly of destination planet on solar orbit
if Dest.y < 0
    sol.nu_dest = 2*pi - sol.nu_dest;
end % quad check
sol.nu_DV = sol.nu_dest - (pi/2);
 % true anomaly of inclination change

r_DV = sol.p/(1+(sol.e*cos(sol.nu_DV)));
 % Position of inclination change
V_DV = sqrt(Sol.mu*((2/r_DV)-(1/sol.a)));
 % inclination change initial velocity

DV = 2*V_DV*sin(Dest.i(T)/2);
 % Delta-V

if sol.e < 1
    sol.E_DV = acos((sol.e+cos(sol.nu_DV))/(1+(sol.e*cos(sol.nu_DV))));
    if sol.nu_DV > pi
        sol.E_DV = 2*pi - sol.E_DV;
    end % quad check
    sol.TOF = (1/sol.n)*(sol.E_DV-(sol.e*sin(sol.E_DV)));
else
    sol.F_DV = acosh((sol.e+cos(sol.nu_DV))/(1+(sol.e*cos(sol.nu_DV))));
    sol.TOF = (1/sol.n)*((sol.e*sinh(sol.F_DV))-sol.F_DV);
end
TOF = sol.TOF;
```

```
end
```

Appendix C. Gravity Assist Trajectory Patched Conic Model

Main Function

```
% Programmer: Will Ziehm
% Project: Delta V Calculations to an Outer Planet on a Flyby Transfer
% Date: January 2023

clc
clear variables
close all

[Sol,Earth,Jupiter,Saturn,Uranus,Neptune,Pluto,Quaoar] = GetEphemeris();

% DEPARTURE BODY (Earth)

earth.a = 2000 + Earth.r;
earth.e = 0;
 % Initial Earth orbit

% FLYBY BODY
Dest1 = Jupiter;

dest1.r_p = 12.5*Dest1.r;
 % Flyby periapsis radius
%dest1.tol = 1e-4;
 % tolerance on rp match

% DESTINATION BODY
Dest2 = Quaoar;

dest2.a = 50*Dest2.r; % use 50*R for STK
dest2.e = 0.95;
 % Final destination orbit

% EVENT TIMES

T1 = 4:.006:10; % (Quaoar)
%T1 = 28:.006:34; % (Pluto)
 % Departure Date, years past J2000
T2 = 0.5:.003:2; % years
 % TOF Departure to Flyby, range
T3i = 5; % years
 % TOF Flyby to Arrival, initial guess

% LAMBERT INPUTS

n = 100;
 % fraction levels
tol = 1e-8;
 % output tolerance
```

```
kmax = 300;
 % maximum number of iterations

TT_FOM = zeros(length(T2),1);
TT_DV_1 = zeros(length(T2),1);
TT_DV_2 = zeros(length(T2),1);
TT_Earth = cell(length(T2),1);
TT_earth = cell(length(T2),1);
TT_Dest1 = cell(length(T2),1);
TT_dest1 = cell(length(T2),1);
TT_Dest2 = cell(length(T2),1);
TT_dest2 = cell(length(T2),1);
TT_sol1 = cell(length(T2),1);
TT_sol2 = cell(length(T2),1);
TT_T3 = zeros(length(T2),1);

all_DV1 = zeros(length(T1),length(T2));
all_DV2 = zeros(length(T1),length(T2));
all_DV = zeros(length(T1),length(T2));
all_T3 = zeros(length(T1),length(T2));
all_Earth = cell(length(T1),length(T2));
all_earth = cell(length(T1),length(T2));
all_Dest1 = cell(length(T1),length(T2));
all_dest1 = cell(length(T1),length(T2));
all_Dest2 = cell(length(T1),length(T2));
all_dest2 = cell(length(T1),length(T2));
all_sol1 = cell(length(T1),length(T2));
all_sol2 = cell(length(T1),length(T2));

opt_FOM = zeros(length(T1),1);
J = zeros(length(T1),1);
opt_DV_1 = zeros(length(T1),1);
opt_DV_2 = zeros(length(T1),1);
opt_Earth = cell(length(T1),1);
opt_Dest1 = cell(length(T1),1);
opt_Dest2 = cell(length(T1),1);
opt_sol1 = cell(length(T1),1);
opt_sol2 = cell(length(T1),1);
opt_T2 = zeros(length(T1),1);
opt_T3 = zeros(length(T1),1);

%for i = 1:length(TOF) % iterates through TOF in years
%    for j = 1:length(DDate) % iterates through depature dates

for i = 1:length(T1) % Iterates through departure date
    fprintf('Progress: %0.3f Complete\n',i/length(T1))
    for j = 1:length(T2) % Iterates through transfer time for each dd

        % Planet Positions
        [Earth] = Planet_Position(Sol,Earth,T1(i));
        [Dest1] = Planet_Position(Sol,Dest1,T1(i)+T2(j));

        % Lamberts Black Box
        % (discontinuity when transfer angle is ~ 0 rads)
```

```
        [sol1.a,sol1.p,Earth.Vdep,Dest1.Varr,~,G1,ta1] = ...
            Lambert(Earth.R,Dest1.R,T2(j)*(365.25*24*3600),Sol.mu,1,n,tol,kmax);
         % Transfer Arc between Earth and Dest1
        if abs(pi-ta1) < 0.08
            sol1.a = NaN;
            sol1.p = NaN;
            Earth.Vdep = [NaN,NaN,NaN];
            Dest1.Varr = [NaN,NaN,NaN];

            DV1 = NaN;
            DV2 = NaN;
        else

            % Earth Departure
            [Earth,DV1] = Departure(Earth,earth);

            % Fly-by
            [Dest1,dest1] = Flyby(Dest1,dest1);

            conv = false;
            k = 0;
            T3s = linspace(T3i,T3i+kmax*0.05,kmax);
            kconv = kmax;
            for k = 1:kmax
                [Dest2] = Planet_Position(Sol,Dest2,T1(i)+T2(j)+T3s(k));
                [sol2.a,sol2.p,Dest1.Vdep,Dest2.Varr,~,~,~] = ...
                    Lambert(Dest1.R,Dest2.R,T3s(k)*(365.25*24*3600),Sol.mu,1,n,tol,kmax);
                Dest1.Vinfp = Dest1.Vdep - Dest1.V;
                Dest1.visvisa_p(k) = dot(Dest1.Vinfp,Dest1.Vinfp);
                %T3 = T3 + 0.1;
                if k > 1 && ~conv
                    if Dest1.visvisa_m < Dest1.visvisa_p(k-1) && Dest1.visvisa_m >
Dest1.visvisa_p(k)
                        if
acos(dot(Dest1.Vinfp,Dest1.Vinfm)/(norm(Dest1.Vinfm)*norm(Dest1.Vinfp))) < dest1.delta
                            conv = true;
                            kconv = k;
                        end
                    end
                end
            end
            T3 = T3s(kconv);% = T3 - 0.1*(kmax-kconv);
            [Dest2] = Planet_Position(Sol,Dest2,T1(i)+T2(j)+T3);
            [sol2.a,sol2.p,Dest1.Vdep,Dest2.Varr,~,~,~] = ...
                Lambert(Dest1.R,Dest2.R,T3*(365.25*24*3600),Sol.mu,1,n,tol,kmax);

            if conv == false
                DV2 = NaN;
            else
                % Destination Arrival
                [Dest2,DV2] = Arrival(Dest2,dest2);
            end
        end
```

```
        Earth.ta = acos(dot(Earth.R,[1;0;0])/(norm(Earth.R)));
        if Earth.R(2) < 0
            Earth.ta = 2*pi - Earth.ta;
        end
        Dest1.ta = acos(dot(Dest1.R,[1;0;0])/(norm(Dest1.R)));
        if Dest1.R(2) < 0
            Dest1.ta = 2*pi - Dest1.ta;
        end
        Dest2.ta = acos(dot(Dest2.R,[1;0;0])/(norm(Dest2.R)));
        if Dest2.R(2) < 0
            Dest2.ta = 2*pi - Dest2.ta;
        end

        FOM = (T2(j) + T3) + 0.5*(DV1 + DV2);

        TT_FOM(j) = FOM;
        TT_DV_1(j) = DV1;
        TT_DV_2(j) = DV2;
        TT_T3(j) = T3;
        TT_Earth(j) = {Earth};
        TT_earth(j) = {earth};
        TT_Dest1(j) = {Dest1};
        TT_dest1(j) = {dest1};
        TT_Dest2(j) = {Dest2};
        TT_dest2(j) = {dest2};
        TT_sol1(j) = {sol1};
        TT_sol2(j) = {sol2};
        %all_vdep(j) = Dest1.vdep;
    end

    [opt_FOM(i),J(i)] = min(TT_FOM);
    %opt_DV_1(i) = TT_DV_1(J(i));
    %opt_DV_2(i) = TT_DV_2(J(i));
    %opt_T2(i) = T2(J(i));
    %opt_T3(i) = TT_T3(J(i));
    %opt_Earth(i) = TT_Earth(J(i));
    %opt_Dest1(i) = TT_Dest1(J(i));
    %opt_Dest2(i) = TT_Dest2(J(i));
    %opt_sol1(i) = TT_sol1(J(i));
    %opt_sol2(i) = TT_sol2(J(i));

    all_DV1(i,:) = TT_DV_1;
    all_DV2(i,:) = TT_DV_2;
    all_DV(i,:) = TT_DV_1 + TT_DV_2;
    all_T3(i,:) = TT_T3;
    all_Earth(i,:) = TT_Earth;
    all_earth(i,:) = TT_earth;
    all_Dest1(i,:) = TT_Dest1;
    all_dest1(i,:) = TT_dest1;
    all_Dest2(i,:) = TT_Dest2;
    all_dest2(i,:) = TT_dest2;
    all_sol1(i,:) = TT_sol1;
    all_sol2(i,:) = TT_sol2;
end
```

```
[opt.FOM,I] = min(opt_FOM);
opt.DV1 = all_DV1(I,J(I));
opt.DV2 = all_DV2(I,J(I));
opt.DV = opt.DV1 + opt.DV2;
opt.T2 = T2(J(I));
opt.T3 = all_T3(I,J(I));
opt.Earth = all_Earth(I,J(I));
opt.earth = all_earth(I,J(I));
%opt.Dest1 = opt_Dest1(I);
opt.Dest1 = all_Dest1(I,J(I));
opt.dest1 = all_dest1(I,J(I));
opt.Dest2 = all_Dest2(I,J(I));
opt.dest2 = all_dest2(I,J(I));
opt.sol1 = all_sol1(I,J(I));
opt.sol2 = all_sol2(I,J(I));
opt.DD = T1(I);
```

```
fprintf('Minimum FOM: %0.3f\n',opt.FOM)
fprintf('Optimum TOF: %0.2f years\n',opt.T2 + opt.T3)
fprintf('Optimum DV: %0.3f km/s\n',opt.DV)
fprintf('Transfer angles: %0.2f rads, %0.2f rads\n',...

acos(dot(opt.Earth{1,1}.R,opt.Dest1{1,1}.R)/(norm(opt.Earth{1,1}.R)*norm(opt.Dest1{1,1}.R
))),...

acos(dot(opt.Dest1{1,1}.R,opt.Dest2{1,1}.R)/(norm(opt.Dest1{1,1}.R)*norm(opt.Dest2{1,1}.R
))))
%{
figure
plot(T1 + 2000,opt_DV_1 + opt_DV_2)
hold on
xSpline = interp1(T1 + 2000,opt_DV_1 + opt_DV_2,T1 + 2000,'spline');
plot(T1 + 2000,xSpline)
ylabel('Delta-V (km/s)')
xlabel('Departure Date')
%}

for d = 1:length(T1)
    T_transit(d) = T2(J(d)) + all_T3(d,J(d));
    if T_transit(d) == 20.5
        T_transit(d) = 25;
    end
end
figure
plot(T1+2000,T_transit,'o')
xlabel('Departure Date')
ylabel('Transfer Time (years)')
ylim([8 22])
xlim([2004 2010])

figure
plot(T1 + 2000,all_DV(:,J(I)),'o')
%hold on
```

```
%xSpline2 = interp1(T1 + 2000,PCDV(:,J(I)),T1 + 2000,'spline');
%plot(T1 + 2000,xSpline2)
ylabel('Delta-V (km/s)')
xlabel('Departure Date')

figure
plot(T2 + all_T3(I,:),all_DV(I,:))
ylabel('Delta-V (km/s)')
xlabel('Transfer Time (years)')
xlim([8 20])
ylim([14 30])
%{
for a = 1:i
    Earth_ta(a) = all_Earth{a,J(I)}.ta;
    Dest1_ta(a) = all_Dest1{a,J(I)}.ta;
    Dest2_ta(a) = all_Dest2{a,J(I)}.ta;
end

figure
plot(T1 + 2000,Earth_ta)
hold on
plot(T1 + 2000,Dest1_ta)
hold on
plot(T1 + 2000,Dest2_ta)

figure
plot(T1 + 2000,Dest1_ta-Earth_ta)
hold on
plot(T1 + 2000,Dest1_ta-Dest2_ta)
%}

c = I;
%for b = 1:j
Dest1_vsvs_p = all_Dest1{c,J(I)}.visvisa_p;
Dest1_vsvs_m = all_Dest1{c,J(I)}.visvisa_m;
%end

f = figure;
h1 = plot(T3s,Dest1_vsvs_p);
hold on
h2 = plot(T3s,Dest1_vsvs_m*ones(kmax,1));

e1 = sqrt(1-opt.sol1{1,1}.p/opt.sol1{1,1}.a);
e2 = sqrt(1-opt.sol2{1,1}.p/opt.sol2{1,1}.a);
if e1 < 1
    theta1 = acos((opt.sol1{1,1}.a-
opt.Earth{1,1}.r)/(opt.sol1{1,1}.a*e1)):0.01:acos((opt.sol1{1,1}.a-
opt.Dest1{1,1}.r)/(opt.sol1{1,1}.a*e1));
    r1 = opt.sol1{1,1}.a*(1-e1*cos(theta1));
else
    theta1 = acosh((opt.sol1{1,1}.a-
opt.Earth{1,1}.r)/(opt.sol1{1,1}.a*e1)):0.01:acosh((opt.sol1{1,1}.a-
opt.Dest1{1,1}.r)/(opt.sol1{1,1}.a*e1));
    r1 = opt.sol1{1,1}.a*(1-e1*cosh(theta1));
```

```
end

if e2 < 1
    theta2 = acos((opt.sol2{1,1}.a-
opt.Dest1{1,1}.r)/(opt.sol2{1,1}.a*e2)):0.01:acos((opt.sol2{1,1}.a-
opt.Dest2{1,1}.r)/(opt.sol2{1,1}.a*e2));
    r2 = opt.sol2{1,1}.a*(1-e2*cos(theta2));
else
    theta2 = acosh((opt.sol2{1,1}.a-
opt.Dest1{1,1}.r)/(opt.sol2{1,1}.a*e2)):0.01:acosh((opt.sol2{1,1}.a-
opt.Dest2{1,1}.r)/(opt.sol2{1,1}.a*e2));
    r2 = opt.sol2{1,1}.a*(1-e2*cosh(theta2));
end

figure
polarplot(linspace(0,2*pi,100),opt.Earth{1,1}.r*ones(1,100))
hold on
polarplot(linspace(0,2*pi,100),opt.Dest1{1,1}.r*ones(1,100))
hold on
polarplot(theta1,r1)
hold on
polarplot(theta2+(theta1(end)-theta2(1)),r2)
```

```
[m_p,m_o,m_t,L] = MassCalcs(T2,all_DV,I,all_T3);
M_P = m_p(J(I));
M_O = m_o(J(I));
M_T = m_t(J(I));
LL = L(J(I));
```

Definition of Planetary Ephemeris

```
function [Sol,Earth,Jupiter,Saturn,Uranus,Neptune,Pluto,Quaoar] = GetEphemeris()

% SOL

Sol.mu = 1.327e11; % km^3/s^2
 % Gravitational parameter of Sol
Sol.AU = 1.496e8; % km
 % Definition of 1 astronomical unit

% EARTH

Earth.mu = 3.9860e5; % km^3/s^2                    %%
 % Gravitational parameter of Earth
Earth.r = 6378.14; % km                            %%
 % Radius of Earth
Earth.a =@(T) (1.00000261+(T*0.00000562))*Sol.AU; % km
 % Semi-major axis of Earth orbit
Earth.e =@(T) 0.01671123-(T*0.00004392);
 % Eccentricity of Earths orbit
```

```
Earth.i =@(T) (-0.00001531-(T*0.01294668))*pi/180; % rads
 % inclination of Earths orbit
Earth.L =@(T) (100.46457166+(T*35999.37244981))*pi/180; % rads
 % mean longitude
Earth.theta =@(T) (102.93768193+(T*0.32327364))*pi/180; % rads
 % longitude of perihelion
Earth.RAAN =@(T) (0.0+(T*0.0))*pi/180; % rads
 % Longitude of ascending node

% JUPITER
Jupiter.mu = 1.26687e8; % km^3/s^2               %%
Jupiter.r = 69911; % km                          %%
Jupiter.a =@(T) (5.20288700-(T*0.00011607))*Sol.AU; % km
Jupiter.e =@(T) 0.04838624-(T*0.00013253);
Jupiter.i =@(T) (1.30439695-(T*0.00183714))*pi/180; % rads
Jupiter.L =@(T) (34.39644051+(T*3034.74612775))*pi/180; % rads
Jupiter.theta =@(T) (14.72847983+(T*0.21252668))*pi/180; % rads
Jupiter.RAAN =@(T) (100.47390909+(T*0.20469106))*pi/180; % rads

% SATURN

Saturn.mu = 3.7931e7; % km^3/s^2
Saturn.r = 58232; % km
Saturn.a =@(T) (9.53667594-(T*0.00125060))*Sol.AU; % km
Saturn.e =@(T) 0.05386179-(T*0.00050991);
Saturn.i =@(T) (2.48599187+(T*0.00193609))*pi/180; % rads
Saturn.L =@(T) (49.95424423+(T*1222.49362201))*pi/180; % rads
Saturn.theta =@(T) (92.59887831-(T*0.41897216))*pi/180; % rads
Saturn.RAAN =@(T) (113.66242448-(T*0.28867794))*pi/180; % rads

% URANUS

Uranus.mu = 5.7940e6; % km^3/s^2
Uranus.r = 25362; % km
Uranus.a =@(T) (19.18916464-(T*0.00196176))*Sol.AU; % km
Uranus.e =@(T) 0.04725744-(T*0.00004397);
Uranus.i =@(T) (0.77263783-(T*0.00242939))*pi/180; % rads
Uranus.L =@(T) (313.23810451+(T*428.48202785))*pi/180; % rads
Uranus.theta =@(T) (170.95427630+(T*0.40805281))*pi/180; % rads
Uranus.RAAN =@(T) (74.01692503+(T*0.04240589))*pi/180; % rads

% NEPTUNE

Neptune.mu = 6.8351e6; % km^3/s^2
Neptune.r = 24624; % km
Neptune.a =@(T) (30.06992276+(T*0.00026291))*Sol.AU; % km
Neptune.e =@(T) 0.00859048+(T*0.00005105);
Neptune.i =@(T) (1.77004347+(T*0.00035372))*pi/180; % rads
Neptune.L =@(T) (-55.12002969+(T*218.45945325))*pi/180; % rads
Neptune.theta =@(T) (44.96476227-(T*0.32241464))*pi/180; % rads
Neptune.RAAN =@(T) (131.78422574-(T*0.00508664))*pi/180; % rads

% PLUTO
```

```
Pluto.mu = 8.724e2; % km^3/s^2
Pluto.r = 1195; % km
Pluto.a =@(T) (39.48211675-(T*0.00031596))*Sol.AU; % km
Pluto.e =@(T) 0.24882730+(T*0.00005170);
Pluto.i =@(T) (17.14001206+(T*0.00004818))*pi/180; % rads
Pluto.L =@(T) (238.92903833+(T*145.20780515))*pi/180; % rads
Pluto.theta =@(T) (224.06891629-(T*0.04062942))*pi/180; % rads
Pluto.RAAN =@(T) (110.30393684-(T*0.01183482))*pi/180; % rads

% QUAOAR (Horizons Small Body Database Lookup)

Quaoar.mu = 93.4332; % km^3/s^2
Quaoar.r = 555; % km
Quaoar.a =@(T) (43.38833028+(T*0))*Sol.AU; % km
Quaoar.e =@(T) 0.04028864+(T*0);
Quaoar.i =@(T) (7.99130083+(T*0))*pi/180; % rads
Quaoar.L =@(T) (281.22046283+(T*125.6157883))*pi/180; % rads
Quaoar.theta =@(T) (346.79068308+(T*0))*pi/180; % rads
Quaoar.RAAN =@(T) (189.10126806+(T*0))*pi/180; % rads

end
```

Calculation of Planet Positions

```
function [Planet] = Planet_Position(Sol,Planet,T)

T = T/100;
 % converts T to centuries for ephemeris functions

Planet.E1 = newton(1,Planet.e(T),Planet.L(T)-Planet.theta(T),1000,1e-8);
 % uses Newtons method to solve Keplers equation

while Planet.E1 > 2*pi
    Planet.E1 = Planet.E1 - (2*pi);
end % quad check
Planet.rs = Planet.a(T)*(1 - (Planet.e(T)*cos(Planet.E1)));
 % position magnitude

nu1 = (2*atan((((1+Planet.e(T))/(1-Planet.e(T)))^(1/2))*tan(Planet.E1/2)));
O1 = Planet.theta(T)-Planet.RAAN(T)+nu1;
U1 = Planet.RAAN(T);
i1 = Planet.i(T);
 % classical orbital angles

Planet.DCM = [(cos(U1)*cos(O1))-(sin(U1)*sin(O1)*cos(i1)),-(cos(U1)*sin(O1))-
(sin(U1)*cos(O1)*cos(i1)),(sin(U1)*sin(i1));...
    (sin(U1)*cos(O1))+(cos(U1)*sin(O1)*cos(i1)),-
(sin(U1)*sin(O1))+(cos(U1)*cos(O1)*cos(i1)),-(cos(U1)*sin(i1));...
    (sin(O1)*sin(i1)),(cos(O1)*sin(i1)),cos(i1)];
```

```
 % Directional Cosine Matrix

Planet.v = sqrt(Sol.mu*((2/Planet.rs)-(1/Planet.a(T))));
Planet.h = sqrt(Sol.mu*Planet.a(T)*(1-Planet.e(T)^2));
Planet.y = acos(Planet.h/(Planet.v*Planet.rs));
if Planet.E1 > pi
    Planet.y = -Planet.y;
end % quad check

Planet.R = Planet.DCM*[Planet.rs;0;0];
Planet.V = Planet.DCM*[Planet.v*sin(Planet.y);Planet.v*cos(Planet.y);0];
 % complete cartesian elements of Planet at time T
end
```

Newton Method Solution of Kepler's Equation

```
function num = newton(x_o,c1,c2,max,tol)
% Purpose:  Using Newtons method to numerically approximate any given value
% Inputs:   c1-c3 - variable or constant values needed in chosen equation
%           tol - tolerance for numerical approximation
%           max - maximum number of iterations in loop
% Outputs:  numerically approximated value
    x = zeros(1,max);

    f =@(E,e,M) M - E + e*sin(E);
    fp =@(E,e) e*cos(E) - 1;

    for i = 1:max
        if i == 1
            y = f(x_o,c1,c2);
            yp = fp(x_o,c1);
            x(1,i) = x_o - (y/yp);
            % calculations for initial run
        else
            y = f(x(1,i-1),c1,c2);
            yp = fp(x(1,i-1),c1);
            x(1,i) = x(1,i-1) - (y/yp);
            % calculations for non-initial run

            if abs(x(1,i)-x(1,i-1)) < tol
                break;
            end
            % ends loop when tolerance is met
        end
    end
    num = x(1,i);
    % final value
end
```

Lambert Solver

```
function [A,P,V1,V2,conv,G,ta] = Lambert(R1,R2,TOF,mu,JJ,n,tol,kmax)
%{
    Programmer: Grant Hecht
    Date:       3/11/2019
    File:       Lambert.m
    Purpose:    This function solves Lambert's Problem using Battin's
                method.

    Inputs:
    R1:     Vector to Pt#1
    R2:     Vector to Pt#2
    TOF:    Time of Flight
    mu:     Gravitational parameter for central body
    JJ:     Integer that determines initial guess for x
                (set JJ = 1 for an ellipse)
                (set JJ = 0 for a parabola or hyperbola)
    n:      Number of continued fracton levels
                (set n = 0 for default of 10)
                (recomend setting n >= 100 for most accurate results)
    tol:    Tolerance to exit iterations
    kmax:   Maximum Iterations


    Outputs:
    V1:     Velocity Vector at Pt#1
    V2:     Velocity Vector at Pt#2
    conv:   Boolean to indicate convergence.

%}
% Defalt Value for n
n_default = 10;

% If does not converge, set as false
conv = true;

% Sets n to defalt value if n = 0 is passed
if n == 0
    n = n_default;
end

% Find Transfer Angle
ta = acos(dot(R1,R2)/(norm(R1)*norm(R2)));
if R1(1)*R2(2)-R1(2)*R2(1) < 0
    ta = 2*pi - ta;
end

% Find Chord
c = sqrt(norm(R1)^2 + norm(R2)^2 - 2*norm(R1)*norm(R2)*cos(ta));
```

```
% Find Semi-Perimeter
s = (norm(R1) + norm(R2) + c)/2;

% Find Lambda
lambda = sqrt(norm(R1)*norm(R2))*cos(ta/2)/s;

% Find w
w = atan((norm(R2)/norm(R1))^0.25)-(pi/4);

% Find l
if (0 < ta) && (ta < pi)
    l = (sin(ta/4)^2+tan(2*w)^2)/(sin(ta/4)^2+tan(2*w)^2+cos(ta/2));
elseif (pi <= ta) && (ta < 2*pi)
    l = (cos(ta/4)^2+tan(2*w)^2-cos(ta/2))/(cos(ta/4)^2+tan(2*w)^2);
else
    fprintf('Cannot Compute for Transfer Angle of 0 or 360 degrees.');
    return
end

% Find m
m = (8*mu.*TOF.^2)/(s^3*(1+lambda)^6);

% For Eliptical Transfer Orbit Use x = l for Initial Guess
% For Hyperbolic or Parabolic Transfer Orbit Use x = 0.
if JJ == 0
    x = 0;
else
    x = l;
end

%Define Velocity Vectors
V1 = zeros(3,1);
V2 = zeros(3,1);

%Define delta x and counter
DX = 100;
k  = 0;

%Iterate to solve
while abs(DX) > tol

    % Breaks Itteration and sets conv = false if k = kmax
    if k >= kmax
        conv = false;
        break
    end

    % Calculates Continued Fraction PHI for 'n' Levels
    eta = x/(sqrt(1+x)+1)^2;
    f   = 1;
    % Itterate to Calculate levels 4 -> n
    for j = n:-1:4
        ceta = j^2/((2*j)^2-1);
```

```
        f = 1 + ceta*eta/f;
    end
    % Finishes Calculation of PHI with levels 1 -> 3
    PHI = 8*(sqrt(1+x)+1)/(3+1/(5+eta+(9/7)*eta/f));

    h1 = (l+x)^2*(1+3*x+PHI)/((1+2*x+l)*(4*x+PHI*(3+x)));
    h2 = m*(x-l+PHI)/((1+2*x+l)*(4*x+PHI*(3+x)));
    B  = 27*h2/(4*(1+h1)^3);
    u  = B/(2*(sqrt(1+B)+1));

    % Calculates Continued Fraction K(u) for 'n' Levels
    f = 1;
    r = n/2-1;
    % Iterate to Calculate Levels 3 -> n
    for j = r:-1:1
        g2n  = 2*(3*j+1)*(6*j-1)/(9*(4*j-1)*(4*j+1));
        g2n1 = 2*(3*j+2)*(6*j+1)/(9*(4*j+1)*(4*j+3));
        f = 1 + g2n*u/(1 + g2n1*u/f);
    end
    % Finishes Calculation of K(u) with levels 1 -> 2
    K = (1/3)/(1+(4/27)*u/f);

    % Calculates New Values for y and x
    yNew = ((1+h1)/3)*(2+sqrt(1+B)/(1+2*u*K^2));
    xNew = sqrt(((1-l)./2).^2+m/yNew.^2)-(1+l)/2;

    % Compares xNew with x
    DX = abs(xNew - x);

    % Sets x and y to xNew and yNew
    x = xNew;
    y = yNew;

    k = k + 1;
end

%Computes Orbit Parameters and Initial and Final Velocity
A  = m.*s.*(1+lambda).^2/(8.*x.*y.^2);
P0 = c^2*(1+x)^2/(16*A*x);
P  = 4*norm(R1)*norm(R2)*P0*sin(ta/2)^2/c^2;
F  = 1-(norm(R2)/P)*(1-cos(ta));
G  = norm(R1)*norm(R2)*sin(ta)/sqrt(mu*P);
FDOT = sqrt(mu/P)*tan(ta/2)*((1-cos(ta))/P-1/norm(R2)-1/norm(R1));
GDOT = 1-(norm(R1)/P)*(1-cos(ta));
for K=1:3
    V1(K)=(1/G)*(R2(K)-(F*R1(K)));
    V2(K)=FDOT*R1(K)+GDOT*V1(K);
end
end
```

Departure Burn Analysis

```
function [Earth,DV1] = Departure(Earth,earth)

Earth.Vinf = Earth.Vdep - Earth.V;

hyper_a = -Earth.mu/(norm(Earth.Vinf)^2);
r_p = earth.a*(1-earth.e);

hyper_v = sqrt(Earth.mu*((2/r_p)-(1/hyper_a)));
ellip_v = sqrt(Earth.mu*((2/r_p)-(1/earth.a)));

DV1 = hyper_v - ellip_v;
Earth.DV1 = Earth.DCM*[0;DV1;0];

end
```

Gravity Assist Analysis

```
function [Dest,dest] = Flyby(Dest,dest)

% Varr, Vdep, Vbody

Dest.Vinfm = Dest.Varr - Dest.V;
Dest.varr = norm(Dest.Varr);
Dest.vinf = norm(Dest.Vinfm);
%Dest.Vinfp = Dest.Vdep - Dest.V;
Dest.visvisa_m = dot(Dest.Vinfm,Dest.Vinfm);

dest.a = -Dest.mu/(Dest.vinf^2);
dest.e = 1 - (dest.r_p/dest.a);
dest.delta = 2*asin(1/dest.e);

Dest.dv = Dest.vinf*sqrt(2*(1-cos(dest.delta)));

dest.beta = 0.5*(pi-dest.delta);
dest.Gamma = acos(dot(Dest.Vinfm,Dest.Varr)/(Dest.vinf*Dest.varr));
dest.d = dest.beta + dest.Gamma;
Dest.vdep = sqrt((Dest.dv^2)+(Dest.varr^2)-(2*Dest.dv*Dest.varr*cos(dest.d)));

end
```

Arrival Burn Analysis

```
function [Dest,DV2] = Arrival(Dest,dest)

Dest.Vinf = Dest.Varr - Dest.V;

hyper_a = -Dest.mu/(norm(Dest.Vinf)^2);
r_p = dest.a*(1-dest.e);

hyper_v = sqrt(Dest.mu*((2/r_p)-(1/hyper_a)));
ellip_v = sqrt(Dest.mu*((2/r_p)-(1/dest.a)));

DV2 = hyper_v - ellip_v;
Dest.DV2 = Dest.DCM*[0;DV2;0];

end
```

Injection Stage Mass Calculations

```
function [m_p,m_o,m_t,L] = MassCalcs(T2,all_DV,I,all_T3)

g = 9.81; % m/s^2
 % gravitational accleration on Earth

% CNTP Performance
Isp = 1600; % s
 % Specific Impulse
m_e = 1650; % kg
 % engine mass

% LV Constraints
R = 4.3; % m
 % max tank diameter

m = [800,1000,1200];

figure
for m_ldry = m
    m_o = zeros(length(T2),1);
    m_p = zeros(length(T2),1);
    m_t = zeros(length(T2),1);
    L = zeros(length(T2),1);

    for k = 1:length(T2)

        m_l = 1.5*m_ldry; % kg

        % Tank estimates
```

```
        m_ts = 0; % kg
         % tank mass estimate for LH2
        tank_margin = 2;

        while tank_margin > 1
            m_t2 = m_ts;
            m_f = m_l + m_e + m_t2; % kg
             % final mission mass
            m_ps = m_f*(exp((all_DV(I,k))*1000/(g*Isp))-1); % kg
             % propellant mass
            V_p = m_ps*1.03/71; % m^3
             % full prop volume
            V_pl = V_p - ((4/3)*pi*R^3);
             % cylindrical prop volume
            Ls = V_pl/(pi*R^2); % m
             % tank cylindrical length
            %if L < 0
            %    R = R - 0.01;
            %    tank_margin = 2;
            %    fprintf('Warning! Tank not full!\n')
            %end
            m_ts = (m_ps*0.128) + (2.88*((2*R*pi*Ls)+(4*pi*R^2)));
             % new tank mass
            tank_margin = abs(m_ts - m_t2);
        end
        L(k) = Ls;
        m_t(k) = m_ts;
        m_p(k) = m_ps;
        m_o(k) = m_ps + m_f; % kg
         % initial mission mass
    end

    %plot(opt_DV_1 + opt_DV_2,m_o)
    mass_transit = T2 + all_T3(I,:);
    plot(T2 + all_T3(I,:),m_o/1000)
    hold on
end

xlim([8 20])
ylim([0 40])
xlabel('Transfer Time (years)')
ylabel('Initial Vehicle Mass (mT)')
legend('Payload Dry Mass: 800 kg','1000 kg','1200 kg')

%figure
%plot(m,m_o)

%fprintf('Required Propellant Mass: %0.2f kg\n',m_p)
%fprintf('Spacecraft Total Mass: %0.2f kg\n',m_o)

end
```